

PULSE SHAPE DESIGN FOR ULTRA WIDE BAND  
COMMUNICATIONS

WEIHUA GAO







PULSE SHAPE DESIGN FOR ULTRA WIDE BAND COMMUNICATIONS

BY

WEIHUA GAO

A thesis submitted to the  
School of Graduate Studies  
in partial fulfillment of the  
requirements for the degree of  
Master of Engineering

FACULTY OF ENGINEERING AND APPLIED SCIENCE

MEMORIAL UNIVERSITY OF NEWFOUNDLAND

2008

MASTER OF ENGINEERING THESIS  
OF  
WEIHUA GAO

APPROVED:  
Supervisor

---

---

---

MEMORIAL UNIVERSITY OF NEWFOUNDLAND

2008

# Abstract

Ultra Wideband (UWB) technology is promising for high-speed short-range communication applications due to its large bandwidth, high data rate, low power requirement and short-range characteristics. Instead of exploring new unused frequency band, the UWB communication follows the overlay principle. The great potential of UWB lies in the fact that it can co-exist with the already licensed spectrum users and can still pave the way for a wide range of applications. Pulse shape design is a key technique in the UWB system. This thesis concentrates on pulse shaping techniques for UWB communication system.

This thesis first summarizes the main pulse shaping schemes, and then describes the design of a pulse shaping method based on combining Gaussian derivative pulses for impulse based UWB systems. New pulse shapes are created to satisfy the Federal Communications Commission (FCC) spectral mask by this method. Since the objective function of the received signal-to-noise ratio (SNR) optimization is affected by different factors, multiple parameters are also designed to try to achieve the best received SNR. The performance of new pulses and other frequently used UWB pulses

are compared through theoretical calculations and simulations coded in MATLAB.

The main contributions of this thesis include the new determined way of combining certain numbers of Gaussian derivative pulses to create a single pulse that not only conforms to the FCC spectral mask, but also effectively exploits the permitted frequency spectrum, as well as the development of an end-to-end UWB signal transmission simulation chain that can use Time Hopping Pulse Position Modulation (TH-PPM) modulation and Time Hopping Binary Phase Shift Keying (TH-BPSK) modulation through an Additive White Gaussian Noise (AWGN) channel and the IEEE 802.15.3a standard channel model.

Comparisons have been done of the overall performance of the systems using different pulses in various scenarios such as: single link system use AWGN channel and IEEE standard channel and multiuser system using AWGN channel and IEEE standard channel. In order to exploit the temporal diversity of the multi-path IEEE channel to improve performance of the decision process, a perfect RAKE receiver simulation model is used in the simulation chain. The theoretical calculation and simulation results indicate that the proposed pulses outperform other pulses to different extents under different situations. Discussions on the implementation issues of the pulse shaper are also provided in this thesis.

The work reported here could act as a starting point from which improvements and extensions can be made and incorporated.

## Acknowledgments

Time flies, and the time has come for me to put a period to my two years Masters study here in Memorial University.

First of all, I wish to express my sincere gratitude to my supervisors, Dr. Ramachandran Venkatesan and Dr. Cheng Li. I would say it is impossible for me to finish this thesis without their excellent guidance and immense patience. I would like to take this opportunity to thank Dr. Venkatesan for his constant help, support, encouragement and guidance throughout my study and research. It has truly been a great privilege to work with him. My deepest gratitude also goes to Dr. Li, who suggested this as my research topic, provided me complete freedom to try ideas and gave help whenever it was needed. The wide knowledge and insightful viewpoints and expert advices of both my supervisors provided me a sense of direction through all phases of this research. In addition to being productive professors, they are both splendid human beings and I have been thoroughly enriched working with and knowing them. My special thanks goes to Dr. Octavia Dobre and Dr. Weimin Huang

in Department of Engineering and Applied Science, and Dr. Yuanzhu Chen in Department of Computer of Science, for their interests on my research and constructive tips and advice on my work. Many thanks to my friends and colleagues in CERL. Working with fellow graduate students in the CERL lab allowed for the exchange of ideas as well as many educational discussions and debates. In particular, I would like to express my appreciation to Reza Shahidi. He took time from his busy PhD. studies and gave me great help on all kinds of technical problems during my days at CERL. I wish to thank Ling Wu, Zhiwei An, Liang Zhang, Pu Wang, Ali Kashif, Fahed Hameed and Shi Chen in CERL, without you guys, the life of 90 hours per week in CERL in the last two years would not have been that productive and interesting for me.

I wish to thank the Faculty of Engineering and Applied Science and CERL, Memorial University of Newfoundland, for providing much needed laboratory space, equipment, and technical services to finish this work.

Thanks also go to my roommates Jianlong Qi and Haifeng Lin (both graduate students in Computer Science), who shared the experience of living in an extremely friendly house and always help me and support me.

This work would not have been completed without the support from my dear parents Shexue Gao Yuqiao Sun and my beautiful girlfriend Yu Zhu who provided me unconditional love and support and were always there to accentuate the positive side of post-graduate studies.

# Contents

<b>Abstract</b>	i
<b>Acknowledgments</b>	iii
<b>Table of Contents</b>	v
<b>List of Figures</b>	1
<b>List of Tables</b>	6
<b>List of Abbreviations</b>	7
<b>1 Introduction</b>	9
1.1 Overview of UWB technology . . . . .	9
1.1.1 General introduction . . . . .	9
1.1.2 A brief history of UWB . . . . .	11
1.1.3 UWB standards and regulations . . . . .	13
1.1.4 UWB advantages . . . . .	22

1.1.5	UWB applications . . . . .	26
1.2	Research motivation . . . . .	29
1.3	Organization of thesis . . . . .	30
<b>2</b>	<b>UWB pulse shaping overview</b>	<b>31</b>
2.1	Introduction . . . . .	31
2.2	Background knowledge . . . . .	32
2.2.1	Effective isotropically radiated power . . . . .	32
2.2.2	UWB modulation schemes . . . . .	34
2.3	UWB pulse shaping literature review . . . . .	38
2.3.1	UWB pulse shaping filter design methods . . . . .	39
2.3.2	Different pulse shapes chosen for UWB systems . . . . .	51
2.4	Pulse generator review . . . . .	69
2.4.1	Avalanche pulse generator . . . . .	69
2.4.2	Step recovery diode pulse generator . . . . .	70
2.4.3	CMOS monocycle generator . . . . .	72
2.4.4	Fifth-derivative Gaussian pulse generator . . . . .	74
2.5	Chapter summary . . . . .	77
<b>3</b>	<b>A new pulse shaping method</b>	<b>79</b>
3.1	Introduction . . . . .	79
3.2	Gaussian derivatives and PSD . . . . .	80

3.3	New UWB pulse design . . . . .	85
3.3.1	Method description . . . . .	85
3.3.2	More pulse shape design considerations . . . . .	86
3.3.3	System models for the pulse shape design . . . . .	88
3.3.4	Pulse shape design in multi-user system with AWGN channel .	89
3.4	Chapter summary . . . . .	98
<b>4</b>	<b>Simulation and comparison</b>	<b>99</b>
4.1	Introduction . . . . .	99
4.2	Newly designed pulses and other pulses for comparison . . . . .	100
4.2.1	Pulses generated by random combining method . . . . .	100
4.2.2	Pulses generated by our design method . . . . .	104
4.3	Performance comparisons . . . . .	110
4.3.1	BER comparisons of different pulses . . . . .	112
4.3.2	Maximum user number comparisons for different pulses . . . .	120
4.3.3	Transmission distance comparisons of different pulses . . . .	121
4.4	Simulation comparisons of pulse performance in system model using UWB standard channel . . . . .	126
4.4.1	IEEE 802.15.3 UWB channel model . . . . .	126
4.4.2	Channel model realizations . . . . .	129
4.4.3	Simulation comparisons of pulse performance . . . . .	131

4.5 Chapter summary . . . . .	134
<b>5 Conclusion and future work</b>	<b>135</b>
5.1 Conclusions . . . . .	135
5.2 Recommendations for future work . . . . .	137
<b>References</b>	<b>139</b>

## List of Figures

1.1	The spectrum of UWB system compared with existing systems . . . . .	11
1.2	Time and frequency waveforms of DS-UWB proposal . . . . .	15
1.3	Band allocation of MBOA proposal . . . . .	16
1.4	Time and frequency waveforms of the MBOA proposal . . . . .	16
1.5	FCC spectral mask for various UWB applications-1 . . . . .	19
1.6	FCC spectral mask for various UWB applications-2 . . . . .	20
1.7	FCC spectral mask for various UWB applications-3 . . . . .	21
1.8	UWB capacity vs. other WLAN technologies . . . . .	23
2.1	FCC Indoor power spectral density mask . . . . .	34
2.2	Pulse amplitude modulation . . . . .	35
2.3	On-Off keying modulation . . . . .	36
2.4	Pulse position modulation . . . . .	36
2.5	Bi-phase shift keying . . . . .	37

2.6 Fourier transform of pulse shapers for single-band UWB (Taken from [19]) . . . . .	42
2.7 Results for a spectral utilization problem : spectrum vs. frequency . . . . .	45
2.8 The spectrum shaping results compared with the FCC mask . . . . .	47
2.9 Transmission filter frequency response . . . . .	49
2.10 The power spectral density for the first-derivative Gaussian pulse for various pulse widths. The FCC spectral mask for indoor systems is shown for comparison . . . . .	53
2.11 PSD of the higher-order derivatives of the Gaussian pulse for UWB indoor systems . . . . .	54
2.12 The power spectral density of pulse shapes obtained from the pulse design algorithm for the single bandpass frequency mask (a) $\varphi_1(f)$ (b) $\varphi_2(f)$ . . . . .	56
2.13 Pulses which comply with the FCC spectral mask . . . . .	59
2.14 The power spectral densities of (a) the pulse $p_3^e(t)$ and (b) the pulse $p_4^e(t)$ and the FCC masks . . . . .	62
2.15 The power spectral density of the pulse $p_2^o(t)$ and (a) the FCC indoor spectral emission mask (b) the FCC outdoor spectral emission mask . . . . .	63
2.16 PSD of the base functions and of the combined waveform . . . . .	65
2.17 PSD of the linear combination of Gaussian waveforms versus FCC indoor emission mask . . . . .	66

2.18 Avalanche pulse generator . . . . .	70
2.19 Step recovery diode pulse generator . . . . .	71
2.20 Gaussian $1^{st}$ and $2^{nd}$ derivatives pulse generator . . . . .	73
2.21 Fifth-derivative Gaussian pulse generator (a) Schematic (b) Signal shape on each node . . . . .	75
3.1 Amplitude normalized Gaussian $1^{st}$ to $16^{th}$ derivative pulses . . . . .	81
3.2 Amplitude normalized Gaussian second-derivative pulse . . . . .	82
3.3 Power spectral density of amplitude normalized Gaussian second- derivative pulse . . . . .	82
3.4 Gaussian second-derivatives with different $\sigma$ values . . . . .	83
3.5 Power spectral density of Gaussian second-derivatives with different $\sigma$ values . . . . .	84
3.6 Power spectral density of Gaussian $1^{st}$ to $16^{th}$ derivatives . . . . .	84
3.7 Power spectral density of Gaussian $3^{rd}$ and $14^{th}$ derivatives . . . . .	87
4.1 PSD of the 5 best results of random combination by two derivatives, coefficient range $[-6, +6]$ . . . . .	102
4.2 PSD of the 5 best results of random combination by three derivatives, coefficient range $[-6, +6]$ . . . . .	103
4.3 PSD of combination of $7^{th}$ $9^{th}$ and $11^{th}$ Gaussian derivatives, coefficient range $[-6, +6]$ . . . . .	104

4.4 PSD of combination of 7 <sup>th</sup> , 9 <sup>th</sup> and 11 <sup>th</sup> Gaussian derivatives, coefficient range [-10,+10] . . . . .	105
4.5 Pulse combined by 7 <sup>th</sup> and 14 <sup>th</sup> Gaussian derivatives . . . . .	106
4.6 PSD of combination of 7 <sup>th</sup> and 14 <sup>th</sup> Gaussian derivatives . . . . .	106
4.7 Pulse combined by 7 <sup>th</sup> , 10 <sup>th</sup> and 15 <sup>th</sup> Gaussian derivatives . . . . .	107
4.8 PSD of combination of 7 <sup>th</sup> , 10 <sup>th</sup> and 15 <sup>th</sup> Gaussian derivatives . . . . .	108
4.9 PSD of two 2 <sup>nd</sup> Gaussian derivative pulses . . . . .	110
4.10 System model for the single link UWB transmission chain with AWGN channel . . . . .	112
4.11 Comparison of indoor Single Link TH-PPM UWB systems using different pulses . . . . .	114
4.12 Comparison of indoor TH-PPM UWB systems using different pulses with 7 asynchronous interferers . . . . .	114
4.13 Comparison of indoor TH-PPM UWB systems using different pulses with 15 asynchronous interferers . . . . .	115
4.14 Comparison of indoor Single Link TH-BPSK UWB systems using different pulses . . . . .	116
4.15 Comparison of indoor TH-BPSK UWB systems using different pulses with 7 asynchronous interferers . . . . .	116
4.16 Comparison of indoor TH-BPSK UWB systems using different pulses with 15 asynchronous interferers . . . . .	117

4.17 BER comparison of two pulses from candidate pool . . . . .	119
4.18 Comparison both theoretical and simulation results of indoor TH-BPSK UWB systems using different pulses with 7 asynchronous interferers . . . . .	120
4.19 Maximum number of users vs. system data rate for system BER at $10^{-3}$ using different pulses . . . . .	122
4.20 Maximum transmission distance vs. system data rate for signal representing by different pulses . . . . .	125
4.21 Channel impulse response for CM1 . . . . .	130
4.22 Discrete time channel impulse response for CM1 . . . . .	131
4.23 Comparison of indoor Single Link TH-BPSK UWB systems using different pulses through IEEE standard channel . . . . .	132
4.24 Comparison of indoor TH-BPSK UWB systems using different pulses with 7 asynchronous interferers through IEEE standard channel . . .	133
4.25 Comparison of indoor TH-BPSK UWB systems using different pulses with 15 asynchronous interferers through IEEE standard channel . . .	133

# List of Tables

1.1	Summary of FCC restrictions on UWB operation . . . . .	18
4.1	Pulse energy of the 5 best results of random combination by two derivatives, coefficient range [-6,+6] . . . . .	101
4.2	Pulse energy of the 5 best results of random combination by three derivatives, coefficient range [-6,+6] . . . . .	102
4.3	Pulse energy of combination of 7 <sup>th</sup> 9 <sup>th</sup> and 11 <sup>th</sup> Gaussian derivatives, coefficient range [-6,+6] . . . . .	103
4.4	Pulse energy of combination of 7 <sup>th</sup> , 9 <sup>th</sup> and 11 <sup>th</sup> Gaussian derivatives, coefficient range [-10,+10] . . . . .	104
4.5	Parameters of different pulses . . . . .	107
4.6	Parameters of two pulses from candidate pool . . . . .	109
4.7	Theoretical BER comparison of two pulses from candidate pool . . .	109
4.8	Parameters of the simulation UWB systems . . . . .	111

## List of Abbreviations

**AWGN** Additive White Gaussian Noise

**BER** Bit Error Rate

**BPSK** Binary Phase Shift Keying

**DARPA** Defense Advanced Research Projects Agency

**DS** Direct Sequence

**DTFT** Discrete Time Fourier Transform

**EIRP** Effective Isotropically Radiated Power

**FAA** Federal Aviation Administration

**GPR** Ground Penetrating Radar

**GPS** Global Positioning System

**IPI** Inter Pulse Interference

**IR** Impulse Radio

**LSE** Least Square Error

**MBOA** Multiband OFDM Alliance

**MUI** Multi User Interference

**NTIA** National Telecommunications and Information Administration

**OFDM** Orthogonal Frequency Division Multiplexing

**OOK** On Off Keying

**PAM** Pulse Amplitude Modulation

**PN** Pseudo Noise

**PPM** Pulse Position Modulation

**RF** Radio Frequency

**SNR** Signal to Noise Ratio

**SRD** Step Recovery Diode

**TH** Time Hopping

**TWI** Through Wall Imaging

**UWB** Ultra Wide Band or Ultra Wideband

**WLAN** Wireless Local Area Network

# Chapter 1

## Introduction

### 1.1 Overview of UWB technology

#### 1.1.1 General introduction

Ultra wideband (UWB) acouwb technology is currently being investigated as a promising solution for bandwidth, cost, power consumption, and physical size requirements of the next-generation short range wireless communications systems.

Generally speaking, it is defined as any wireless transmission scheme in which the fractional bandwidth is greater than 0.25 or the bandwidth (as defined by the -10 dB points) occupies 1500 MHz or more of the spectrum [1]. The fractional bandwidth is defined as

$$B_f = 2 \frac{f_H - f_L}{f_H + f_L}, \quad (1.1)$$

where  $f_H$  and  $f_L$  are the upper and lower -10 dB emission points of the signal spectrum, respectively. The center frequency of the transmission is defined as the average of the upper and lower 10 dB points, i.e.  $(f_H + f_L)/2$ . Unlike conventional wireless communications systems, UWB systems transmit information using narrow time-duration (typically a few tens of picoseconds to a few nanoseconds) pulses that spread the energy from near DC to a few gigahertz without using a frequency carrier. On February 14, 2002, the Federal Communications Commission (FCC) specified that the UWB systems must operate with their -10 dB bandwidth within the frequency [3.1-10.6] GHz for indoor communications and their -20 dB bandwidth within the [3.1-10.6] GHz range for outdoor communications [2]. The wide spectrum allows devices to obtain very high data rate. The FCC also imposed strict broadcast power restrictions on UWB. The transmitted power spectrum density (PSD) is limited to -41 dBm/MHz. Figure 1.1 shows the spectrum of UWB systems compared with existing systems. Following the regulation, UWB devices can make use of an extremely wide frequency band (7.5 gigahertz) while not emitting too much energy. Hence, interference with existing wireless devices can be minimized. The low energy density in spectrum also brings in a Low Probability of Detection (LPD) characteristic, which is significant for both military and commercial applications. Since UWB is a carrier-less technique, the system complexity and cost will be greatly reduced. UWB systems can be made nearly “all-digital”, with minimal RF or microwave electronics. This feature avoids interference with existing services, while fully utilizing

the available spectrum. With the characteristics of wide bandwidth, low power, low cost, and very high data rates at limited range, UWB is a promising candidate for future short range wireless communications.

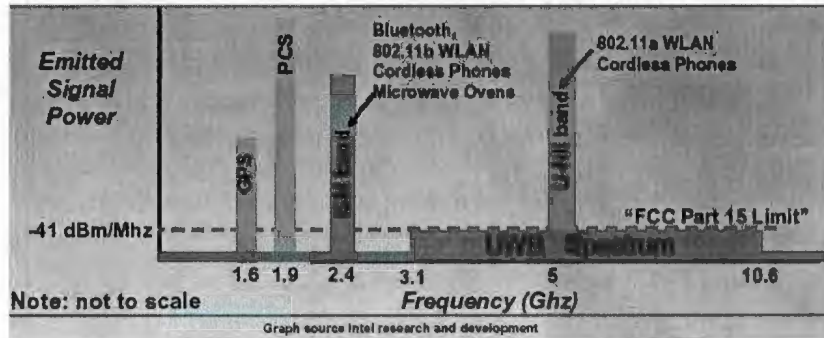


Figure 1.1: The spectrum of UWB system compared with existing systems (Taken from [3])

### 1.1.2 A brief history of UWB

Ultra wideband (UWB) radio is the modern reincarnation of a century old type of communication. The first cross-Atlantic wireless transmission by Guglielmo Marconi used spark-plug transmitters that can be thought of as impulse based UWB transmission [4]. The modern era in UWB started in the early 1960s from work in time domain electromagnetic to describe the transient behavior of a certain class of microwave networks through their characteristic impulse response [5]. The milestones in UWB development are the advent of the sampling oscilloscope by both Tektronix and Hewlett-Packard in the early 1960s and the breakthrough of techniques for sub-nanosecond pulse generation, that is, providing suitable approximations to

an impulse excitation, the impulse response of microwave networks could be directly observed and measured. In 1972, Ross at Sperry Rand Corporation invented a sensitive baseband pulse receiver that replaces the sampling oscilloscope which led to the first patented design of a UWB communications system [6]. At the same time, extensive research was conducted in the former Soviet Union.

In the early 1970s the basic designs for UWB systems became available. Both radar and communication systems could be constructed by basic components such as pulse train generators, pulse train modulators, switching pulse train generators, detection receivers and wideband antennas. The first ground-penetrating radar based on UWB was commercialized in 1974 by Morey at the Geophysical Survey Systems Corporation [7].

Through the 1980s, this technology was referred to as baseband, carrier-free or impulse radio. The term “ultra wideband” was not used until 1989 by the U.S. Department of Defense. Since then, with the advancement in hardware design, UWB technology has been used in many applications such as communications, radar, automobile collision avoidance, positioning systems, liquid level sensing, and altimetry [7].

Within the academic context, Professor Scholtz and his group in the University of Southern California pioneered UWB investigations since the early 1990s. In 1993, Scholtz published a landmark paper that presented a multiple access technique for UWB communication systems [8]. This technique allocates each user a

unique spreading code that determines specific instances in time when the user is allowed to transmit. This allows UWB to support not only radar and point-to-point communications, but also wireless networks. Being a promising candidate for wireless networks, more and more researchers began to investigate on UWB in the late 1990s and early 2000s. These studies include pulse shape design, multiple access schemes, channel model analysis, antenna response characterization, and transmitter and receiver design in UWB systems. At the same time, there has been a rapid expansion of the number of companies and government agencies involved in UWB, which include Multispectral Solutions, Time Domain, Aether Wire, and Fantasma Networks. These companies and the FCC, National Telecommunications and Information Administration (NTIA), Federal Aviation Administration (FAA), and Defense Advanced Research Projects Agency (DARPA), have spent many years investigating the effect of UWB emissions on existing narrowband systems [9].

### **1.1.3 UWB standards and regulations**

Worldwide regulatory developments for UWB appear to be gathering momentum. A number of initiatives have been taken world-wide to develop standards and regulations for the UWB systems and devices.

As of December 2004, two competing proposals existed for this standard: i) The Direct Sequence (DS) UWB, supported by the UWB Forum, which includes Freescale

Semiconductor and a number of small companies. ii) The Multiband OFDM Alliance (MBOA) standard, supported by a consortium of leading semiconductor and consumer electronics companies such as Intel, TI, ST Microelectronics, Panasonic, Philips, Sony, and many others. Both proposals exhibit competitive features and advantages, from the standpoints of technology and business models.

The DS-UWB proposal divides the entire allocated spectrum into two bands. Though initial proposals covered the entire 7.5 GHz bandwidth, later versions excluded the 802.11a Wireless Local Area Network (WLAN) band. The frequency ranges for this proposal are from 3.2-5.15 GHz and 5.825-10.6 GHz. The DS-UWB scheme uses traditional impulse UWB with M-ary Bi-Orthogonal Keying and a CDMA encoding scheme for multiplexing and channelization. The waveforms in time domain and frequency domain of DS-UWB signals are illustrated in Figure 1.2.

In the Multiband OFDM proposal, the spectrum is divided into 14 bands (each with each band of 528 MHz), and devices are allowed to statically or dynamically select which bands to use for transmission. Further, OFDM is used in each of these bands. The data is then appropriately modulated using a concatenation of these bands.

In the MBOA proposal, the entire spectrum is divided into four distinct groups, as shown in Figure 1.3. Only Group-A spectrum is intended for first generation devices because of current technology limitations. Other groups have been reserved for future use. The time and frequency waveforms of the MBOA scheme are shown

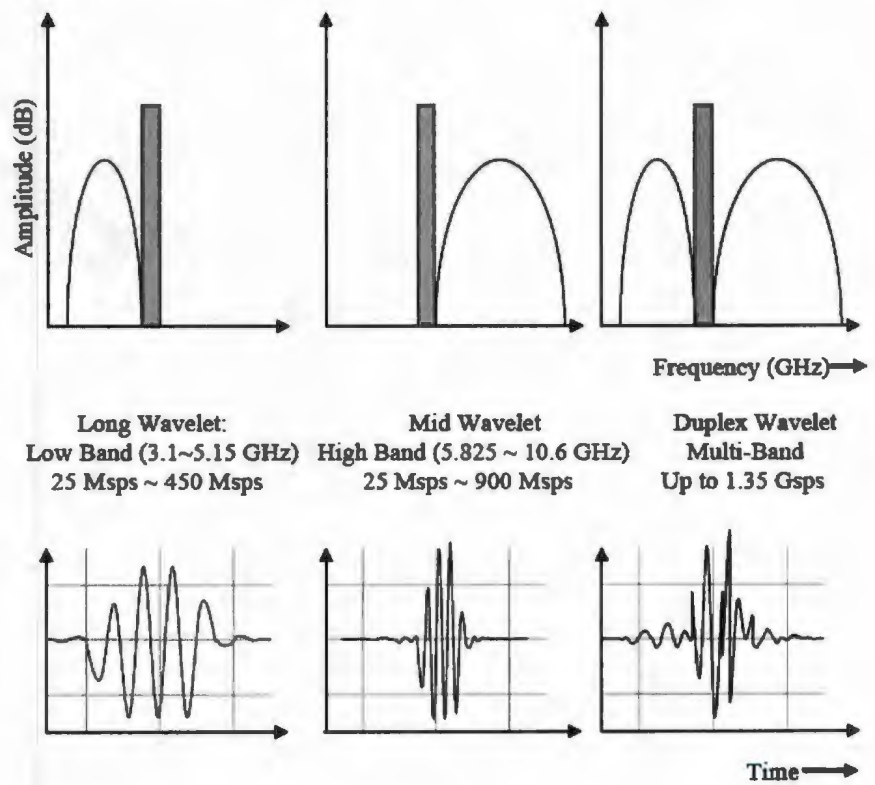


Figure 1.2: Time and frequency waveforms of DS-UWB proposal (Taken from [10])

in Figure 1.4.

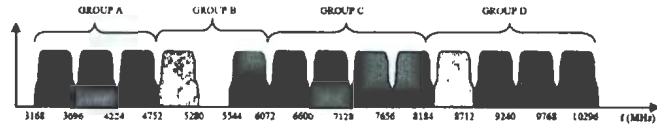


Figure 1.3: Band plan of MBOA proposal (Taken from [11])

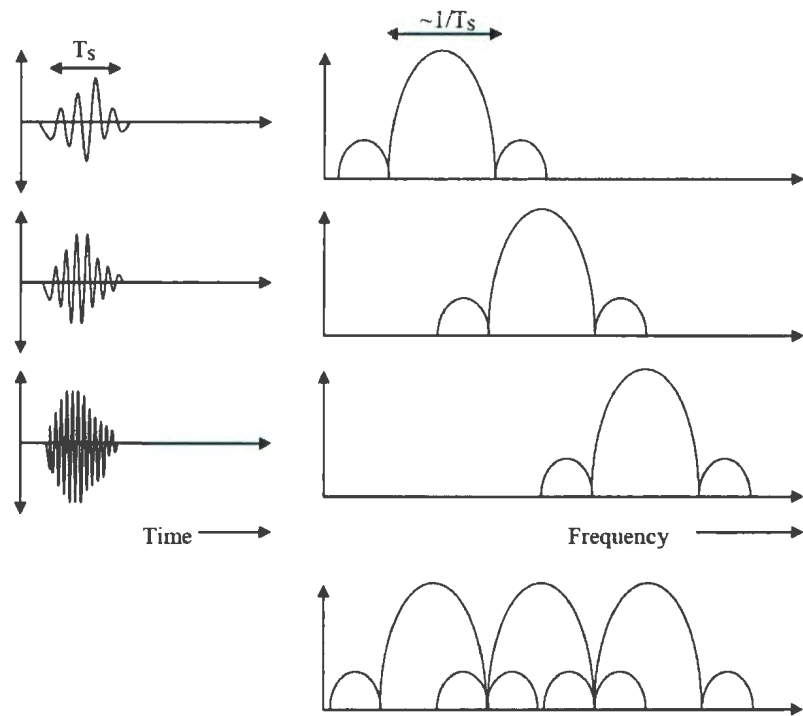


Figure 1.4: Time and frequency waveforms of MBOA proposal (Taken from [11])

Currently, both camps are trying to make a strong case to the IEEE 802.15.3a standards committee. The competition over the UWB standard is very challenging, which might shape the wireless communication landscape for the future. A poll before the IEEE meeting in Berlin in mid-September 2004 indicated that DS-UWB

is currently in the leading position with a majority of 60%. However, in order to be adopted as a standard, 75% in favor would be required [12]. To the best of the author's knowledge, up to now, the standard has not been determined.

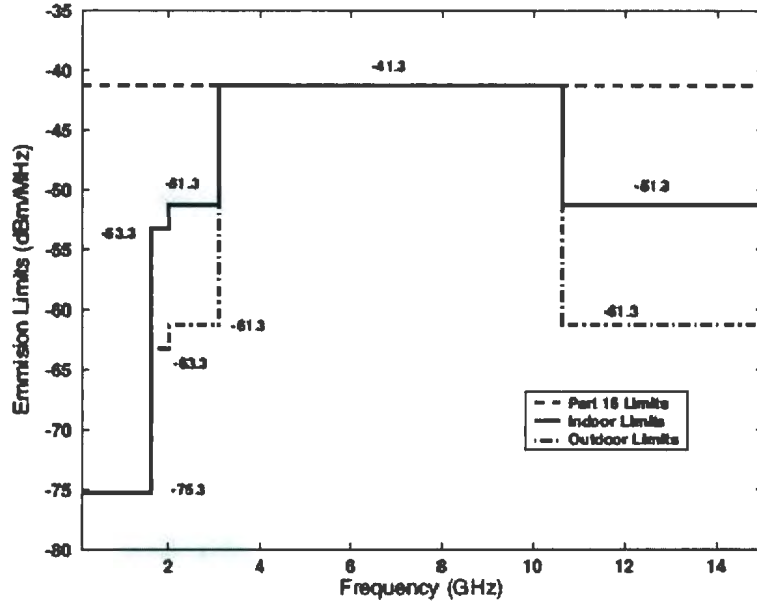
A number of initiatives have been taken world-wide to develop standards and regulations for the UWB systems and devices. At present, the US is the only market where UWB devices are allowed to be operated without a license.

Efforts taken by the Federal Communication Commission (FCC), in the United States, to authorize the use of UWB systems spurred a great amount of interest of UWB technology. In February 2002, the FCC approved the first report and order, allowing the production and operation of unlicensed UWB devices [2]. The report specified three targeted application areas and provided corresponding operating frequency ranges and power limitations. The application areas included vehicular radar systems, communications and measurement systems, and imaging systems. The imaging systems consist of several radar implementations and is divided into the following subclasses: ground penetrating radar, wall imaging, through-wall imaging, medical and surveillance systems [2]. Each category was assigned with a specific spectral mask, as shown from Figure 1.5 to Figure 1.7. Table 1.1 summarizes the various UWB operational categories, their allocated bandwidths, along with restrictions on organizations that are allowed to operate.

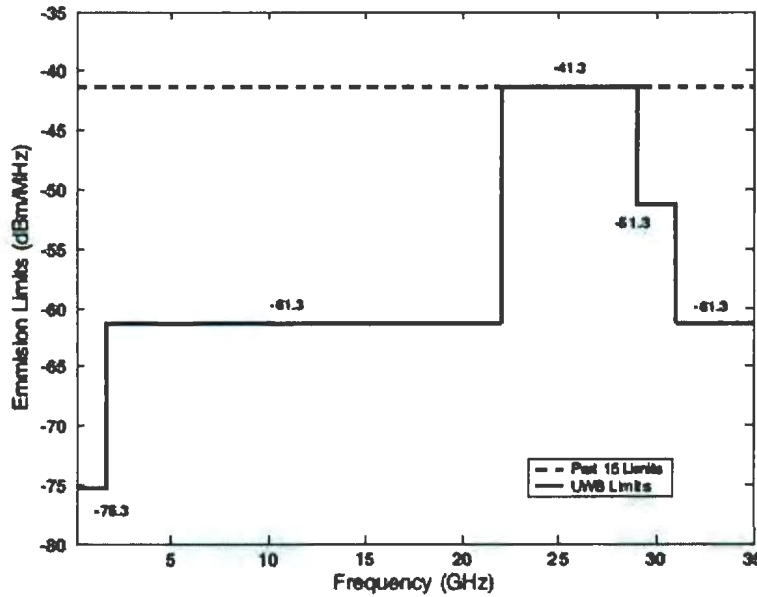
Of all the systems mentioned, measurement and communications systems are currently receiving the most attention in industry and academia alike. Communications

Table 1.1: Summary of FCC restrictions on UWB operation (Taken from[9])

Application	Frequency Band for Operation at Part 15 Limits	User Restrictions
Communications and Measurement Systems (sensors)	3.1-10.6 GHz (different emission limits for indoor and outdoor systems)	None
Vehicular Radar for collision avoidance, airbag activation, and suspension system control	24-29 GHz	None
Ground Penetrating Radar to see or detect buried objects	3.1-10.6 GHz and below 960 MHz	Law enforcement, fire and rescue, research institutions, mining, construction
Wall Imaging Systems to detect objects contained in walls	3.1-10.6 GHz and below 960 MHz	Law enforcement, fire and rescue, mining, construction
Through-wall Imaging Systems to detect location or movement of objects located on the other side of a wall	1.99-10.6 GHz and below 960 MHz	Law enforcement, fire and rescue
Medical Systems for imaging inside people and animals	3.1-10.6 GHz	Medical personnel
Surveillance Systems for intrusion detection	1.99-10.6 GHz	Law, enforcement, fire and rescue, public utilities and industry

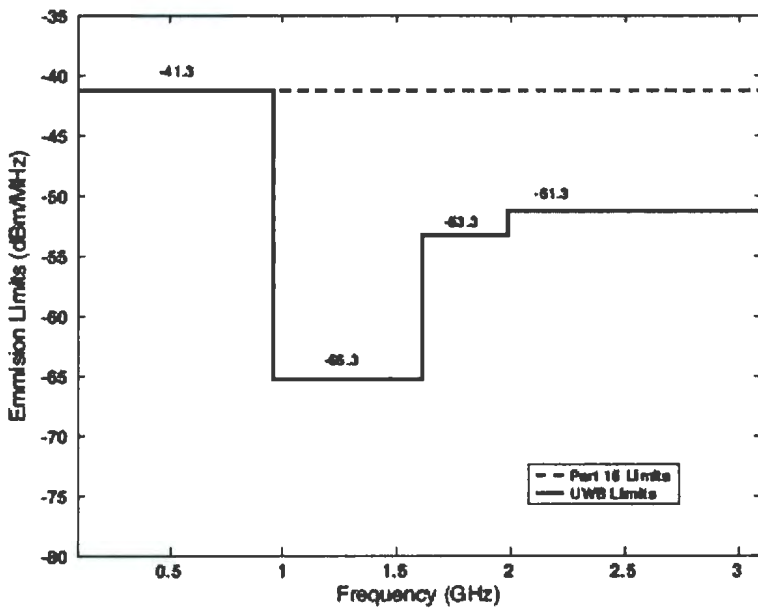


Indoor UWB Communication Systems

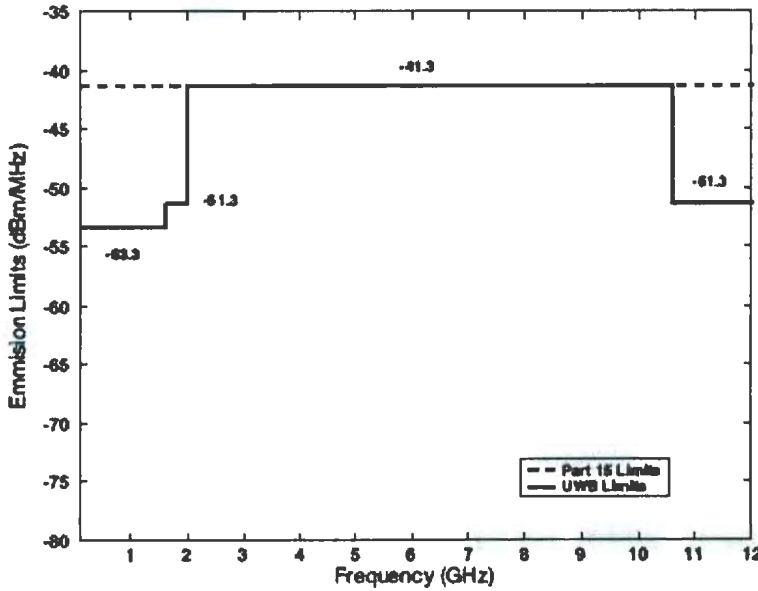


Vehicular Radar

Figure 1.5: FCC allocated spectral mask for various UWB applications (Taken from [2])

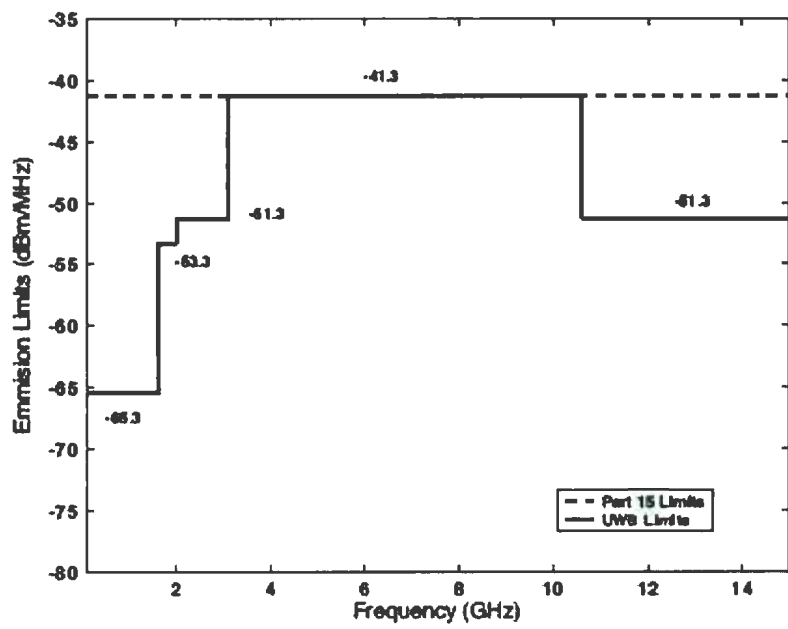


Imaging (Low Frequency)



Imaging (Mid Frequency)

Figure 1.6: FCC allocated spectral mask for various UWB applications (continued)  
(Taken from [2])



Imaging (High Frequency)

Figure 1.7: FCC allocated spectral mask for various UWB applications (continued)  
(Taken from [2])

are the focus of this thesis and most of the discussions henceforth will be in that context.

#### 1.1.4 UWB advantages

There are several advantages in UWB technology compared to traditional wireless technologies.

##### **High data rate**

The 802.15.3 physical layer criterion [13] requires designs to achieve 110 Mb/s for a receiver at a distance of 10 m and 200 Mb/s at 4 m, with options for demonstrating scalability to higher speeds of up to 480 Mb/s at distances less than 4 m.

The principle for the high data rate is based on the Shannon channel capacity theory, which is given by [14]

$$C = W \log_2(1 + SNR), \quad (1.2)$$

where  $C$  is maximum channel capacity,  $W$  is channel bandwidth, and SNR is signal to noise power ratio in Gaussian Channel. Shannon's equation indicates that channel capacity grows linearly with the bandwidth. But it requires exponential increases in power to achieve the same result if the bandwidth and noise level is fixed.

Figure 1.8 compares practical UWB implementations with present wireless technologies. From the figure, we can see those achievable rates for UWB and two other short-range wireless networking technologies notably the 802.11a in the Unlicensed National Information Infrastructure (UNII) radio band (5 GHz) which is divided into three sub-bands, and Bluetooth in the 2.4 GHz industrial, scientific and medical (ISM) radio bands are shown. We can see that UWB provides much higher potential link rates than the other wireless technologies at shorter distances (typically less than 10 m). The picture shows that UWB technology is most suitable for short-range (less than 10 m) applications. Long range flexibility can be served by WLAN applications such as 802.11a.

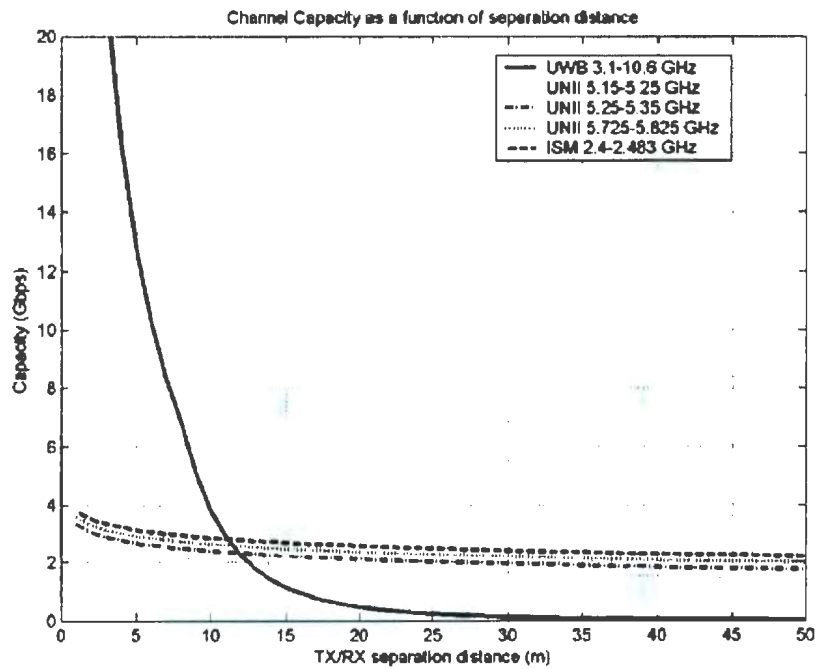


Figure 1.8: UWB capacity vs. other WLAN technologies (Taken from [1])

For communication link design, two metrics are frequently used; namely, bandwidth efficiency, which is measured in b/s/Hz and spatial capacity, which is given by  $b/s/m^2$  that captures the aggregated data intensity in time and space. According to the following example [1], we can clearly see the advantages of UWB over other technologies.

The 2.4 GHz Industrial, Scientific, and Medical (ISM) band contains 80 MHz of usable spectrum which implies that three 22 MHz IEEE 802.11b systems can operate on a non-interfering basis. Each system can provide a peak rate of 11 Mb/s to achieve a total aggregated speed of 33 Mb/s. For an operating range of 100 m, this yields a spatial capacity of approximately  $1 \text{ Kb/s/m}^2$ . Bluetooth in its low-power mode can reach 10 m range and can achieve a peak rate of 1 Mb/s. Studies have shown that approximately ten Bluetooth clusters can operate simultaneously within this range with minimal degradation. This yields an aggregate speed of 10 Mb/s and a spatial capacity of approximately  $30 \text{ Kb/s/m}^2$ . UWB systems are designed for 110 Mb/s at 10 m range with four collocated clusters, which yields a spatial capacity of about  $1.3 \text{ Mb/s/m}^2$ . Thus, the data intensity UWB can potentially support is several orders of magnitude larger than those of the existing WLANs/WPANs. Thus, UWB represents a tradeoff between lower spectral efficiency for increased power efficiency to achieve a given rate/range operating point with limited transmitting power.

### **Robustness to fading and interference**

In traditional UWB systems, the large bandwidth was achieved by using very narrow time-duration baseband pulses of appropriate shape, which include the family of Gaussian shaped pulses and their derivatives [15]. The Fourier Transform (FT) of the pulse indicates that the pulse possesses significant energy from near DC up to the upper limit of the system bandwidth.

These short duration waveforms are relatively immune to multipath cancelation effects as observed in mobile and in-building environments. Multipath cancelation occurs when a strong reflected signal, e.g., signal bounced back from a wall, ceiling, vehicle, building, etc, arrives partially or completely out of phase with the direct path signal, causing a reduced amplitude signal at the receiver. With very short pulses, the direct path signal will have arrived and reflected before the reflected signal arrives, hence, no cancelation will occur. Another important advantage of the UWB technology is that multipath components can be resolved and used to improve signal reception. Furthermore, UWB provides better rejection to the co-channel interference and narrowband jammers and demonstrates the ability to overlay spectrum of the present narrowband solutions.

### **Low system complexity**

UWB radios may provide lower cost architectures when compared to narrow band radios. Narrow band architectures use high-quality oscillators and tuning circuits to

modulate and de-modulate information. UWB transmitters, however, can directly modulate a baseband signal, hence, explicit up and down conversions can be omitted. This results in substantial reduction in area and power for analog circuitry, such as mixers and phase-locked loop. The whole UWB transmitter on a single chip using the low cost CMOS technologies can be realized. The UWB receiver also does not require the reverse process of downconversion. Again, this means a local oscillator in the receiver can be omitted, which means the removal of associated complex delay and phase tracking loops. UWB devices may have a nearly all-digital implementation in CMOS with minimal analog RF electronics. This simple architecture can translate to low power dissipation and low cost, which opens a variety of possible mobile applications.

### **1.1.5 UWB applications**

The applications of UWB can be categorized into four categories, i.e., communications, distance determinations, remote sensing radar, and vehicular radar [2].

#### **Communication and measurement systems**

Communication and measurement systems mainly include WPAN and sensor systems. WPAN, also known as in-home networks, address short-range (generally within 10 - 20 m) ad hoc connectivity among portable consumer electronic and communication devices. They are envisioned to provide high-quality real-time video and audio

distribution, file exchange among storage systems, and cable replacement for home entertainment systems. Sensor networks consist of a large number of nodes spread across a geographical area. The nodes can be either static or mobile, for example, road condition monitoring and pollution tracking, or mobile sensors, when equipped on soldiers, firemen, or robots in military and emergency response situations. Key requirements for sensor networks operating in challenging environments include low cost, low power, and multi-functionality. Typically, energy is more limited in sensor networks than in WPANs because of the nature of the sensing devices and the difficulty in recharging their batteries. Studies have shown that current commercial Bluetooth devices are less suitable for sensor network applications because of their energy requirements and higher expected cost. In addition, exploiting the precise location capability of UWB provides wireless sensor networks with improved positioning accuracy. This is especially useful when GPSs are not available, e.g., due to obstruction [2].

### **Vehicular radar systems**

UWB-based sensing has the potential to improve the resolution of conventional proximity and motion sensors. Relying on the high ranging accuracy and target differentiation capability enabled by UWB, intelligent collision-avoidance and cruise-control systems can be envisioned. These systems can also improve airbag deployment and

adapt suspension/braking systems depending on road conditions. UWB technology can also be integrated into vehicular entertainment and navigation systems by downloading high-rate data from airport off ramp, road-side, or gas station UWB transmitters.

### **Imaging systems**

Imaging systems include Ground Penetrating Radar (GPR), Through-Wall Imaging (TWI) and Surveillance Systems, and Medical Imaging. GPRs operate only when in contact with, or within close proximity of, the ground for the purpose of detecting or obtaining the images of buried objects. Operation is restricted to law enforcement, fire and rescue organizations, scientific research institutes, commercial mining companies, and construction companies. TWI detects the location or movement of persons or objects that are located on the other side of a structure such as a wall. Surveillance systems operate as “security fences” by establishing a stationary RF perimeter field and detecting the intrusion of persons or objects to that field. A medical imaging system may be used for a variety of health applications to “see” inside the body of a person or animal.

In summary, UWB is seen as a potential technology for realizing exciting new applications that to date have not been fulfilled by other wireless short range technologies currently available (e.g., 802.11 LANs and Bluetooth PANs). The development

of this technology has resulted in significant industry interest as indicated by the formation of various new privately funded startup organizations, as well as interest from established silicon vendors aiming to develop new UWB chipset. Correspondingly, there has been a recent upsurge in academic research into UWB.

## 1.2 Research motivation

One of the fundamental functions in communications systems is the representation of a message symbol by a waveform for transmission through a channel. Impulse radio signals in UWB systems utilize an extremely short pulses that spread the energy from near DC to a few gigahertz without using a RF carrier. Since the FCC has introduced strict power restrictions on UWB signals, it is desirable for UWB signals to spread the energy as wide as possible to minimize the power spectral density and hence the potential interference to other systems. Under the condition that the pulses' PSD conforms to the FCC mask, those pulses whose PSD is closer to the FCC mask can transmit more energy and thus can have better error performance. Thus, for an UWB system, the choice of the pulse shape will strongly affect the design of all kinds of filters, the choice of receiver bandwidth, the bit error rate, and the performance in multipath environments. In particular, the pulse shape design is an interesting and critical issue in UWB research. In the literature of UWB pulse shaping, we find that people use those pulses that are complicated to generate, at the

same time constrained by the specific pulse shapes, the PSD of those pulses provide less flexibility in approaching the FCC mask in frequency domain. Hence, we decided to conduct research in this area and try to find a pulse that not only best fits the FCC mask, but also can be easily generated by a simple generator.

### 1.3 Organization of thesis

Chapter 2 contains the literature review of UWB pulse shape design methods and describes the implementation issues of UWB pulses, as pertains to our work. Chapter 3 gives details on the determined method of combining certain numbers of Gaussian derivative pulses to obtain a single pulse that not only conforms to the FCC mask but also exploits the available spectrum efficiently. Chapter 4 compares the various results of our designed pulses and other frequently used UWB pulses to shows that our pulse provides better performance than other pulses. Conclusions and suggestions for future work are presented in Chapter 5.

# **Chapter 2**

## **UWB pulse shaping overview**

### **2.1 Introduction**

One of the fundamental functions in communications systems is the representation of a message symbol by a waveform for transmission through a channel. Impulse UWB technology, also known as Impulse Radio (IR) UWB technology, is the traditional approach for UWB and it is also the focus of this thesis. Impulse UWB is based upon transmitting and receiving very short pulses without a carrier frequency. Thus, pulse generation and pulse shaping are among the most essential problems in these systems. The choice of the pulse shape will strongly affect the design of all kinds of filters, the choice of receiver bandwidth, the bit error rate, and the performance in multipath environments. Spectral masks imposed by FCC regulatory restrictions challenge the design of UWB pulse waveforms. In this chapter, a review of previous

work on impulse UWB pulse shaping techniques will be given. Shaping the spectrum of signals by modifying the pulse waveform is a possibility for both IR and non-IR. In fact, it is well known that the impulse response of the pulse shaper affects the PSD of transmitted signals [16]. In IR-UWB, in particular, the envelope of the ultra wide spectrum has a direct correspondence with the transfer function of the pulse shaper [17]. At the end of the chapter, we also introduce some of the widely used pulse generation techniques unique to UWB communication systems. Particularly, we will introduce an all-digital low-power CMOS pulse generator for UWB systems, because by modifying this system we can generate the pulses that we design.

## 2.2 Background knowledge

In order to understand the advantages and disadvantages of various existing schemes of pulse shaping, it is necessary to have the knowledge of the PSD, Effective Isotropically Radiated Power (EIRP) for a given range of operating frequencies and the UWB modulation schemes.

### 2.2.1 Effective isotropically radiated power

Effective isotropically radiated power (EIRP) is the amount of power that would have to be emitted by an isotropic antenna (that evenly distributes power in all directions) to produce the peak power density observed in the direction of maximum

antenna gain. EIRP takes into account the losses in transmission line and connectors and the gain of the antenna. The EIRP is often stated in terms of decibels over a reference power level, that would be the power emitted by an isotropic radiator with an equivalent signal strength:

$$EIRP(dBm) = (\text{power of transmitter } (dBm)) - \\ (\text{losses in transmission line } (dB)) + (\text{antenna gain } (dB)), \quad (2.1)$$

where antenna gain is expressed relative to a (theoretical) isotropic reference antenna. The EIRP is used to estimate the service area of the transmitter, and to co-ordinate transmitters on the same frequency so that their coverage areas do not overlap [18]. Emission masks typically impose limits on the PSD of emitted signals that is on EIRP spectral density, expressed in dBm/Hz or dBm/MHz.

It is important that UWB devices use a low transmitting power spectral density in order not to interfere with existing narrow band communication systems. For this reason, the FCC has provided a preliminary “conservative” spectral mask for all UWB systems. This thesis concentrates on wireless communication applications of UWB. The FCC indoor spectral mask shown in Figure 2.1 will be the target PSD mask to achieve.

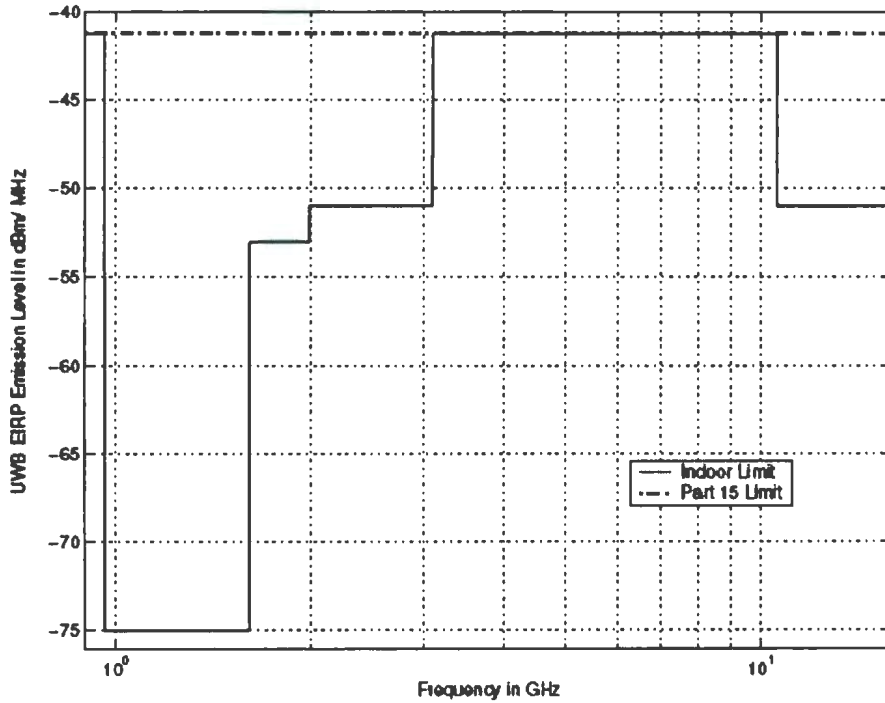


Figure 2.1: FCC Indoor power spectral density mask

### 2.2.2 UWB modulation schemes

The way of forming an UWB signal consists of radiating a train of pulses that are very short in time. The pulses are modulated by the information data symbols in various ways so that different modulation schemes can shape the spectrum of the generated signal. In addition, in the case of multi-user communications, different codes (typically pseudo-random or pseudo-noise (PN) codes) are assigned to different users. This will also affect the spectrum of the train of pulses. Therefore we first study the modulation techniques for UWB.

Modulation techniques commonly used for UWB can take the form of Pulse

Amplitude Modulation (PAM), On-Off Keying (OOK), Pulse Position Modulation (PPM) and Binary Phase Shift Keying (BPSK).

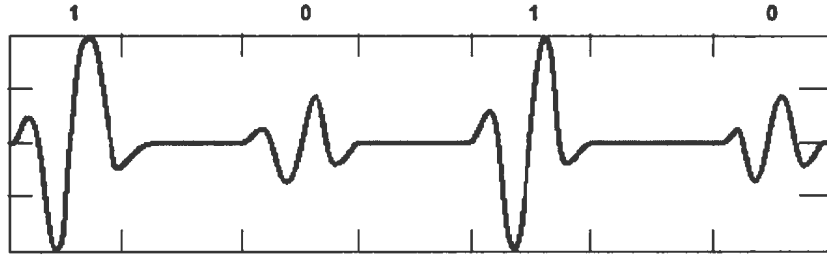


Figure 2.2: Pulse amplitude modulation

PAM is based on the principle of encoding information with the amplitude of the impulses, as shown in Figure 2.2. If we assume that pulses are uniformly spaced in time, the signal can be written as

$$s_{PAM} = \sum_{k=-\infty}^{\infty} a_k p(t - kT), \quad (2.2)$$

where  $p(t)$  is the pulse and  $T$  is the basic time interval between two consecutive pulses. Information bits are coded in sequence of  $a_k$ 's.

The PSD of this PAM signal is:

$$PSD_{PAM} = \frac{\sigma_a^2}{T} |P(f)|^2 + \frac{\mu_a^2}{T^2} \sum_{k=-\infty}^{\infty} \left| P\left(\frac{k}{T}\right) \right|^2 \delta(f - \frac{k}{T}), \quad (2.3)$$

where  $\sigma_a^2$  and  $\mu_a^2$  are the variance and the mean of sequences, respectively;  $P(f)$  is the Fourier transform of the basic pulse, and  $\delta(f)$  is a unit impulse [14].

OOK modulation is a particular case of amplitude modulation, as shown in Figure

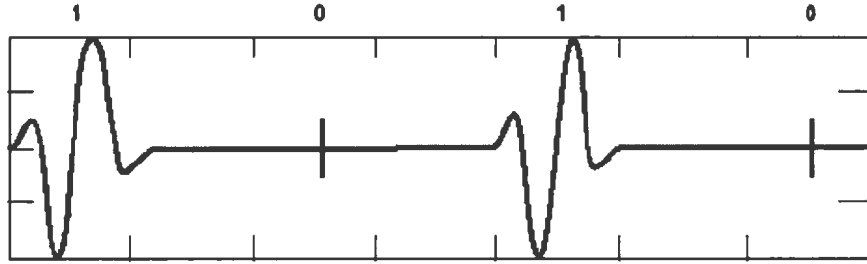


Figure 2.3: On-Off keying modulation

2.3.

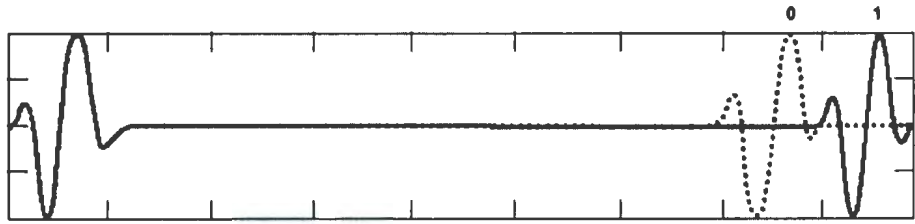


Figure 2.4: Pulse position modulation

PPM consists of encoding the data bits in the pulse stream by advancing or delaying individual pulses in time, relative to some reference, as shown in Figure 2.4. In this case, the signal can be written as:

$$s_{PPM} = \sum_{k=-\infty}^{\infty} p(t - kT - a_k \Delta), \quad (2.4)$$

where  $\Delta$  is the amount of pulse delay in time, relative to the reference position.

The PSD of this PPM signal is

$$PSD_{PPM} = \frac{\sigma_a^2}{T} |B(f)|^2 + \frac{\mu_a^2}{T^2} \sum_{k=-\infty}^{\infty} \left| B\left(\frac{k}{T}\right) \right|^2 \delta(f - \frac{k}{T}), \quad (2.5)$$

where  $B(f)$  is the fourier transform of  $b(t) = 0.5 [p(t - T) - p(t + \Delta)]$  [14].

The modulation here tends to smooth the spectrum but this still contains some spectral lines since the pulses are only delayed by a fractional part of the pulse width.

All those modulation techniques mentioned above would generate what is known as mono-phase ultra-wide band signals. There is another modulation technique which is more widely used and that is BPSK (Bi-Phase Shift Keying). The polarity of the impulses is switched to encode a “0” or a “1”. Only one bit per impulse can be encoded, because there are only two polarities available, as shown in Figure 2.5.

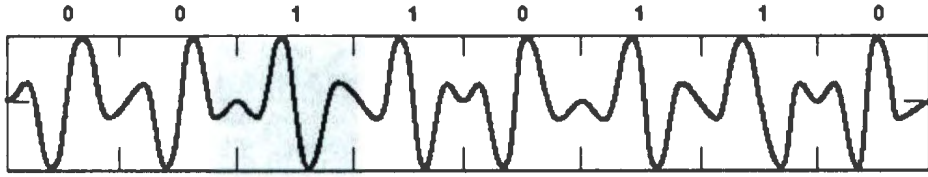


Figure 2.5: Bi-phase shift keying

For this modulation scheme, values of the variance  $\sigma_a^2$  and  $\mu_a^2$  are “1” and “0”, respectively. Then, the discrete portion of the PSD disappears.

$$PSD_{BPSK} = \frac{1}{T} |P(f)|^2. \quad (2.6)$$

These PSD calculations are all derived based on [14]. In the literature, there are various expressions of different signal modulations. This part provides a general information of modulation and PSD of different signals. Expression with minor modifications will be used for later discussions.

## 2.3 UWB pulse shaping literature review

Impulse radio signals in UWB systems utilize extremely broad bandwidth for transmission and coexist with other radio applications in the same frequency spectrum. It is desirable for UWB signals to spread the energy as wide as possible to minimize the power spectral density and hence reduce the potential for interference to other systems.

By far, the most popular pulse shapes discussed in IR-UWB communication literature are the Gaussian pulse and its derivatives, as they provide excellent radiation properties and are easy to describe and work with. However, those Gaussian pulses are not flexible enough to be used in practical systems, because without tuning some of their parameters, their PSD can not fit in the FCC spectral mask.

Therefore, researchers around the world began to design pulses that not only meet the FCC transmission spectral mask, but also utilize this spectrum effectively.

Currently, there are two main design trends in tuning spectral properties of radiated IR-UWB signals to fit in the FCC mask. One approach is shaping the Gaussian pulse with a baseband analog/digital filter to make the output waveform conform to the FCC mask. The other method is tuning parameters of different kinds of waveforms to make them comply with the FCC mask. Next, we briefly review the work that has been conducted for each method.

### 2.3.1 UWB pulse shaping filter design methods

In this section, we study several pulse shaping filter design methods proposed for ultra-wideband communications systems and evaluate the power spectral density of the pulses generated by those filters relative to the FCC UWB masks.

In order to be consistent to the original work, at the following sections, the denotation in the original paper will be used.

#### A. Design of X.Luo et al.

Their approach is to design pulse shapers for UWB using the “workhorse” of digital filter design methods, namely the Parks-McClellan algorithm [19].

As mentioned in section 2.2.2, the second term in both  $PSD_{PAM}$  and  $PSD_{PPM}$  expression, which is composed of discrete spectral lines, will vanish if the information symbols have zero mean. Then, the transmit PSD  $\propto |P(f)|^2$ . In order to utilize the FCC spectral mask efficiently,  $|P(f)|$  needs to closely approximate the shape of the spectral mask. In their design, they define a desired magnitude profile  $P_d(f)$ , which can be chosen to satisfy any desirable specifications. Normalizing the square root of the FCC spectral mask to an Fourier transform mask  $M(f)$ , in this case,  $P_d(f)$  is upper bounded by  $M(f)$ . The approach to design  $p(t)$  is based on this model

$$p(t) = \sum_{n=0}^{M-1} w[n]g(t - nT_0), \quad (2.7)$$

where  $g(t)$  is the Gaussian monocycle expressed as  $g(t) = A \frac{t}{\tau_g} e^{-2(\frac{t}{\tau_g})^2}$ ,  $\tau_g$  is the duration between its minimum and maximum values and  $A$  represents its peak amplitude.  $w[n]$  are the tap coefficients with spacing  $T_0$  to be designed. The Fourier transform of  $p(t)$  is

$$P(f) = \sum_{n=0}^{M-1} w[n] e^{-j2\pi f T_0 n} G(f). \quad (2.8)$$

Hence,  $|P(f)|$  can be controlled by adjusting the weights  $w[n]$ . The problem becomes finding  $M$  tap coefficients:  $\{w[n]\}$ , where  $0 \leq n \leq M$ , so that the Fourier transform  $W(e^{j2\pi f T_0})$  satisfies

$$\begin{aligned} |W(e^{j2\pi f T_0})| &\approx \frac{P_d(f)}{|G(f)|}, f \in \left[0, \frac{1}{2T_0}\right] \\ |W(e^{j2\pi f T_0})| &< \frac{M(f)}{|G(f)|}, f \in \left[\frac{1}{2T_0}, +\infty\right]. \end{aligned} \quad (2.9)$$

This problem now boils down to an FIR filter design problem: Design an  $M$ -tap FIR filter with coefficients  $\{w[n]\}$ , so that its discrete time Fourier transform (DTFT) magnitude  $|W(e^{j2\pi f T_0})|$  approximates the function  $D(\frac{F}{T_0})$ ,  $F \in [0, 0.5]$ , where  $D(f) = \frac{P_d(f)}{|G(f)|}$ ,  $f \in \left[0, \frac{1}{2T_0}\right]$ .

This problem is a classical Chebyshev approximation problem. The authors adopt

the Parks-McClellan algorithm, which leads to pulse shaper designs which can minimize the maximum approximation error over the frequency band of interest [20].

Figure 2.6 shows the designed Fourier transform of pulse shapers. The FIR filter has  $M = 2L + 1$  coefficients, the authors compare (i) the Gaussian monocycle  $g(t)$  with  $T_0 = 73$  ps,  $f_g = 6.85$  GHz, where  $f_g = 1/(\pi\tau_g)$ ; (ii) the pulse shaper  $p_{16}(t)$  they designed for single-band UWB with  $T_0 = 35.7$  ps; and (iii) the “prolate-spheroidal” pulse shaper  $p_{p-s}(t)$  designed in [21] with  $T_p=1.3$  ns. Complying with the FCC spectral mask, while transmitting at the maximum allowable power, their corresponding transmit powers are:  $P_g = 0.00387$  mW,  $P_{16}(t)=0.91$  mW, and  $P_{p-s}(t)=0.25$  mW, respectively. Accordingly, the authors claim their design utilizes the FCC spectral mask most efficiently.

Here, we should point out that the maximum transmitting power of their designed pulse is over that allowed by the FCC mask, which is 0.7 mW. This might be a calculation error. In general, from the graph provided by the authors, we can see their design outperforms the other two pulses. At the same time, they claim that currently available hardware is sufficient to implement their pulse shaper designs: a Gaussian monocycle generator, and a shift register that stores the tap coefficients.

## B. Design of X.Wu et al.

Paper [22] proposed a convex optimization based waveform design method. The authors resort the pulse design problem to a semi-definite program (SDP) over the

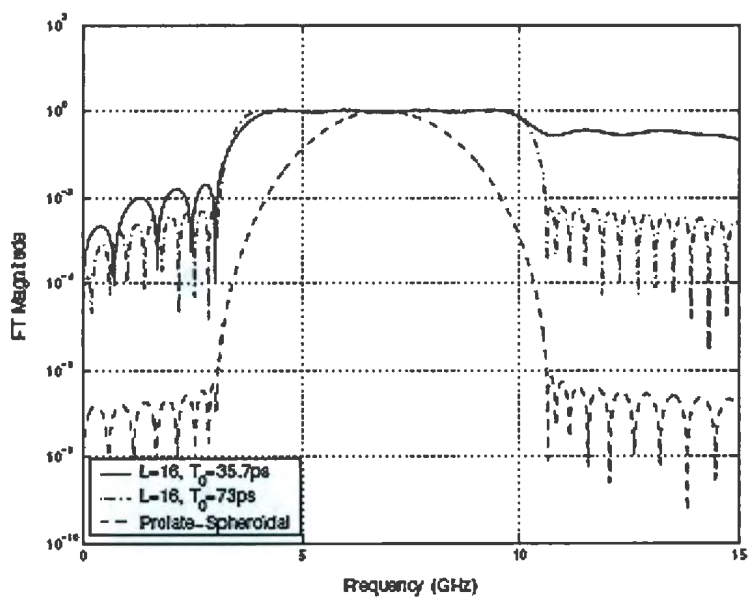


Figure 2.6: Fourier transform of pulse shapers for single-band UWB (Taken from [19])

pulse autocorrelation and design a global optimal waveform. The FCC spectral mask in this paper is  $S(f)$ . The efficiency of spectrum utilization can be measured by the normalized effective signal power (NESP)  $\varphi$

$$\varphi = \frac{\int_{-\infty}^{\infty} |P(f)|^2 df}{\int_{-\infty}^{\infty} S(f) df}. \quad (2.10)$$

The objective of their pulse design problem is to find  $p(t)$  that maximizes the NESP under the spectral mask constraint. This can be mathematically formulated as follows:

$$\max \varphi_{p(t)} \text{ subject to } |P(f)|^2 \leq S(f), \forall f. \quad (2.11)$$

Then the authors transform this problem to a semi-definite programming problem according to [23]

$$\min \operatorname{tr}(CX) \text{ subject to } \operatorname{tr}(A_k X) = b_k, X \geq 0, \quad (2.12)$$

where  $X$  is the (symmetric) matrix variable,  $C$  and  $A_k$  are symmetric matrices describing the objective and the  $k^{th}$  linear constraint, respectively. There are finite number of linear equality constraints.

In this way, the design problem can now be written as the following convex optimization problem:

$$\min - \varphi$$

$$S_p(f) \leq 0dB, \forall f$$

$$S_p(f) \leq -15dB, f > 10.6GHz$$

$$S_p(f) \leq -41dB, 0 \leq f < 3.1GHz \quad (2.13)$$

Their synthesized pulse  $p(t)$  can also be written as

$$p(t) = \sum_{i=0}^{L-1} g_i q(t - iT_q), \quad (2.14)$$

where  $T_q$  is the sampling interval,  $q(t)$  is Gaussian monocycle and the set  $\{g_i\}_{i=0}^{L-1}$  contains the  $L$  pulse coefficients to be designed. The power spectrum  $S_p(f) = |P(f)|^2$  of  $p(t)$  is

$$S_p(f) = |Q(f)|^2 \left| \sum_{i=0}^{L-1} g_i e^{-j2\pi f T_q} \right|^2 \approx \left| \sum_{i=0}^{L-1} g_i e^{-j2\pi f T_q} \right|^2, \quad (2.15)$$

where  $Q(f)$  is the FT of  $q(t)$ . By carefully choosing  $T_q$  and using the proposed method to find the set  $\{g_i\}_{i=0}^{L-1}$ , the optimum pulse can be designed. The authors solve this Spectral Utilization Problem (SUP) (with  $L = 33$ ) numerically by using the SeDuMi SDP package for MATLAB. The generated pulse spectrum is depicted in Figure 2.7. Compliant to the FCC mask, the synthesized pulse achieves a maximum

NESP of  $\varphi = 83.77\%$ . In contrast, the method in [21] uses a sampling rate of 64 GHz to yield a NESP value of approximately 39%.

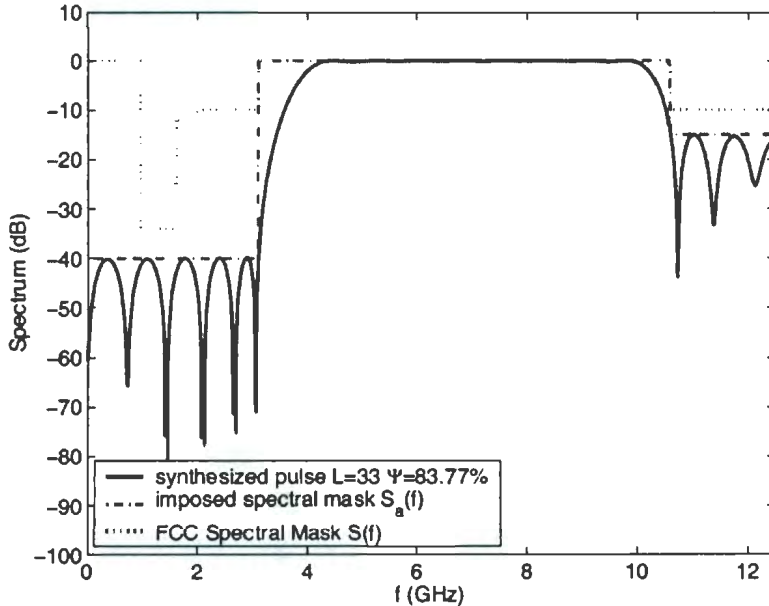


Figure 2.7: Results for a spectral utilization problem ( $L=33$ ): spectrum vs. frequency (GHz) (Taken from [22])

The advantages of this convex optimization based pulse design framework is that it can take multiple system-level constraints into consideration simultaneously, for example, when robustness to timing jitter is also consider in the waveform design.

### C. Design of Y.Wu et al.

The authors of [24] treat the pulse design problem as a problem that has three challenges: (i) it is minimum with quadratic constraints; (ii) a single-sided distortion function is used and (iii) delay positions are treated as tuning parameters. Their

approach is to construct a bootstrapping solution by approximating the single-sided min-max problem with a least squares formulation. A linear FIR filter can be used to shape the spectrum of  $p(t)$  in order to fit better in the mask. The signals that come out of the shaper can be written as

$$s(t) = \sum_{i=0}^M s_i p(t - \tau_i), \quad (2.16)$$

where  $s_i$  are filter coefficients,  $M$  is the number of number of filter coefficients.

The PSD expression of this signal is

$$S(j\Omega) = \sum_{i=0}^M s_i P(j\Omega) e^{-j\Omega\tau_i}. \quad (2.17)$$

The spectrum shaping problem can now be formulated as follows:

$$\max_{s,\tau} \langle s(t), s(t) \rangle, \text{ subject to } |S(j\Omega)|^2 \leq M(\Omega), \forall \Omega \in [-\Omega_m, \Omega_m], \quad (2.18)$$

where

$$\langle s(t), s(t) \rangle \equiv \int_{-\infty}^{\infty} s(t) s^*(t) dt, \quad (2.19)$$

$M(\Omega)$  is the regulated upper-bound on the squared magnitude response and  $\Omega_m$  is set to 11 GHz. The authors constructed a 2-norm approximation, in an effort to find a good bootstrapping solution. That results in a FIR filter design problem with

least-squares formulation:

$$\min \int_{-\Omega_m}^{\Omega_m} |S(j\Omega) - M(\Omega)|^2. \quad (2.20)$$

The authors use quadratic approximation by discretely spacing the delays. The approximation is pursued mainly because the joint optimizations over the weight and delay can be easily solved with its special structure. Figure 2.8 demonstrates the performance of the proposed procedure.

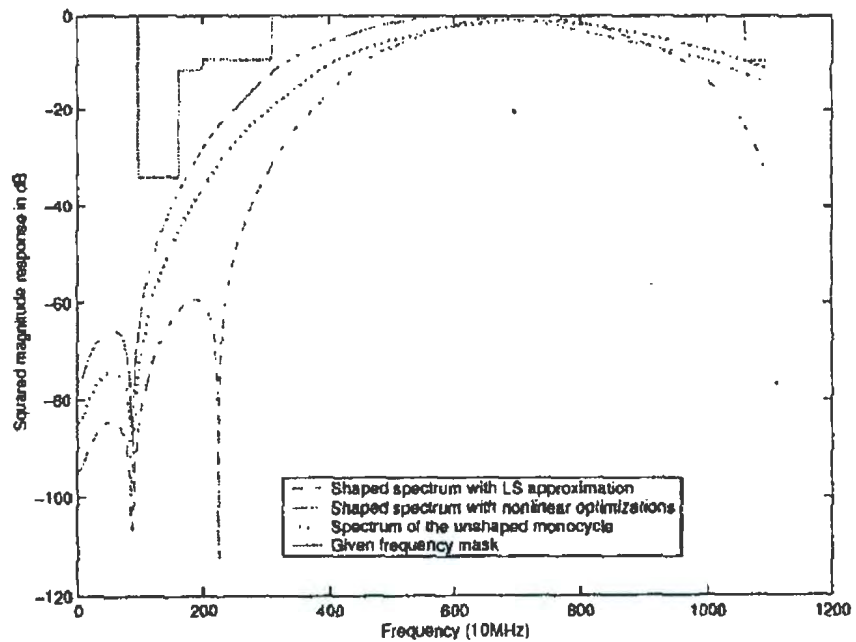


Figure 2.8: The spectrum shaping results compared with the FCC mask (Taken from [24])

The advantage of this design is that the design can be used to fit an arbitrary spectrum mask. With the least square solution serving as an initialization, nonlinear

optimization techniques can be employed to fine tune the solutions.

#### D. Design of D.Zeng et al.

In the transmission filter optimization of [25], the problem can be mathematically formulated as

$$\min_G \epsilon = \int_0^{f_s} W(f)(G(f) - D(f))^2 df. \quad (2.21)$$

In this equation,  $\epsilon$  is the objective function,  $W(f)$  is a non-negative weight function,  $G(f)$  is the frequency response of the actual transmission pulse, and  $D(f)$  is the ideal transmission mask. Notation  $f_s$  is the sampling frequency. The frequency response  $G(f)$  is expressed as:

$$\min_G G(f) = \sum_{n=0}^{Y_n} a(n) \cos(2\pi n f), \quad (2.22)$$

where  $a(0) = g(Y_n)$ ,  $a(n) = 2g(Y_n - n)$ , for  $1 \leq n \leq Y_n$  and  $Y_n = (N - 1)/2$ . The filter coefficients  $g(m)$ , ( $1 < m < N$ ) are symmetric about the middle point. This optimization can be solved by zero first derivative method. To minimize the mean square error  $\epsilon$ , the first derivative of  $\epsilon$  was set to zero, i.e.,

$$\frac{\partial \epsilon}{\partial a(k)} = 0. \quad (2.23)$$

Through a series of manipulations, the authors got the transmission FIR filter coefficient vector  $g^*$  as

$$g^* = [a(Y_n)/2, \dots, a(1)/2, a(0), a(1)/2, \dots, a(Y_n)/2]. \quad (2.24)$$

The order of the transmission filter is related to the minimum mean square error  $\epsilon_{min}$ . The lower the mean square error is, the higher order the transmission filter is, and the closer its frequency response is to the desired spectrum.

The frequency response of two filters with 41 and 81 taps are compared in Figure 2.9.

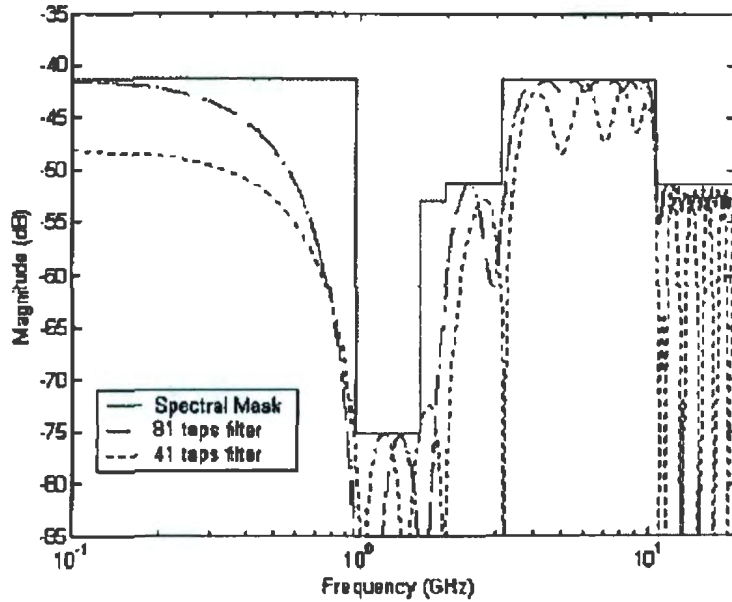


Figure 2.9: Transmission Filter Frequency Response (Taken from [25])

From the figure, we can see that the frequency response of the 81-tap filter is

closer to the ideal spectrum mask than the 41-tap filter. The paper concluded that if all other conditions are the same, the power of the resulting pulse from the 81-tap filter has 2.4 dB gain over that of the 41-tap filter.

## Discussion

In the previous four sections, we have studied four different pulse shaping filter design methods. These methods represent the main schemes in pulse shaping filter design in the literature. Although the researchers use different algorithms to do the calculation, they all concentrated on finding the best coefficients of those FIR filters.

To summarize, these different methods share the following characteristics:

- (i) All FIR filters are symmetric. The number of the coefficients are varying. However, when the realization complexity is considered, they are under some limit, for example, 100 taps.
- (ii) In theory, these filters can process any kind of pulse shapes, not only Gaussian pulse and its derivatives.
- (iii) In theory, coefficients of those FIR filters can be flexibly selected to meet arbitrary spectral specifications.

However, the algorithms for calculating the coefficients are all complicated. There is no easy way to find the optimum coefficients set. All the results are basically based on numerical approximations, not on closed-form expressions. Thus, there are possibilities that the maximum results those researchers have gotten may not be the

global maximum values but values trapped in local maximum points. Furthermore, when the implementation issues are considered, the pulse shaping filter actually can be integrated into the pulse generator, it is not necessarily an independent part because it has to process the pulse coming from the pulse generator. If we can find the optimal pulse shape, and if it is comparatively easy to be generated then the pulse shaping filter can be removed. Thus come the second pulse shaping design trend, to find the very good pulse shape.

### 2.3.2 Different pulse shapes chosen for UWB systems

In this section, several types of pulses previously proposed for ultra-wideband communications systems are introduced. The power spectral density of these pulses relative to the FCC UWB masks will also be illustrated here. The design goal is to obtain a pulse that matches the FCC PSD mask as closely as possible, which is the same as the previous pulse shape filters approach, although different schemes are used.

#### A. Pulses based on higher-order Gaussian derivatives

In [26], a general Gaussian pulse is given by:

$$x(t) = \frac{A}{\sqrt{2\pi}\sigma} \exp^{-\frac{t^2}{2\sigma^2}}, \quad (2.25)$$

and its  $n^{th}$  derivative can be determined by the recursive function given by

$$x^n(t) = -\frac{n-1}{\sigma^2}x^{n-2}(t) - \frac{t}{\sigma^2}x^{n-1}(t). \quad (2.26)$$

Usually people also use  $x'(t)$  for the first derivative, which is the same as  $x^1(t)$ .

The Fourier transform of the  $n^{th}$  order derivative pulse is

$$X_n(f) = A(j2\pi f)^n \exp\left\{-\frac{(2\pi f\sigma)^2}{2}\right\}. \quad (2.27)$$

In Figure 2.10, the PSD of the first derivative ( $n = 1$ ) of the Gaussian pulse is normalized to 0 dB and plotted for several values of the pulse width  $T_p$ . Note the  $T_p$  values is in unit  $ps$ . It is clear from the figure that the PSD of the first derivative pulse does not meet the FCC requirement no matter what value of the pulse width is used. In the time domain, the higher-order derivatives of the Gaussian pulse has higher center frequency, that make them possible candidates for UWB transmission. In the authors's algorithm, by gradually changing the parameters  $n$  and  $\sigma$ , some of the pulse's PSD can satisfy the FCC mask.

In Figure 2.11, the PSD for the first-order through tenth-order derivatives of the Gaussian pulse is normalized to 0 dB and shown for indoor systems.

It is clear that the fifth-order derivative is the best choice for indoor systems. The parameter  $\sigma$  is equal to 51 ps here. The authors also find that the seventh or higher order derivative Gaussian pulse can be used in outdoor systems.

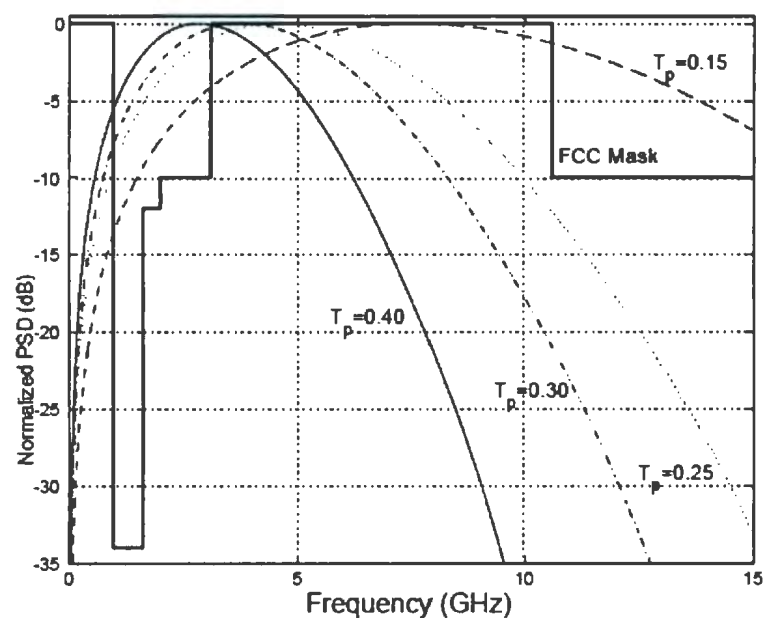


Figure 2.10: The power spectral density for the first-derivative Gaussian pulse for various values of the pulse width. The FCC spectral mask for indoor systems is shown for comparison (Taken from [26])

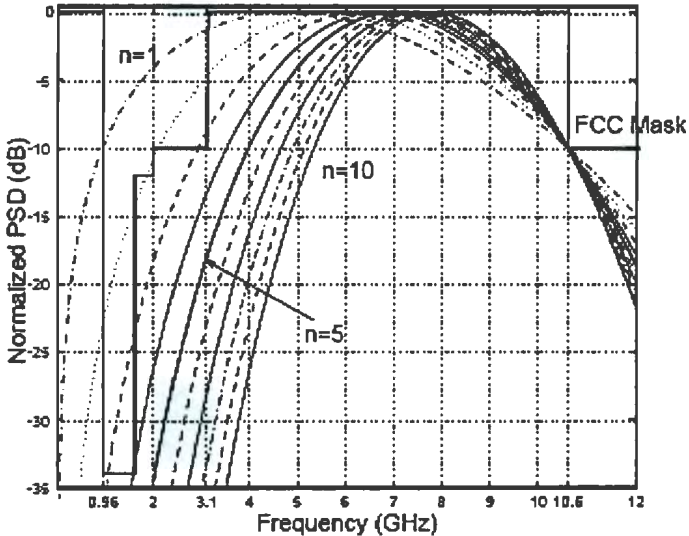


Figure 2.11: PSD of the higher-order derivatives of the Gaussian pulse for UWB indoor systems (Taken from [26])

### B. Pulses based on prolate spheroidal (PS) functions

In [21], a new algorithm to numerically generate pulses that based on PS functions was proposed. A pulse signal that is time-limited to  $T_m$  (impulse pulse period) seconds that meets the desired frequency mask satisfies the form:

$$\lambda \varphi(t) = \int_{-T_m/2}^{T_m/2} \varphi(\tau) h(t - \tau) d\tau, \quad (2.28)$$

where  $\lambda$  is the coefficient of the virtual filter,  $h(t)$  is the impulse response of the virtual filter. Their algorithm provides a numerical solution through the discretion of 2.28. The convolution can be turned into a matrix multiplication of a Toeplitz matrix  $H$  with the sample vector  $\varphi$

$$\lambda \underbrace{\begin{Bmatrix} \varphi[-\frac{N}{2}] \\ \vdots \\ \varphi[0] \\ \vdots \\ \varphi[\frac{N}{2}] \end{Bmatrix}}_{\varphi} = \underbrace{\begin{Bmatrix} h[0] & \dots & h[-N] \\ \vdots & \ddots & \vdots \\ h[\frac{N}{2}] & \dots & h[-\frac{N}{2}] \\ \vdots & \ddots & \vdots \\ h[N] & \dots & h[0] \end{Bmatrix}}_H \times \underbrace{\begin{Bmatrix} \varphi[-\frac{N}{2}] \\ \vdots \\ \varphi[0] \\ \vdots \\ \varphi[\frac{N}{2}] \end{Bmatrix}}_{\varphi}, \quad (2.29)$$

where  $\varphi$  is an eigenvector of  $H$ . Applying the theory of prolate spheroidal wave functions, only the eigenvectors corresponding to large eigenvalues should be taken as pulse designs and selected for implementation. The greater the eigenvalue, the better the power spectrum fits. Concerning to the FCC mask, example numerical pulses in the time domain are provided for a bandpass frequency mask between 3.1 and 10.6 GHz represented as

$$h(t) = 2f_U sinc(2f_U t) - 2f_L sinc(2f_L t), \quad (2.30)$$

where  $f_L=3.1$  GHz and  $f_U=10.6$  GHz. The authors generated two relatively large eigenvalues with  $N = 64$  and  $T_m = 1$  numerically by using MATLAB. The corresponding eigenvectors suggested for UWB pulse designs can be obtained. Figure 2.12 show that the majority of their power is concentrated in the 3.1-10.6 GHz frequency band and they comply with the FCC indoor/outdoor mask.

The selection of  $T_m$  has a significant effect on the frequency content of the pulse.

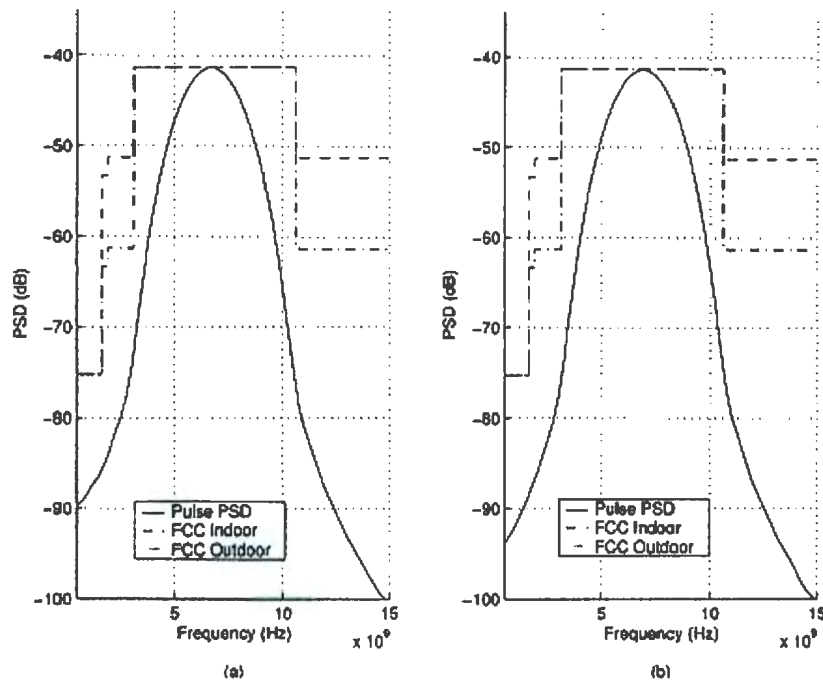


Figure 2.12: The power spectral density of pulse shapes obtained from the pulse design algorithm for the single bandpass frequency mask (a)  $\varphi_1(f)$  (b)  $\varphi_2(f)$  (Taken from [21])

By decreasing  $T_m$ , we can get a pulse whose -10 dB bandwidth can be exactly fitted into the specified bandwidth. However, the pulse has large sidelobes which will cause strong adjacent channel interference. Thus,  $T_m$  must be carefully selected.

The proposed pulses have several advantages: the short duration the pulses result in higher data rates; no frequency shifting is required; no big or multiple lobes existing which make a bandpass filter not necessary and two strong pulses are orthogonal when assuming that the two users who use them have perfect timing synchronizations.

### C. Modified hermite polynomial based pulses

In [27], a set of pulses based on modified Hermite Polynomials (HP) are proposed. These polynomials are defined by

$$h_{e_0}(t) = 1 \quad (2.31)$$

$$h_{e_n}(t) = (-1)^n e^{\frac{t^2}{2}} \frac{d^n}{dt^n} (e^{-\frac{t^2}{2}}), \quad (2.32)$$

where  $n = 1, 2, \dots$  are the orders. Originally, they are not orthogonal. However, they can be modified to become orthogonal as follows

$$h_n(t) = e^{-\frac{t^2}{4}} h_{e_n}(t) = (-1)^n e^{-\frac{t^2}{4}} \frac{d^n}{dt^n} (e^{-\frac{t^2}{2}}). \quad (2.33)$$

Although the authors claimed that the modified HP pulses are orthogonal and can

be assigned to different users in a multi-user system to enhance the data rate, those pulses can not be used in the current practical commercial systems for the following reasons. First, those pulses are not designed to fit in the FCC mask, they need frequency shifting to meet the FCC mask; Second, HP pulses with higher order have multiple large side lobes that have to be removed using bandpass filters. Otherwise, they will generate strong adjacent channel interference which will deteriorate the useful signal and reduce Signal to Noise Ratio (SNR) at the receiver side; Third, the pulses containing DC component are not efficient to radiate in real UWB systems.

#### D. Pulses based on B-splines

As discussed in [28], the B-splines functions have the following properties: (i) The B-splines are time-limited piecewise polynomials. (ii) They are rectangular pulses when their orders are one and they converge to band-limited functions at the limit that their order tends to be infinity. (iii) There are an analog circuit and a fast digital filter for the generation of B-splines. Those properties make B-splines functions good candidates of basis functions employed for designing pulses for UWB system. The B-spline of order  $m$  having the knot interval  $T > 0$  is defined by:

$$\varphi_m(t) := T \int_{-\infty}^{\infty} \left( \frac{\sin \pi f T}{\pi f T} \right)^m e^{i 2 \pi f (t - \frac{m}{2} T)} df, m = 1, 2, 3, \dots \quad (2.34)$$

Its Fourier transform is

$$\widehat{\varphi}_m(f) := T \left( \frac{\sin \pi f T}{\pi f T} \right)^m e^{-i 2 \pi (f \frac{m}{2}) T}, m = 1, 2, 3, \dots \quad (2.35)$$

UWB pulses are constructed as linear combinations of the B-splines of order  $m$ , i.e.

$$\psi_l(t) = \sum_{k=0}^L c_{l,k} \varphi_m(t - kT), l = 1, 2, \dots, L \quad (2.36)$$

Pulses design using the B-splines is to determine  $c_{l,k}$  under the basic conditions that the template pulses  $\varphi_m(t)$  must not have direct current component and they are orthonormal to each other.

Because there are several constraints, the authors use the Lagrange method to get the results. Figure 2.13 shows example pulses for  $m = 4$  and  $T = 61ps$ . There are four orthonormal pulses complying with the FCC spectral mask at the cost of  $L + 1 = 11$  shift versions of the B-splines.

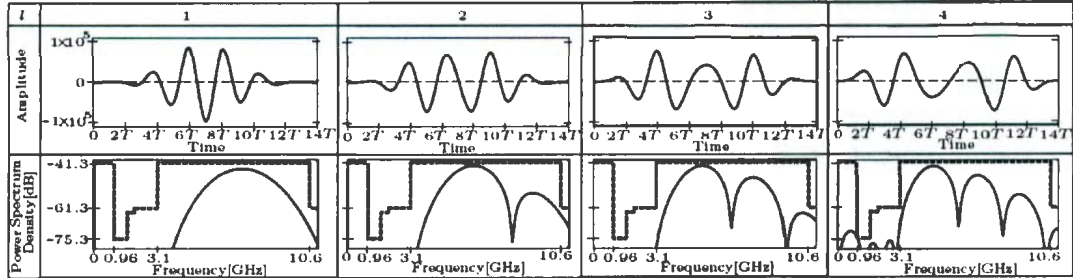


Figure 2.13: Pulses which comply with the FCC spectral mask (Taken from [28])

The authors shows the possibility of constructing UWB pulses in terms of B-splines. However, performance analysis of these pulses under jitter, white noise, and other interfering signals have not been done yet.

### E. Pulses based on gated sine and cosine functions

In [29], a little different construction of UWB pulses using gated *sine* and *cosine* functions was discussed. The discussion considered pulses having even symmetry and pulses having odd symmetry separately. For a given frequency mask, a center frequency  $f_c$  for the mask should be determined first. In this paper,  $f_c$  is set to be 6.85 GHz in order to fit in the FCC indoor and outdoor masks.

For even pulses, a candidate pulse can be obtained by windowing the *cosine* function  $f(t) = \cos(2\pi f_c t)$  according to

$$p_1^e(t) = f(t) \times w_1\left(\frac{t}{\tau}\right), \quad (2.37)$$

where  $p_1^e(t)$  is a time-limited pulse and  $w_1\left(\frac{t}{\tau}\right)$  is a window function given by

$$w_1(x) = \begin{cases} 1 & \text{if } |x| < \frac{1}{2} \\ \frac{1}{2} & |x| = \frac{1}{2} \\ 0 & |x| > \frac{1}{2} \end{cases} \quad (2.38)$$

The parameter  $\tau$  determines the time duration of the window, and thus the pulse duration of  $p_1^e(t)$ . When the rectangular window  $w_1(t/\tau)$  is used, the pulse obtained

from 2.37 as  $p_1^e(t)$  has frequency spectrum as

$$P_1^e(f) = \frac{1}{2} [\delta(f - f_c) + \delta(f + f_c)] * W_1(f) = \frac{\tau}{2} \{ \text{sinc}[\tau(f - f_c)] + \text{sinc}[\tau(f + f_c)] \} \quad (2.39)$$

where  $*$  denotes the convolution operation.

In a more general way, the window  $w_n(t/\tau)$  can be generated by multiple convolution of the rectangular windows  $w_1(t/\tau)$ , which is given by

$$w_n\left(\frac{t}{\tau}\right) = \underbrace{w_1\left(\frac{t}{\tau}\right) * w_1\left(\frac{t}{\tau}\right) * \cdots * w_1\left(\frac{t}{\tau}\right)}_n, \quad (2.40)$$

where  $n$  denotes the number of rectangular windows involved. Then, the designed pulse will be:

$$p_n^e(t) = w_n\left(\frac{t}{\tau}\right) \cos(2\pi f_c t), \quad (2.41)$$

where pulse spectrum  $P_n^e(f)$  must meet the desired frequency mask.

$$P_n^e(f) = \frac{\tau^n}{2} \{ \text{sinc}^n[\tau(f - f_c)] + \text{sinc}^n[\tau(f + f_c)] \}. \quad (2.42)$$

A set of pulses can be generated by adjusting suitable combinations of the values of  $\tau$  and  $n$  to approach the desired power spectrum.

For odd pulses, *sine* function is used, which is  $f(t) = \sin(2\pi f_c t)$ . Other procedures are quite similar as in the previous discussion.

Figures 2.14 and 2.15 show the power spectral densities of the pulse  $p_3^e(t)$  and the pulse  $p_4^e(t)$ , respectively.

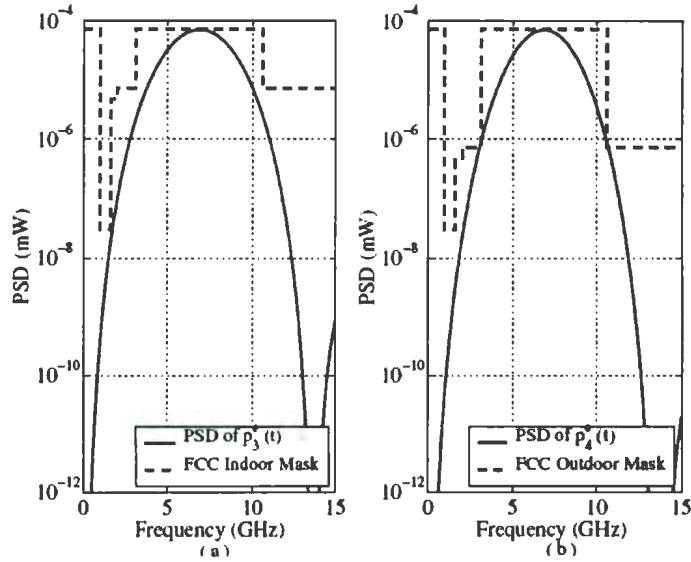


Figure 2.14: The power spectral densities of (a) the pulse  $p_3^e(t)$  and (b) the pulse  $p_4^e(t)$  and the FCC masks (Taken from [29])

There are a few advantages of this design method and the resulting pulses: First, two parameters  $n$  and  $\tau$  can be adjusted, which provide more flexibility than the Gaussian monocycles and the modified Hermite polynomial function based pulses at a given center frequency. Second, this approach provides an effective and flexible way for designing pulses to satisfy arbitrary emission masks. Third, the pulses generated are time-limited so as to reduce the interference and simplify implementation.

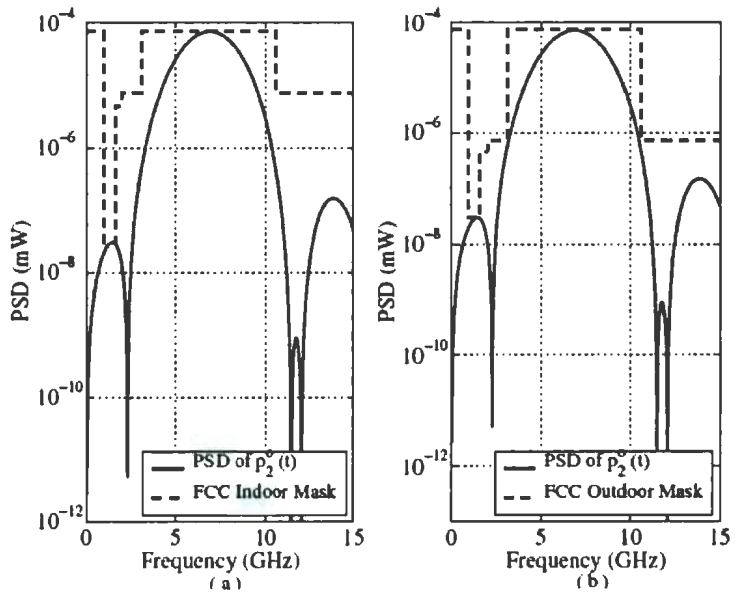


Figure 2.15: The power spectral density of the pulse  $p_2^o(t)$  and (a) the FCC indoor spectral emission mask (b) the FCC outdoor spectral emission mask (Taken from [29])

## F. Pulses based on linear combinations of Gaussian derivatives

In [30], the authors proposed a pulse shaping method based on the linear combination of a set of base waveforms obtained by the differentiation of the Gaussian pulse. The time domain representation for the Gaussian pulse is

$$p_G(t) = \pm \frac{1}{\sqrt{2\pi\sigma^2}} e^{-(\frac{t}{2\sigma^2})} = \pm \frac{\sqrt{2}}{\alpha} e^{-\frac{2\pi t^2}{\alpha^2}}, \quad (2.43)$$

where  $\alpha^2 = 4\pi\sigma^2$  is the shape factor and  $\sigma^2$  is the variance of the Gaussian pulse. Properties of Gaussian derivatives are also investigated in [26], where a method for selecting a single derivative of the Gaussian pulse which fits the FCC mask is proposed. In this paper, both differentiation and width variation of the pulse affect the PSD of the transmitted waveform, and can be used to shape the PSD of the transmitted signal. However, as none of the derivatives of the Gaussian pulse leads to an efficient approximation of the FCC mask, the authors proposed a method linearly combined a set of different derivatives of the Gaussian pulse. The authors give an example of a pulse combined by using the first 15 derivatives of the Gaussian pulse with  $\alpha = 0.714ns$ . The strategies for selecting linear combination coefficients are by iteration. First, choose a set of Gaussian derivatives; Then, the coefficients are randomly generated.

The combined pulse's PSD will be checked to see if meet the FCC mask. If yes, the result will be stored, and the procedure will be repeated again. If a better waveform

is obtained in the next round, the previous result will be overwritten. The whole procedure will stop until the distance between the mask and PSD of the generated signal falls within a pre-defined threshold. Figure 2.16 shows that combination of several Gaussian derivative pulses leads to a better approximation of the emission mask.

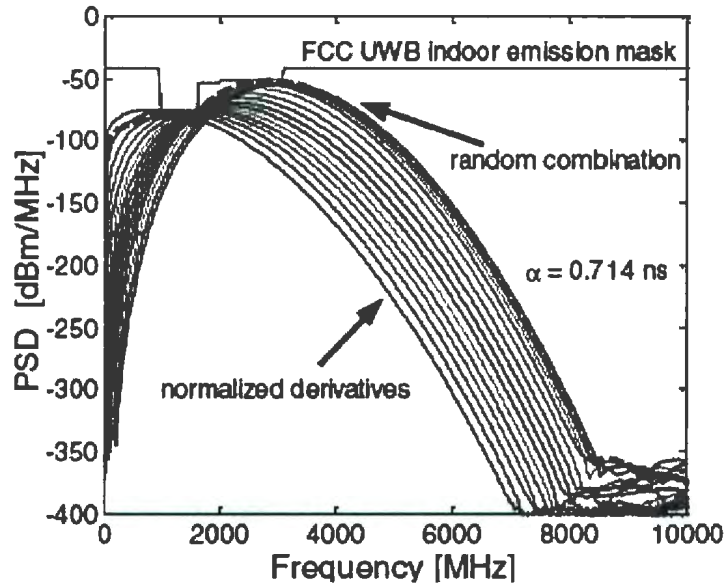


Figure 2.16: PSD of the base functions and of the combined waveform (Taken from [30])

Random selection of coefficients is one possibility in the choice of the linear combination. The other approach is to use the Least-Square-Error (LSE) standard procedure, in which the following error function must be minimized

$$e_s(t) = \int_{-\infty}^{+\infty} |e(t)|^2 dt = \int_{-\infty}^{+\infty} \left| f(t) - \sum_{k=0}^{N-1} a_k f_k(t) \right|^2 dt, \quad (2.44)$$

where  $f(t)$  is the target function. This criterion leads to a global minimized distance between the target and generated spectra. However, this could also lead to a generated PSD which violates the mask, as shown in Figure 2.17.

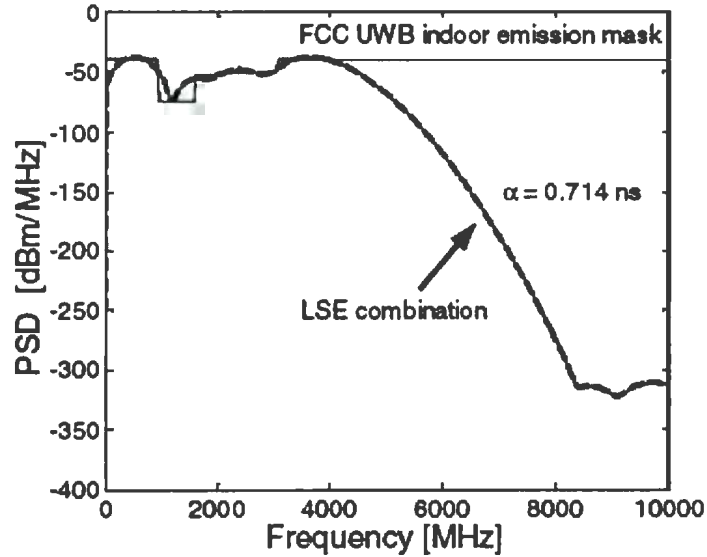


Figure 2.17: PSD of the linear combination of Gaussian waveforms versus FCC indoor emission mask (Taken from [30])

Overall, in this paper, results showed that better approximation of the mask can be achieved by adopting the linear combination in place of a single pulse. However, the two methods of determining the coefficients for a set of base waveforms obtained by differentiation of Gaussian pulse both have their own disadvantages: First, both methods consider using some of the base waveforms. In order to obtain good results, usually the number of base waveforms are more than 10. This makes the transmitter and receiver structure very complicated and costly. Because the transmitter has to

first generate the many base functions individually and then combine them, generation and synchronization problems must be considered. Similar problems also exist in the receiver, because the correlator has to generate the same template pulse for detector uses. Second, the LSE method generates a pulse that violates the FCC mask, which makes this method not feasible to be used in practical realization. Third, the method of random selection of coefficients has several uncertain factors that affect the final results, such as the randomness of data and the huge number of iterations that need to run in the coefficients calculation. Moreover, the result got by this method may not be reproduced.

## Discussion

In the previous sections, different pulse designs for UWB systems were introduced. These pulses and design approaches cover the main research effort in pulses and pulse design trends since 2002. Except modified HP-based pulses, the other four kinds of pulses were all designed to comply with the FCC spectrum mask. Compared to the pulse shape filter design, using different kind of pulses has several advantages:

- (i) The pulses are either existed or easily generated ones, which simplify the implementation. By tuning the parameters of the pulses, researchers can make pulses comply to the FCC mask while make good use of the allowed frequency spectrum.
- (ii) Some pulses can be designed as two or more orthogonal pulses, which make them good candidates in multi-user UWB systems for transmitting different users'

information while maintaining good SNR at the receiver side.

(iii) Some pulses, like Gaussian higher order derivatives and PS pulses, do not need frequency shift to fit in the FCC mask, thus a very simple transmitter is required.

However, those pulses also have disadvantages. The duration of pulses introduced here are all in nanosecond range. Implementing them entails D/A conversion operations at tens of giga hertz rate. For example, the D/A converter has to work at 64 GHz to realize the pulses in [21]. Some pulses such as modified HP pulses need frequency shift, which make the implementation more complicated. Some pulses such as PS pulses have strong sidelobes in the PSD. Bandpass filters have to be added to the transmitter. Constrained by the specific pulse shapes, the PSD of those pulses provide less flexibility in approaching the FCC mask in frequency domain while pulse shape filter did this generally better. We feel that if pulse shaping filter is integrated into the pulse generator given that the optimal pulse can been found, the transmitter structure can be less complex. The best way to do that is to find a pulse that not only best fits the FCC mask, but also can be easily generated by a simple generator.

## 2.4 Pulse generator review

In this section, we describe some of the widely used pulse generation techniques unique to UWB communication systems. Particularly, we will introduce an all-digital low-power CMOS pulse generator for UWB systems, because by modifying this system we can generate the pulses that we design.

The heart of any Impulse UWB system is some type of fast-rise time step or pulse generator. These pulse generators are used for both transmitter and receiver. Impulse UWB transmitters convert data bits directly to fast-rise time pulses. Matched filter correlation receivers must generate a template pulse that matches the incoming waveforms. The pulse generator is the basis for the UWB communication systems.

### 2.4.1 Avalanche pulse generator

In [31] an avalanche transistor is used to generate a monocyte pulse. The pulse generation is based on operating the transistor in avalanche mode, which requires a high voltage. The bias circuit of the pulse generator, as shown in Figure 2.18, provides a fixed bias voltage across the capacitor  $C7$ . This voltage is also provided across charging capacitor  $C8$ , which dumps a large charge through transistor  $TR3$  when the avalanche breakdown voltage is reached. This is achieved by the pulse position modulated message signal, which is fed to the base of the avalanche transistor. As the avalanche breakdown takes place, the emitter voltage of  $TR3$  rises dramatically

for a short time ( $\approx 10$  ns), and then falls to negative equivalent voltage due to the inductance connected between the emitter and earth. After the charging capacitor  $C_8$  has dumped its charge, it takes a few tens of microseconds to attain the level required for a new avalanche break down. This pulse generation method is feasible for applications with high voltage levels and moncycles with relatively large length, such as radar.

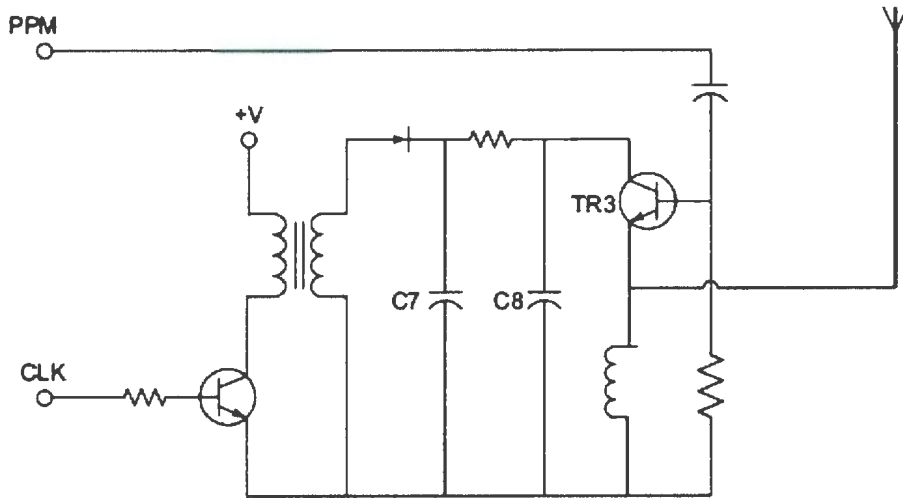


Figure 2.18: Avalanche pulse generator (Taken from [31])

#### 2.4.2 Step recovery diode pulse generator

Step Recovery Diode (SRD) or “snap off” diodes can be used to make very fast-rise time pulses. A recent pulse generation method [32] is based on SRD, Schottky diode and charging and discharging circuitry are shown in Figure 2.19. The SRD provides an impulse, which is high-pass filtered in a RC-circuit. The result is a Gaussian-like

pulse, which is fed to a pair of transmission lines. The generated pulse is divided in two and propagates in both branches after the capacitor C. The first half of the pulse propagates directly to the load resistor, and the other half of the pulse propagates to the short. The transmission lines are designed to have such a length that the propagation delay of the second half of the pulse (the one propagating to the short) is equal to the length of the pulse. The pulse will be inverted when the pulse reflects from the short circuit in the end of the transmission line. The resulting pulse seen across the load is the superposition of the two branches. The pulse width is controlled by the SRD.

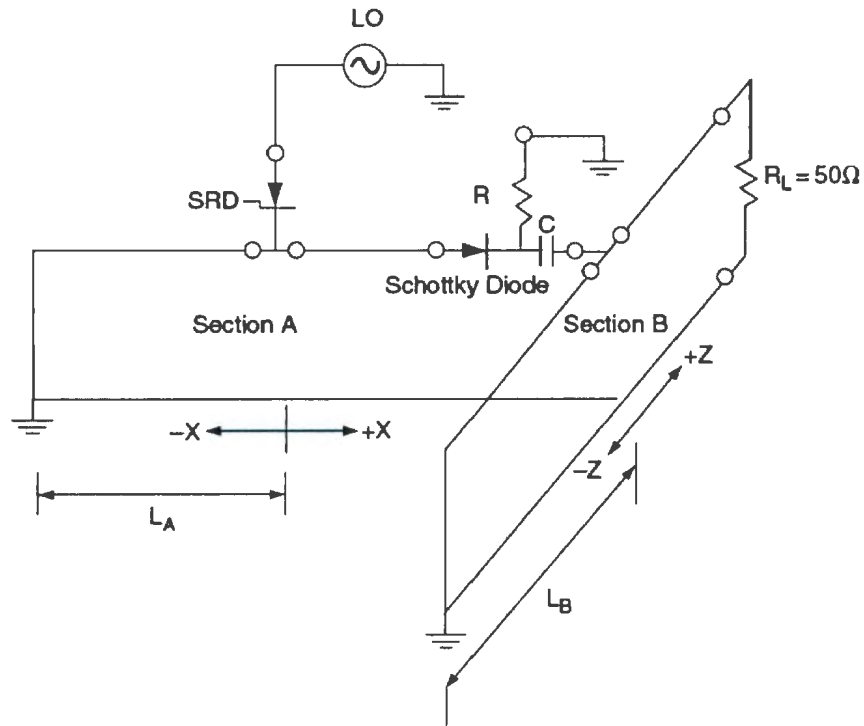


Figure 2.19: Step recovery diode pulse generator (Taken from [32])

### 2.4.3 CMOS monocycle generator

The previous two UWB pulse generators have limited utility in integrated configurations. It is highly desirable to design Impulse UWB transmitters that are compatible with CMOS and other IC technology. An integrated implementation of the 1<sup>st</sup> and 2<sup>nd</sup> derivatives of the Gaussian pulse generator was published in [33]. The proposed schematic is shown in Figure 2.20.  $Q1 - Q5$  form a squaring circuit, and the L and C perform a double differentiation on  $Q5$ 's collector.

The circuit squares the input current, and a Gaussian pulse can be approximated by squaring a  $\tanh(t)$  input current. As the circuit squares the input current, a Gaussian pulse can be approximated by a  $\text{sech}^2(t)$  function [33].

$$e^{-t^2} = 1 - t^2 + \frac{t^4}{2!} - \frac{t^6}{3!} + \dots \quad (2.45)$$

$$e^{-t^2} \propto \text{sech}^2(t) = 1 - t^2 + \frac{16t^4}{24} - \frac{152t^6}{720} + \dots \quad (2.46)$$

The input current is a  $\tanh(t)$  function that can be obtained by the exponential function in the bipolar junction transistor. The collector current of  $Q5$  is the square of the input current

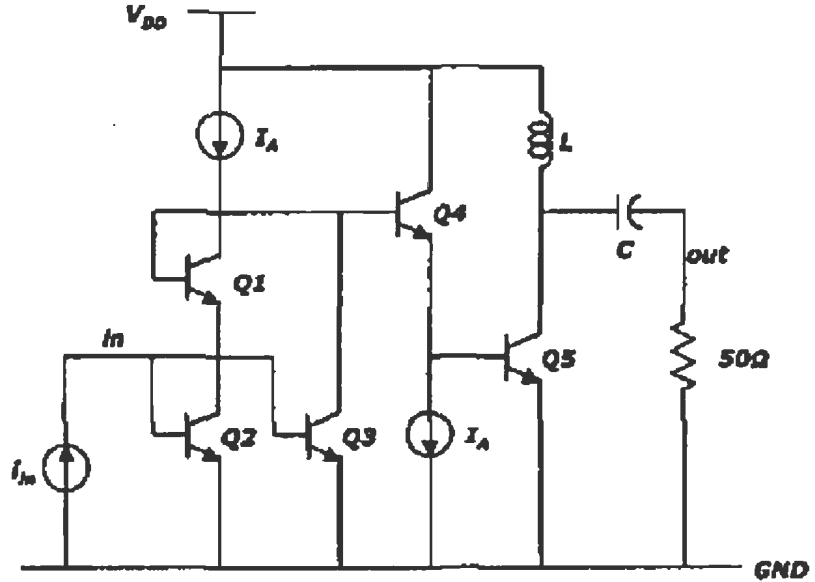


Figure 2.20: Gaussian 1<sup>st</sup> and 2<sup>nd</sup> derivatives pulse generator (Taken from [33])

$$\begin{aligned}
 I_{CQ_5} &= a - I_{in}^2 \\
 &= a - \tanh^2(t) \\
 &= a - (1 - \operatorname{sech}^2(t)) \\
 &= b - \tanh^2(t)
 \end{aligned} \tag{2.47}$$

The collector current of  $Q_5$  is a Gaussian impulse. Due to the inductor in  $Q_5$ 's collector circuit, the collector voltage is proportional to the derivative of the collector current. The resulting collector voltage is a Gaussian monocyte. Due to the coupling

capacitor, the voltage across the load is the derivative of the collector voltage. The output voltage is the second derivative of  $Q5$ 's collector current. The resulting output is a Gaussian  $2^{nd}$  derivative monocycle.

#### 2.4.4 Fifth-derivative Gaussian pulse generator

Although the  $1^{st}$  and the  $2^{nd}$  derivatives of the Gaussian pulse, which were popular in traditional impulse radio, were proposed to be designed on CMOS technology [32], they must be filtered out to satisfy the FCC regulation. In addition, the current source to generate the pulse dissipates constant power at all times which increases the power consumption. To solve this problem, the pulse, which originally complies with the FCC regulation, should be designed with a power efficient scheme. In [26], it was reported that the  $5^{th}$  derivative of the Gaussian pulse is a single pulse with the most effective spectrum under the FCC limitation floor, and this pulse can be transmitted without any filtering. A simple all-digital, low-power CMOS UWB pulse generator which generates the  $5^{th}$  derivative of the Gaussian pulse shape was proposed in [34]. The output pulse width is 2.4 ns, and the average power consumption is 1.159 mW with pulse repletion frequency (PRF) of 20 MHz.

The equation of the  $5^{th}$  derivative of the Gaussian pulse can be written as follows:

$$Gaussian_{5^{th}}(t) = A \left( -\frac{t^5}{\sqrt{2\pi}\sigma^{11}} + \frac{10t^3}{\sqrt{2\pi}\sigma^9} - \frac{15t}{\sqrt{2\pi}\sigma^7} \right) \exp\left(-\frac{t^2}{2\sigma^2}\right) \quad (2.48)$$

where  $A$  and  $\sigma$  are variables which are chosen to be fitted with the FCC power density limitation [26]. Of course, the 5<sup>th</sup> derivative of the Gaussian pulse can be generated by differentiating Gaussian pulse five times, but this procedure is very complicated and not suited for low-power transceiver design.

The proposed technique to generate the UWB pulse which satisfies the FCC limitation is shown in Figure 2.21 together with the signal shape.

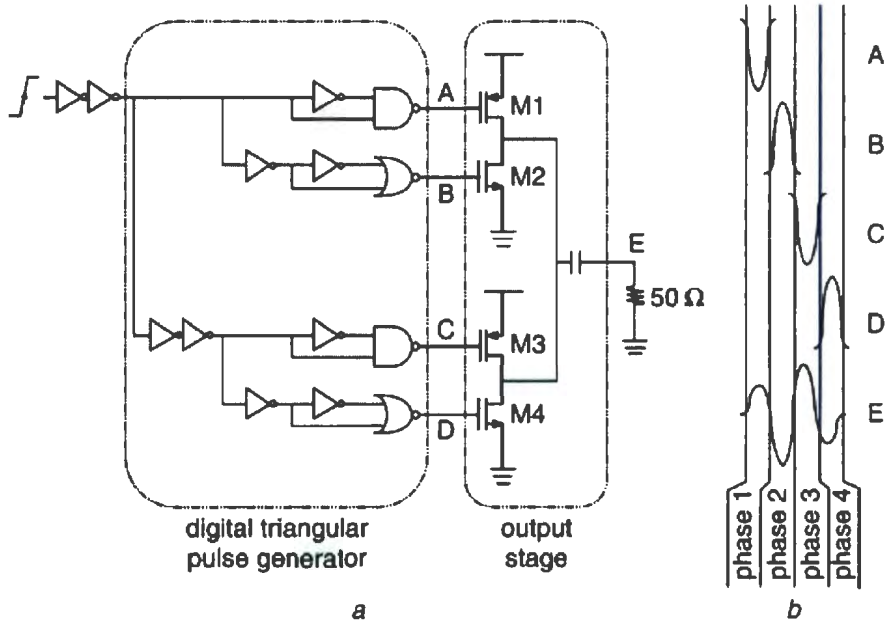


Figure 2.21: Fifth-derivative Gaussian pulse generator (a) Schematic (b) Signal shape on each node (Taken from [34])

It consists of two blocks: a digital triangular pulse generator and an output stage driving a  $50\Omega$  load. The input digital pulse and its inverted pulse which are followed by a NAND or NOR gate to generate the triangular pulse. Since the NAND gate is low only when both inputs are high, and the NOR gate is high only when

both inputs are low, the outputs of NAND and NOR gates are low and high at any given time, respectively. This procedure generates the triangular function as shown in Figure 2.21a. The voltage variations on nodes A and C take the shape of a triangular pulse from  $V_{DD}$  to the ground (negative-peak triangular pulse), and voltage variations on nodes B and D are built up to a triangular pulse from the ground to  $V_{DD}$  (positive-peak triangular pulse). The NOR gate generates a positive-peak triangular pulse, and the negative-peak triangular pulse is constructed by the NAND gate. Each triangular pulse is designed to have the same peak-to-peak amplitude. To organize four phase signals correctly, as shown in Figure 2.21b, the delay times of the four pulses are determined by changing the size and number of the inverters. In the output stage, the four triangular pulses generated in the previous block are combined successively. The output current magnitude is controlled by output transistor (M1-M4) size. Phases 1 and 3 are generated by PMOS and a negative-peak triangular pulse, and phases 2 and 4 are generated by NMOS and a positive-peak triangular pulse. Power consumption is minimized by turning on only one MOS transistor in the output stage during each phase.

In their paper, the proposed 5<sup>th</sup>-derivative of the Gaussian pulse generator has been simulated with AMI 0.5  $\mu m$  and TSMC 0.18  $pm$  CMOS technologies. Meanwhile, a prototype pulse generator is fabricated with the AMI 0.5  $\mu m$  CMOS process. The test results are well matched with simulation when poly sheet resistance effect is considered.

Unlike previously published CMOS pulse generators, the generated UWB pulse complies with the FCC regulations without a filter. For high power efficiency, the entire circuit is made using digital CMOS only and no current source is used. Since no static power is consumed, the proposed pulse generator can be used for low power UWB transceiver design.

The specialty of this design is that the researchers can generate the single  $5^{th}$ -derivative of the Gaussian pulse and make its PSD fit in the FCC mask. This gives us a new approach to generate the pulse combined by several Gaussian derivative pulses that we design in the next chapter.

## 2.5 Chapter summary

In this chapter, the two main pulse shape design trends for UWB systems are examined. The main designed methods in literature are listed and described. We did comparisons and evaluations on various aspects of those methods. We also discussed pulse generation techniques for impulse-based UWB communication systems. Three frequently referenced pulse generators are introduced. Most importantly, an all-digital low-power CMOS Gaussian  $5^{th}$ -derivative pulse generator with simple and power efficient architecture is described. The design of this pulse generator gives us a direction to generate our designed pulses by using a simple and power efficient all-digital CMOS pulse generator. We hope this can be a meaningful reference for

those researchers who are interested in UWB pulse shaping in the future.

# Chapter 3

## A new pulse shaping method

### 3.1 Introduction

In this chapter, a new pulse shaping method will be proposed. This method is based on linear combination of a set of different Gaussian derivatives. New pulses generated by this method will not only conform to the FCC indoor mask, but also effectively exploit the available power spectrum. The performance of our pulses and other frequently used UWB pulses are compared through theoretical calculations and simulations coded in MATLAB. In order to conduct fair comparisons, we established a UWB signal transmission simulation model. On this platform, a series of comparisons of different pulses by simulations will be done.

### 3.2 Gaussian derivatives and PSD

As introduced in [26] and [30], Gaussian pulse can be one candidate for the monocycle in UWB impulse radio systems. However, Gaussian pulse has direct current component, so it can not radiate effectively via antennas. The second derivative of the Gaussian pulse, proposed by Win and Scholtz in [16], has been widely adopted in the investigation of UWB applications. Following [26], the Gaussian pulse in our design has the form:

$$p(t) = \frac{A}{\sqrt{2\pi}\sigma} e^{-\frac{t^2}{2\sigma^2}}, \quad (3.1)$$

where  $A$  is the amplitude of the pulse and  $\sigma$  represents a bandwidth scaling factor. It is regarded that the antenna has the general effect of differentiating the time waveform presented to it [35]. By passing through the transmitter and receiver antennas, the baseband pulse is differentiated twice when it reaches the output of the receiver antenna. The received pulse is given by

$$p^2(t) = A\left(\frac{t^2}{\sqrt{2\pi}\sigma^5} - \frac{1}{\sqrt{2\pi}\sigma^3}\right)e^{-\frac{t^2}{2\sigma^2}}, \quad (3.2)$$

where the superscript n denotes the  $n^{th}$  derivative.

Figure 3.1 shows the amplitude normalized Gaussian 1<sup>st</sup> to 16<sup>th</sup> order derivative waveforms. These waveforms will be fundamental pulses in the design.

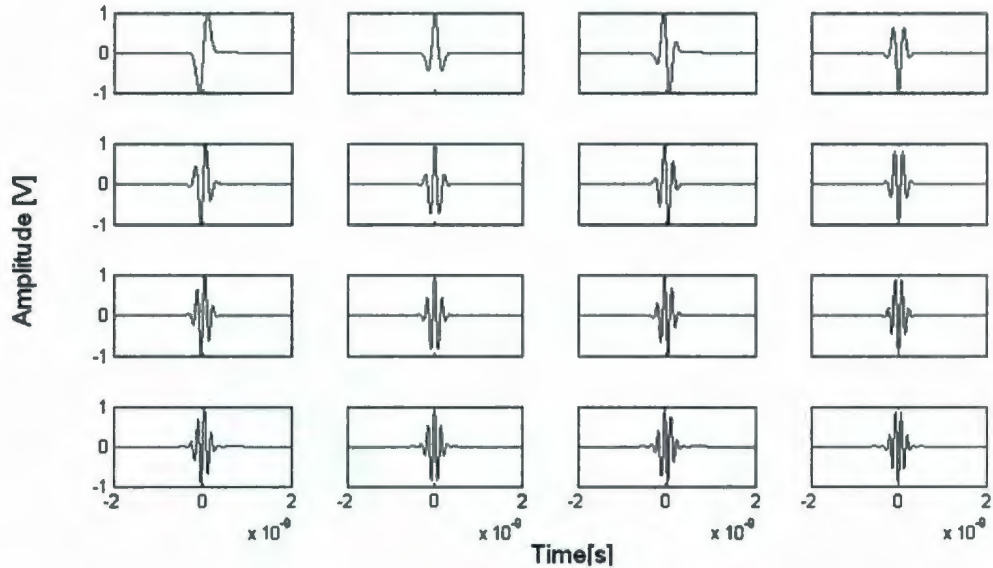


Figure 3.1: Amplitude normalized Gaussian 1<sup>st</sup> to 16<sup>th</sup> derivative pulses

The PSD of a waveform can be expressed as:

$$PSD(f) = |P(f)|^2 = \left| \int_{-\infty}^{+\infty} p(t) e^{-j2\pi f t} dt \right|^2. \quad (3.3)$$

In Figure 3.2 and 3.3, we have generated and depicted the Gaussian second derivative and its PSD respectively.

Since  $\sigma$  is a bandwidth scaling factor, the pulse PSD is closely related to it. The bandwidth of the pulse is approximately 1/(pulse duration), which is the same as the bandwidth of pulse PSD. Figure 3.4 and 3.5 demonstrate how  $\sigma$  affects the pulse duration in the time domain and their PSD in the frequency domain for a Gaussian second derivative pulse. From the two figures, we can see that the bigger  $\sigma$  value,

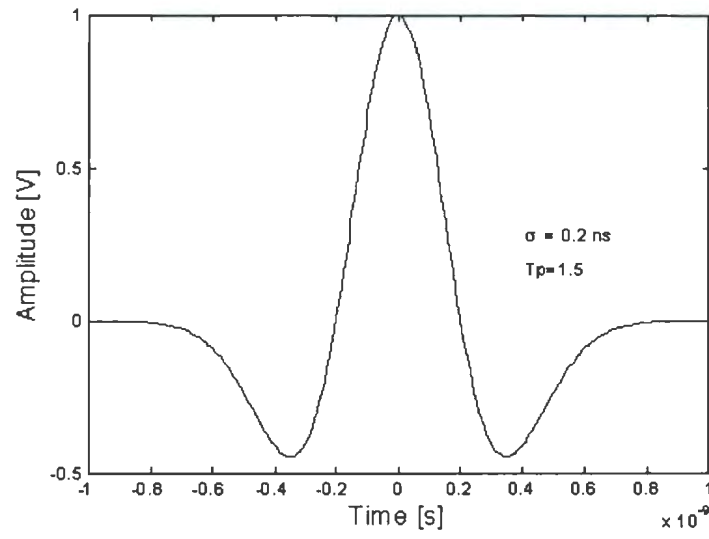


Figure 3.2: Amplitude normalized Gaussian second-derivative pulse

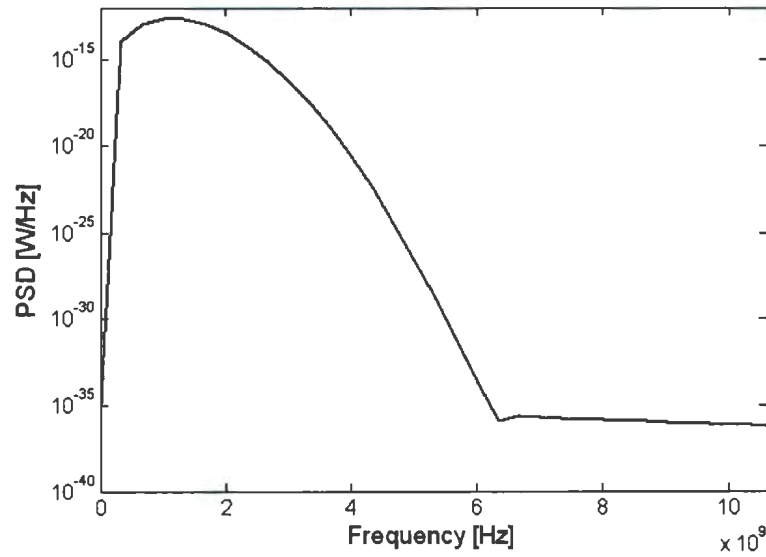


Figure 3.3: Power spectral density of amplitude normalized Gaussian second-derivative pulse

the wider the pulse and the narrower the PSD. If the pulse is too wide in the time domain, the PSD of the pulse will be very narrow in the frequency domain, which makes the pulse not a good choice for fitting in the FCC mask. On the other hand, if the pulse is very narrow in the time domain, a very high precision pulse generator and high speed D/A and A/D converters are required. This trade off must be properly considered in the pulse design.

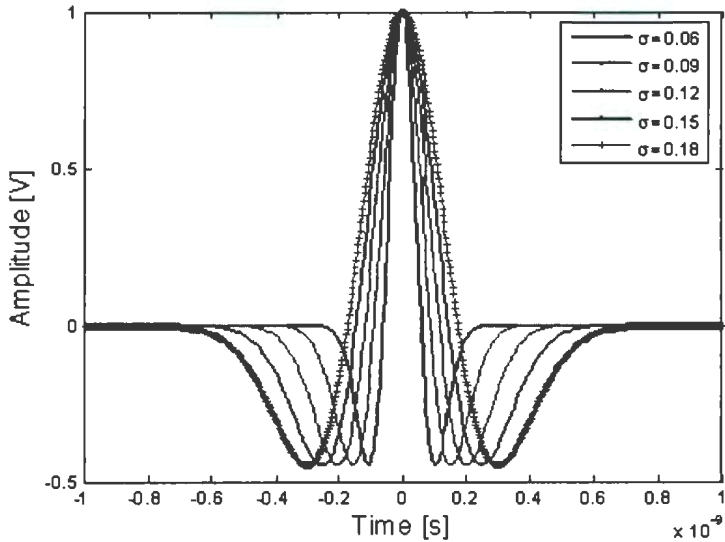


Figure 3.4: Gaussian second-derivatives with different  $\sigma$  values

Our design method is to combine several Gaussian derivatives to form a single pulse, whose PSD will effectively exploit the allowable bandwidth and power. Here, we show the PSD of different Gaussian derivatives. Figure 3.6 is similar to Fig. 7 in [30] with a different set of parameters.

This figure reveals that, as the order of the derivative increases, the energy is

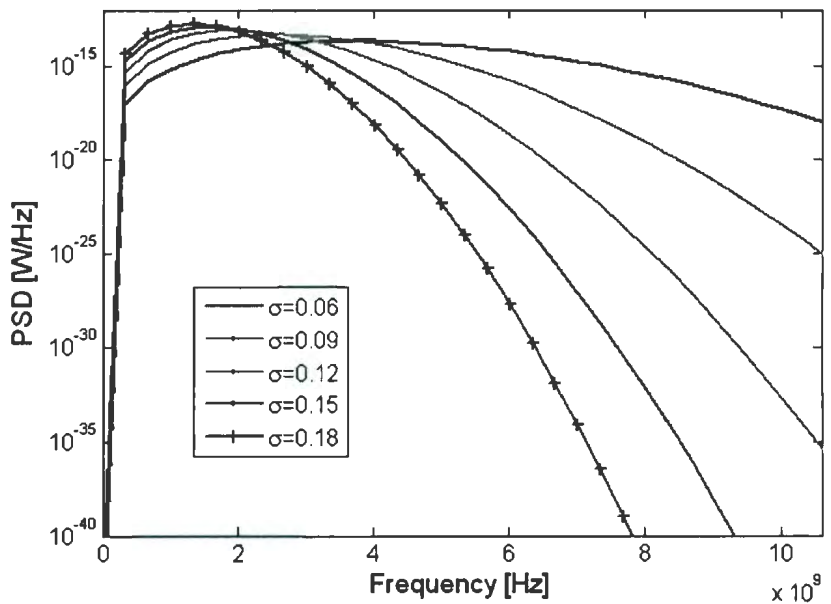


Figure 3.5: Power spectral density of Gaussian second-derivatives with different  $\sigma$  values

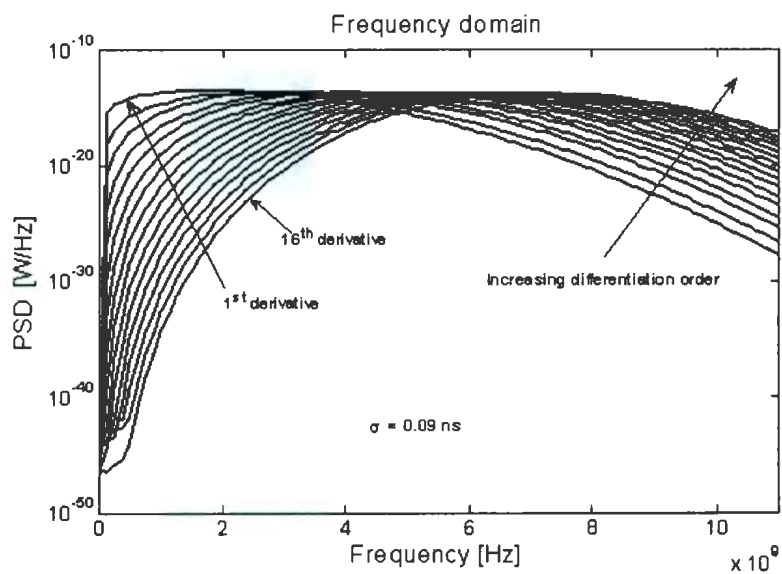


Figure 3.6: Power spectral density of Gaussian 1<sup>st</sup> to 16<sup>th</sup> derivatives

moving to higher frequencies. In [26], by choosing the order of the derivative and a suitable pulse width, the authors can find a pulse that satisfies the FCC mask. Unlike randomly combining different Gaussian derivative pulses, as proposed in [30], in our design, we propose a more determined way to form one pulse that can make best use of the FCC indoor mask.

### 3.3 New UWB pulse design

#### 3.3.1 Method description

From the previous section, we can clearly see that both differentiation and pulse width variation affect the PSD of the transmitted waveform, and can be used to shape the PSD of the transmitted signal. However, the flexibility in shaping the spectrum guaranteed by a single waveform is not sufficient to fulfill such requirements. Single Gaussian derivative pulse either does not fit in the FCC mask, or can be fit in the mask but does not exploit the allowed spectrum efficiently. Linearly combining certain numbers of Gaussian derivative pulses to form one single pulse is a simple, effective and flexible way of designing pulses to comply with the mask. At the same time, pulse shapes' effect on the mitigation of Multi-User Interference(MUI) is also considered in our design, which will be verified using the FCC indoor communication emission mask. The new pulse shape design method has the following steps:

1. Increase the amplitude of every single waveform of Gaussian first 16 derivatives monotonically from  $-M$  to  $M$  ( $M$  is a real number) to make the pulse's PSD conform to the mask, while transmitting as much energy as possible.
2. Use these 16 derivative waveforms as base waveforms.
3. Compare all the possible combinations of any 2 (3, or even more) of the 16 derivatives and search for the best five pulses in terms of energy. During each searching and comparing loop, keep changing those coefficients monotonically in a certain range and record a number of pulses which not only offer efficiency in meeting the FCC mask, but also effectively exploit the allowable bandwidth and power, these pulses will be kept in the candidates pool for further selection.
4. Choose from the pulse candidates pool according to different constraints and get the best result for certain applications.

Figure 3.7 shows the PSD of  $3^{rd}$  and  $14^{th}$  Gaussian derivative waveforms ( $\sigma = 0.09ns$ ) when we try to make them satisfy condition 1 in the first method.

### 3.3.2 More pulse shape design considerations

In the subsection, we explain how we choose the constraints in condition 4 of the first method. In a single link UWB communication system, for simplicity, we assume the channel has no multi-path effects and signals are affected by the Additive White

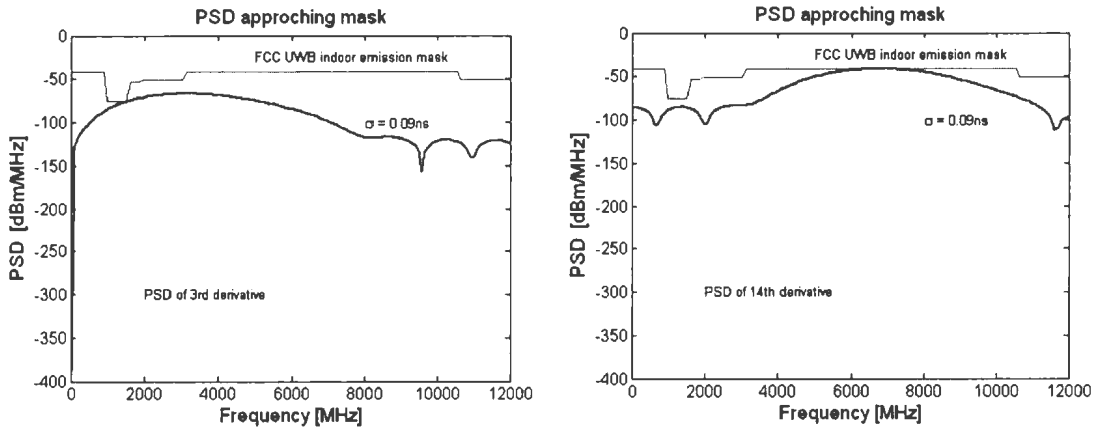


Figure 3.7: Power spectral density of Gaussian  $3^{rd}$  and  $14^{th}$  derivatives

Gaussian Noise (AWGN) only. Under the condition that the pulses' PSD conforms to the FCC mask, those pulses whose PSD is closer to the FCC mask can transmit more energy and thus can have better error performance. This is because the system Bit-Error-Rate (BER) will be based on the Signal-to-Noise Ratio (SNR). Obviously, under the same noise level, more energy for useful signal means better SNR. In this case, the design goal is the same as other pulse shape design methods we have reviewed before.

However, due to the potential large processing gain, a UWB system is capable of supporting multiple users at a high data rate in indoor dense multipath environment. Inter Pulse Interference (IPI) is a primary obstacle to achieving good performance in such systems. Hence, our design will take this into consideration and design the pulse which can reduce IPI.

### 3.3.3 System models for the pulse shape design

We use the classical system framework and notation of [16]. Our system model consists of  $N_u$  active users, transmitting UWB signals simultaneously through an AWGN channel. Each user employs Time Hopping spread spectrum technique. For a binary TH-BPSK UWB system, signal for the  $i^{th}$  bit of the  $k^{th}$  user can be represented as

$$s_{tr}^{(k)}(t, i) = \sum_{j=iN_s}^{(i+1)N_s-1} d_i^{(k)} p(t - jT_f - c_j^{(k)} T_c) \quad (3.4)$$

and a typical TH-PPM UWB signal takes the form

$$s_{tr}^{(k)}(t, i) = \sum_{j=iN_s}^{(i+1)N_s-1} p(t - jT_f - c_j^{(k)} T_c - \delta d_i^{(k)}), \quad (3.5)$$

where

- $p(t)$  represents the transmitted pulse at the output of transmitter antenna;
- $N_s$  is the number of pulses to represent one data bit;
- $T_f$  is the frame duration (pulse repetition time);
- $T_c$  is the chip duration;
- $\delta$  is the time offset of binary PPM, the limits  $T_p + \delta < T_c$  and  $N_h T_c \leq T_f$  are assumed, here  $T_p$  is the pulse width;

- $c_j^{(k)}$  is the distinct TH Pseudo-random Noise (PN) codes sequence of  $k^{th}$  signal,  $c_j^{(k)} \in [1, N_h]$ ,  $N_h$  is upper bound of the PN code  $c_j^{(k)}$ ;
- $d_i^{(k)}$  is the binary data sequence. In antipodal TH-BPSK UWB systems,  $d_i^{(k)} \in \{1, -1\}$ . In TH-PPM UWB systems,  $d_i^{(k)} \in \{0, 1\}$ .

A frame is divided into many time slots with the time duration  $T_c$ , and the pulse generated from the  $k^{th}$  user occupies only one of these slots, while the rest of the slots can be allocated to other users. In one time slot, there can be only one pulse. Same as in other spread spectrum systems, the distinct PN codes control the allocations of each users' signals.

### 3.3.4 Pulse shape design in multi-user system with AWGN channel

In this subsection, we adopted a TH-BPSK and a TH-PPM system that transmits signals through a AWGN channel, respectively. For simplicity, no multi-path effects are considered. We assume  $s_{rec}^{(k)}(t, i)$  is the received signal corresponding the transmitted signal  $s_{tr}^{(k)}(t, i)$ , and

$$s_{tr}^{(k)}(t) = \sum_{i=0}^n s_{tr}^{(k)}(t, i). \quad (3.6)$$

Without loss of generality, we assume that signal from user 1 ( $k = 1$ ) is studied. When  $N_u$  users are active, the signal at the receiver after passing through an AWGN

channel can be modeled as

$$r(t) = \sum_{k=1}^{N_u} A_k s_{rec}^{(k)}(t - \tau_k) + n(t), \quad (3.7)$$

where  $A_k$  is the propagation attenuation over path for the  $k^{th}$  user.  $\tau_k$  is the time asynchronism between  $k^{th}$  user and receiver.  $n(t)$  is the Additive White Gaussian Noise (AWGN).

The well-known optimal processor for a single bit of a binary modulated impulse radio signal through AWGN channel is correlator plus maximum likelihood detection. The template signal in the correlator is  $v(t)$ . It takes different forms given by the equation 3.4 and 3.5 in the case of TH-BPSK and TH-PPM UWB systems, correspondingly. The decision statistic at the output of the correlator is:

$$z = \sum_{j=0}^{N_s-1} \int_{jT_f}^{(j+1)T_f} r(t)v(t - jT_f - \tau_1)dt. \quad (3.8)$$

### **Analysis of the TH-BPSK system**

In this system, the receiver is assumed to be perfectly synchronized with the desired user (user 1). The template waveform  $v(t)$  adopts the pulse  $p'(t)$ , the derivative of  $p(t)$ , because the antenna has the general effect of differentiating the time waveform

presented to it [35]. Substituting  $v(t)$  by  $p'(t)$  in 3.8 yields

$$z = z_{S(BPSK)} + z_{I(BPSK)} + z_n, \quad (3.9)$$

where  $z_{S(BPSK)}$  and  $z_{I(BPSK)}$  represent the useful signal and the multi-user interference, respectively.  $z_n$  represents other interference (e.g., receiver noise and thermal noise) present at the correlator output. We model  $z_n$  as Gaussian noise with zero mean and variance  $\sigma_n^2$ . Define the correlation function of the pulse  $p'(t)$  as

$$R(\delta) = \int_{-\infty}^{+\infty} p'(t)p'(t - \delta)dt. \quad (3.10)$$

The energy of one bit of data at the output of the correlator,  $E_b$ , is given by

$$\begin{aligned} E_b &= (z_{S(BPSK)})^2 \\ &= (A_1 \sum_{j=0}^{N_s-1} \int_{jT_s+c_j^{(1)}T_c}^{jT_s+c_j^{(1)}T_c+T_p} p'_1(t - jT_s - c_j^{(1)}T_c)v(t - jT_s - c_j^{(1)}T_c)dt)^2 \\ &= (A_1 \sum_{j=0}^{N_s-1} \int_{jT_s+c_j^{(1)}T_c}^{jT_s+c_j^{(1)}T_c+T_p} p'_1(t - jT_s - c_j^{(1)}T_c)p'_1(t - jT_s - c_j^{(1)}T_c)dt)^2 \\ &= A_1^2(N_s \int_0^{T_p} p'_1(t)p'_1(t)dt)^2 \\ &= A_1^2 N_s^2 (\int_0^{T_p} p'_1(t)p'_1(t)dt)^2 \\ &= A_1^2 N_s^2 R(0)^2. \end{aligned} \quad (3.11)$$

Because  $v(t) = p'(t)$ , this equation can be simply written as

$$E_b = A^2 N_s^2 \left( \int_0^{T_p} p_{rec}(t) v(t) dt \right)^2, \quad (3.12)$$

where  $T_p$  is the pulse width,  $p_{rec}(t)$  represents the received pulse at the output of the receiver antenna  $p'(t)$ , which is also the input signal to the correlator [17].

We assume the PN code elements  $c_j^{(k)}$  for different  $k$  and  $j$  are independently and identically distributed (i.i.d.) random variables in their range. We also assume the relative transmission delay compared to the target user  $(\tau_k - \tau_1)$  is i.i.d. random variable, which can be seen as  $(\tau_k - \tau_1) \bmod T_f$  being uniformly distributed over the range  $[0, T_f]$ . Then, the energy of multi-user interference noise is given by:

$$\begin{aligned} \sigma_{z_{I(BPSK)}}^2 &= \sum_{k=2}^{N_u} \left[ \frac{N_s}{T_f} \int_0^{T_f} \left( A_k \int_0^{2T_p} p'_k(t - \tau_k) v_1(t) dt \right)^2 d\tau_k \right] \\ &= \frac{N_s}{T_f} \sum_{k=2}^{N_u} A_k^2 \int_0^{T_f} \left( \int_0^{2T_p} p'_k(t - \tau_k) p'_1(t) dt \right)^2 d\tau_k \\ &= \frac{N_s}{T_f} \sum_{k=2}^{N_u} A_k^2 \int_0^{T_f} \left( \int_0^{T_p} p'_k(t - \tau_k) p'_1(t) dt \right)^2 d\tau_k \\ &= \frac{N_s}{T_f} \sum_{k=2}^{N_u} A_k^2 \int_0^{T_f} (R_{1k}(\tau))^2 d\tau_k \\ &= \frac{N_s}{T_f} \sum_{k=2}^{N_u} A_k^2 \int_0^{T_f} (R(\tau))^2 d\tau. \end{aligned} \quad (3.13)$$

During the derivation of this equation, we assume that all users utilize the same

pulse shape in this multi-user system. Since all the delays and codes are supposed to be independent, pulse collision in one frame is assumed to be independent from collisions occurring in all other frames. Based on these assumptions, the above equation can be simply rewritten as

$$\sigma_{z_{I(BPSK)}}^2 = \frac{N_s}{T_f} \sum_{k=2}^{N_u} A_k^2 \int_0^{T_f} \int_0^{T_p} (p_{rec}(t - \tau)v(t)dt)^2 d\tau = \frac{N_s}{T_f} \sigma_N^2 \sum_{k=2}^{N_u} A_k^2. \quad (3.14)$$

The term  $\sigma_N^2$  is the energy term of the correlation of template pulse and received pulse, it can be given by

$$\sigma_N^2 = \int_0^{T_f} \int_0^{T_p} (p_{rec}(t - \tau)v(t)dt)^2 d\tau \quad (3.15)$$

In this system, a perfect power control is also assumed. That means  $A_i = A, \forall i$ .

By considering the Multiple User Interference (MUI) as noise, the system SNR expression can be obtained as:

$$\begin{aligned}
SNR_{out(BPSK)} &= \frac{E_b}{\sigma_n^2 + \sigma_{z_I(BPSK)}^2} \\
&= \frac{A^2 N_s^2 R(0)^2}{\sigma_n^2 + \frac{N_u}{T_f} \sum_{k=2}^{N_u} A_k^2 \sigma_N^2} \\
&= \frac{A^2 N_s^2 (\int_0^{T_p} p_{rec}(t)v(t)dt)^2}{\sigma_n^2 + \frac{N_u}{T_f} \sigma_N^2 \sum_{k=2}^{N_u} A_k^2} \\
&= \frac{A^2 N_s^2 (\int_0^{T_p} p_{rec}(t)v(t)dt)^2}{\sigma_n^2 + \frac{N_u}{T_f} \int_0^{T_f} \int_0^{T_p} (p_{rec}(t-\tau)v(t)dt)^2 d\tau \sum_{k=2}^{N_u} A_k^2} \\
&= \frac{1}{\frac{\sigma_n^2}{E_b} + \frac{1}{N_u T_f} \eta (N_u - 1)} \\
&= \frac{1}{SNR_{single}^{-1} + R_d \eta (N_u - 1)}, \tag{3.16}
\end{aligned}$$

where  $SNR_{single}$  denotes the signal to noise ratio in a single user environment. It is defined as a constant value since we normalized the signal energy and assume the same noise level in different scenarios.  $\eta$  is what we called normalized mean-squared partial pulse correlation given by

$$\eta = \frac{\int_0^{T_f} \int_0^{T_p} (p_{rec}(t-\tau)v(t)dt)^2 d\tau}{(\int_0^{T_p} p_{rec}(t)v(t)dt)^2}. \tag{3.17}$$

We can see that the value of  $\eta$  can directly affect SNR. The smaller the value of  $\eta$ , the higher the SNR and the better the error performance. In a TH-BPSK UWB system, since  $v(t) = p_{rec}(t)$ ,  $\eta$  clearly depends on the autocorrelation characteristic of the

pulse itself. Hence, when we design the pulse for a multi-user TH-BPSK system, the value of  $\eta$  should be taken into consideration. This can be the constraint in condition 4 of our design procedure.

### Analysis of TH-PPM system

Similar to the TH-BPSK system, the decision statistic  $z_{PPM}$  is expressed by:

$$z_{PPM} = z_{S(PPM)} + z_{I(PPM)} + z_n. \quad (3.18)$$

The template pulse waveform in TH-PPM system is  $v(t) = p'(t) - p'(t - \delta)$ . Then, the useful signal energy  $E_b$  can be expressed as

$$\begin{aligned} E_b &= (z_{S(PPM)})^2 \\ &= (A_1 \sum_{j=0}^{N_s-1} \int_{jT_s+c_j^{(1)}T_c}^{jT_s+c_j^{(1)}T_c+T_p} p'_1(t - jT_s - c_j^{(1)}T_c) v(t - jT_s - c_j^{(1)}T_c) dt)^2 \\ &= A_1^2 (N_s \int_0^{T_p} p'_1(t) (p'_1(t) - p'_1(t - \delta)) dt)^2 \\ &= A_1^2 N_s^2 (\int_0^{T_p} p'_1(t) p'_1(t) dt - \int_0^{T_p} p'_1(t) p'_1(t - \delta) dt)^2 \\ &= A_1^2 N_s^2 (R(0) - R(\delta))^2. \end{aligned} \quad (3.19)$$

This equation can also be simply written as [16]:

$$E_b = A^2 N_s^2 (\int_0^{T_p} p_{rec}(t) v(t) dt)^2. \quad (3.20)$$

where  $p_{rec}(t)$  represents the received pulse at the output of the receiver antenna, which is also the input signal to the correlator.  $v(t) = p'(t) - p'(t - \delta)$  is the template pulse waveform. This equation takes the same form as equation 3.12. However, the  $v(t)$  here is different from that in equation 3.12. The energy of multi-user interference noise is given by

$$\begin{aligned}
\sigma_{z_{I(PPM)}}^2 &= \sum_{k=2}^{N_u} \left[ \frac{N_s}{T_f} \int_0^{T_f} \left( A_k \int_0^{2T_p} p'_k(t - \tau_k) v_1(t) \right)^2 d\tau_k \right] \\
&= \frac{N_s}{T_f} \sum_{k=2}^{N_u} A_k^2 \left( \int_0^{T_f} \left( \int_0^{2T_p} p'_k(t - \tau) v_1(t) dt \right)^2 d\tau \right)^2 \\
&= \frac{N_s}{T_f} \sum_{k=2}^{N_u} A_k^2 \int_0^{T_f} \left( \int_0^{2T_p} p'_k(t - \tau) (p'_1(t) - p'_1(t - \delta)) dt \right)^2 d\tau \\
&= \frac{N_s}{T_f} \sum_{k=2}^{N_u} A_k^2 \int_0^{T_f} \left( \int_0^{T_p} p'(t - \tau) p'(t) dt - \int_{\delta}^{T_p + \delta} p'(t - \tau) p'(t - \delta) dt \right)^2 d\tau \\
&= \frac{N_s}{T_f} \sum_{k=2}^{N_u} A_k^2 \int_0^{T_f} (R_{1k}(\tau) - R_{1k}(\tau - \delta))^2 d\tau \\
&= \frac{N_s}{T_f} \sum_{k=2}^{N_u} A_k^2 \int_0^{T_f} (R(\tau) - R(\tau - \delta))^2 d\tau. \tag{3.21}
\end{aligned}$$

As already discussed in the last section, the above equation also can be written as

$$\begin{aligned}
\sigma_{z_{I(PPM)}}^2 &= \frac{N_s}{T_f} \sum_{k=2}^{N_u} A_k^2 \int_0^{T_f} \int_0^{T_p} (p_{rec}(t - \tau) v(t) dt)^2 d\tau \\
&= \frac{N_s}{T_f} \sigma_N^2 \sum_{k=2}^{N_u} A_k^2, \tag{3.22}
\end{aligned}$$

where  $\sigma_N^2$  stays the same as in the previous section.

Thus, the SNR expression of this system is the same as that in the TH-BPSK system.

$$\begin{aligned}
SNR_{out(PPM)} &= \frac{E_b}{\sigma_n^2 + \sigma_{z_{I(PPM)}}^2} \\
&= \frac{A^2 N_s^2 (\int_0^{T_p} p_{rec}(t) v(t) dt)^2}{\sigma_n^2 + \frac{N_s}{T_f} \sigma_N^2 \sum_{k=2}^{N_u} A_k^2} \\
&= \frac{A^2 N_s^2 (\int_0^{T_p} p_{rec}(t) v(t) dt)^2}{\sigma_n^2 + \frac{N_s}{T_f} \int_0^{T_f} \int_0^{T_p} (p_{rec}(t - \tau) v(t) dt)^2 d\tau \sum_{k=2}^{N_u} A_k^2} \\
&= \frac{1}{\frac{\sigma_n^2}{E_b} + \frac{1}{N_s T_f} \eta(N_u - 1)} \\
&= \frac{1}{SNR_{single}^{-1} + R_d \eta(N_u - 1)}. \tag{3.23}
\end{aligned}$$

The parameter  $\eta$  has the same expression as in 3.17, while  $v(t)$  changed from  $p'(t)$  to  $p'(t) - p'(t - \delta)$ . We see here  $\eta$  not only depends on the autocorrelation characteristic of the pulse, but also the index  $\delta$ . The role of  $\delta$  in the reduction of BER has been studied in detail in [36]. We make the choice of pulse and corresponding  $\delta$  as condition 4 in our design procedure for TH-PPM UWB system, thus  $\delta$  does not affect the SNR calculation.

As we can see that all the SNR expressions are made to be the same, it is convenient for us to make programs to numerically generate pulses that have the best parameters.

### 3.4 Chapter summary

In this section, we introduce our new UWB pulse shape design method. As a part of the design method, we investigate the pulse waveform effects on the TH-BPSK and TH-PPM UWB systems' performance on multi-user interference in a multi-path free AWGN channel. We attribute the waveform effect on these interferences to a single parameter that only relates to the waveform. We also make the SNR expression of the TH-BPSK and TH-PPM UWB systems unified in form, which aided in making programs to numerically generate pulses designed by our methods.

# Chapter 4

## Simulation and comparison

### 4.1 Introduction

In this chapter, we first show the results of our designs described in Chapter 3 and compare the pulses with other approaches in terms of the frequency spectrum utilization and energy contained. Second, we examine the BER of single link and multi-user systems that have an AWGN channel using different pulses. Third, system level characteristics such as maximum user number and transmission distance of those systems using different pulses are also examined. Last, we introduce the IEEE standard UWB channel into the simulation systems and compare the BER of single link and multi-user systems using different pulses under the new channel environment.

## 4.2 Newly designed pulses and other pulses for comparison

In this section, we will investigate the possibility of obtaining the waveform by combining different derivative waveforms of Gaussian pulse to approximate the FCC indoor mask at all frequencies. Note that the combination of a number of derivatives and the possibility of choosing different  $\sigma$  values for derivatives provides a high degree of flexibility in the generation of the pulse waveforms. In our case, we set  $\sigma$  to be the same for different derivatives, thus lowering the complexity of design. In the following discussion, our program implements the procedure described in Chapter 3.

### 4.2.1 Pulses generated by random combining method

The following set of parameters are used for calculations in this subsection: the chip time  $T_c=0.9$  ns and the pulse duration  $T_p=0.7$  ns.

We first did some tests by randomly choosing the coefficients for any combination of 2 and 3 different derivatives among 1<sup>st</sup> to 16<sup>th</sup> Gaussian derivatives, to see how good the random coefficients selection approach is. The reasons we choose to combine 2 or 3 Gaussian derivative pulses are that, on one hand, our exhaustive search procedure need a lot of calculation, so we start with combining small number of Gaussian derivative pulses that we can see the results quickly. On the other hand, considering the realization complexity of a real pulse generator, combining 2 or 3 Gaussian

derivatives will not be too complex.

In this approach, the coefficients are randomly picked from -6 to 6, and a large number of iterations will be conducted. The reason that we set the range to be -6 to 6 is that we want to make the coefficient range big enough that when the PSD of the combined pulse is approaching to the mask, the coefficient of the single Gaussian derivative pulse will not be limited by the range. In other words, the coefficient range should be larger than the possible upper limit of the single Gaussian derivative pulse. In our program, we record the best 5 results for one iteration, the better results get from later iterations will be updated for the older ones. Figure 4.1 and 4.2 show the best 5 pulses we get in 500 iterations of our program which combined by randomly picked 2 and 3 derivatives respectively with their coefficients range from -6 to 6.

Because the coefficients are randomly picked from -6 to 6 in this approach, such randomness determines that the results may not be very good. Meanwhile, the more rounds our program runs, the better results we can get. We also find that the range of -6 to 6 can be expanded to a larger scale to make the PSD of the randomly picked pulses more closely approaching the mask.

Table 4.1: Pulse energy of the 5 best results of random combination by two derivatives, coefficient range [-6,+6]

Pulse	Pulse Energy				
1-5	$1.1256 \cdot 10^{-4}$	$1.1165 \cdot 10^{-4}$	$1.1107 \cdot 10^{-4}$	$1.1098 \cdot 10^{-4}$	$1.1003 \cdot 10^{-4}$

From the previous calculation by randomly picking both derivatives and coefficients, we found that pulses combined by 3 different Gaussian derivatives have more

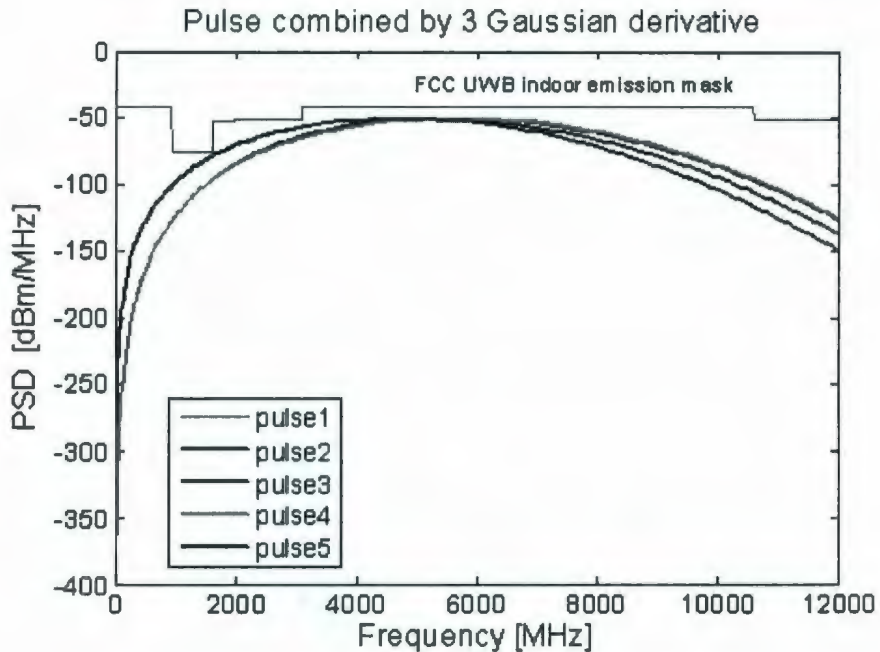


Figure 4.1: PSD of the 5 best results of random combination by two derivatives, coefficient range [-6,+6]

Table 4.2: Pulse energy of the 5 best results of random combination by three derivatives, coefficient range [-6,+6]

Pulse	Pulse Energy				
1-5	$1.7618 \cdot 10^{-4}$	$ 1.7586 \cdot 10^{-4} $	$1.7576 \cdot 10^{-4}$	$ 1.7567 \cdot 10^{-4} $	$1.7558 \cdot 10^{-4}$

energy than the pulses combined by 2 different Gaussian derivatives. That is understandable, because more base waveforms can improve efficiency of spectrum utilization thanks to their different PSD occupations in the frequency domain. During the random selection, we also find that the pulses combined by the 7<sup>th</sup>, 9<sup>th</sup> and 11<sup>th</sup> Gaussian derivatives have comparatively the best performance. We set the 7<sup>th</sup>, 9<sup>th</sup> and 11<sup>th</sup> Gaussian derivatives as base waveforms, change their coefficients at regular step from -6 to 6. From the results we find the -6 to 6 range has limited the combined

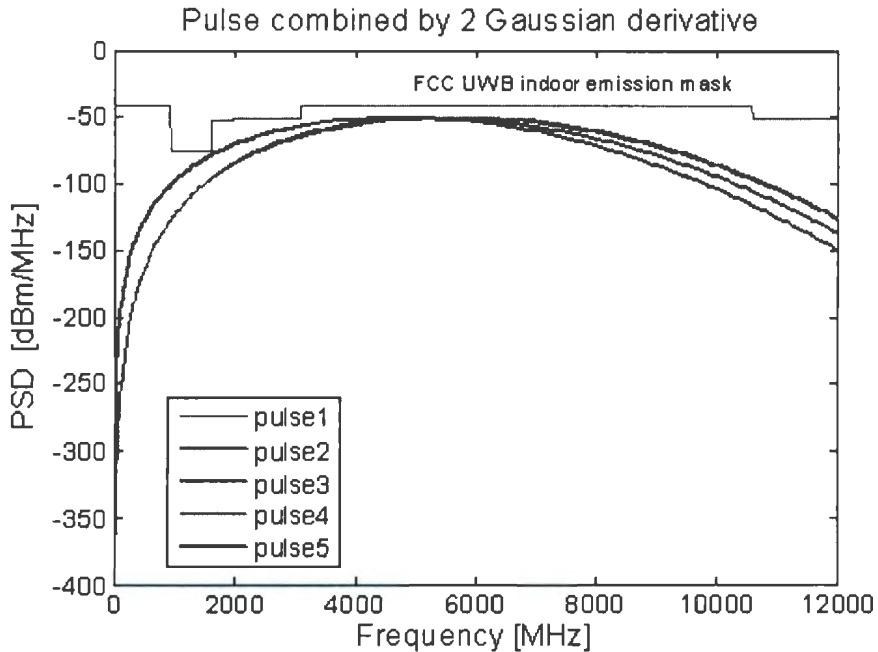


Figure 4.2: PSD of the 5 best results of random combination by three derivatives, coefficient range  $[-6, +6]$

Table 4.3: Pulse energy of combination of  $7^{th}$ ,  $9^{th}$  and  $11^{th}$  Gaussian derivatives, coefficient range  $[-6, +6]$

Pulse	Pulse Energy				
1-5	$1.4898 \cdot 10^{-4}$	$1.4877 \cdot 10^{-4}$	$1.4787 \cdot 10^{-4}$	$1.4699 \cdot 10^{-4}$	$1.4691 \cdot 10^{-4}$

pulse's PSD to approach the mask more closely, then in the second round we change the range to -10 to 10, to get 5 best results as shown in Figure 4.3, Figure 4.4, Table 4.3 and Table 4.4. We can clearly see that enlarging the coefficients can provides more freedom of making pulse approximate the mask more closely and contain more energy. However, the random selection of coefficients does has its limitation that the “best” results obtained from this method are not likely to be the real global best results, so some type of determined method will be needed.

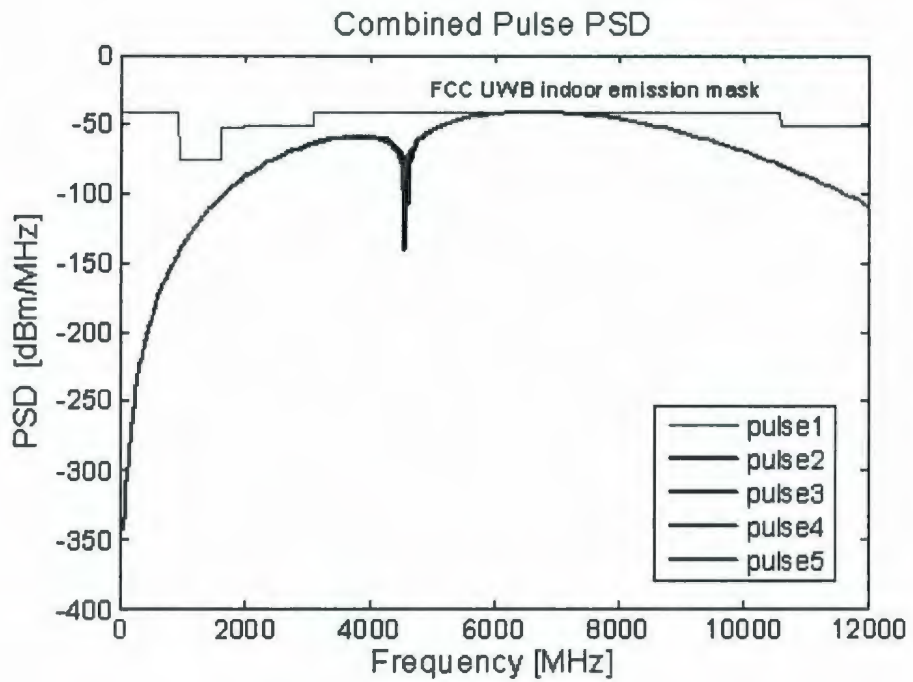


Figure 4.3: PSD of combination of 7<sup>th</sup>, 9<sup>th</sup> and 11<sup>th</sup> Gaussian derivatives, coefficient range [-6,+6]

Table 4.4: Pulse energy of combination of 7<sup>th</sup>, 9<sup>th</sup> and 11<sup>th</sup> Gaussian derivatives, coefficient range [-10,+10]

Pulse	Pulse Energy				
1-5	$2.1496 \cdot 10^{-4}$	$2.1439 \cdot 10^{-4}$	$2.1389 \cdot 10^{-4}$	$2.1327 \cdot 10^{-4}$	$2.0187 \cdot 10^{-4}$

#### 4.2.2 Pulses generated by our design method

As described in Chapter 3, our pulse shape design method uses 1<sup>st</sup> to 16<sup>th</sup> order Gaussian derivative pulses as base waveforms, exhaustively search and compare combinations of any 2 (3 or even more) of the 16 derivatives. During each searching and comparing loop, we keep changing those coefficients step by step in a certain range, record a number of pulses which not only offer efficiency in meeting the FCC mask,

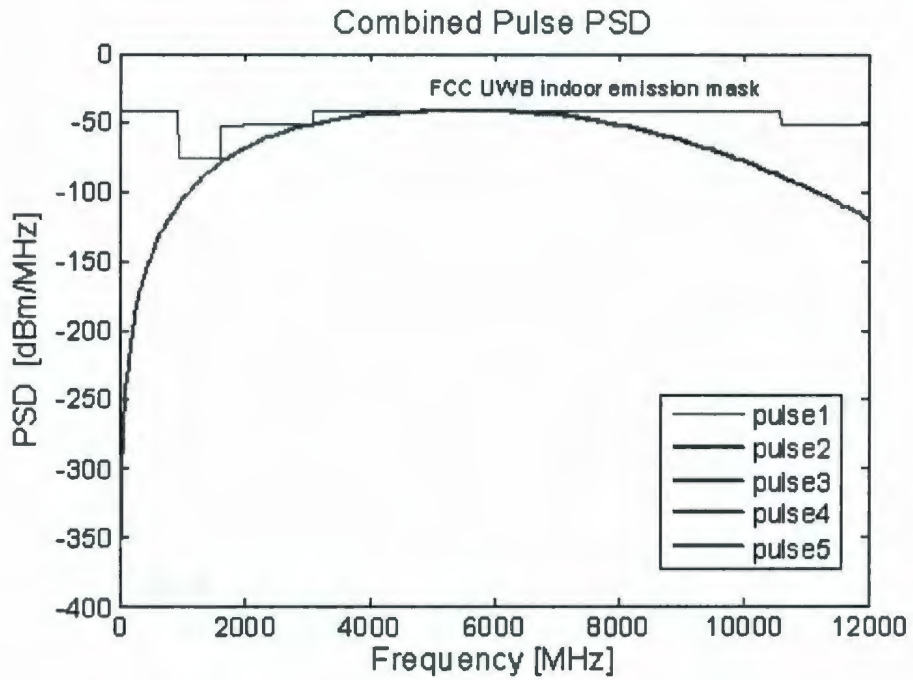


Figure 4.4: PSD of combination of 7<sup>th</sup>, 9<sup>th</sup> and 11<sup>th</sup> Gaussian derivatives, coefficient range [-10,+10]

but also effectively exploit the allowable bandwidth and power. After obtaining a number of candidate pulses, we choose the pulse whose derivative pulse has the smallest  $\eta$  value based on our discussion in Chapter 3. This will make a receiver in the multi-user system has a better SNR. Figure 4.5 show the best pulse in time domain we obtain from our program. We can see from Figure 4.6 that the PSD of this pulse is very close to the FCC mask, which mean that it effectively exploit the allowable frequency spectrum. Its energy is 0.27564 mW and the  $\eta$  value is the smallest among 5 candidate pulses generated by our program.

Same as the pulse designed by combining 2 different derivatives, we also get the

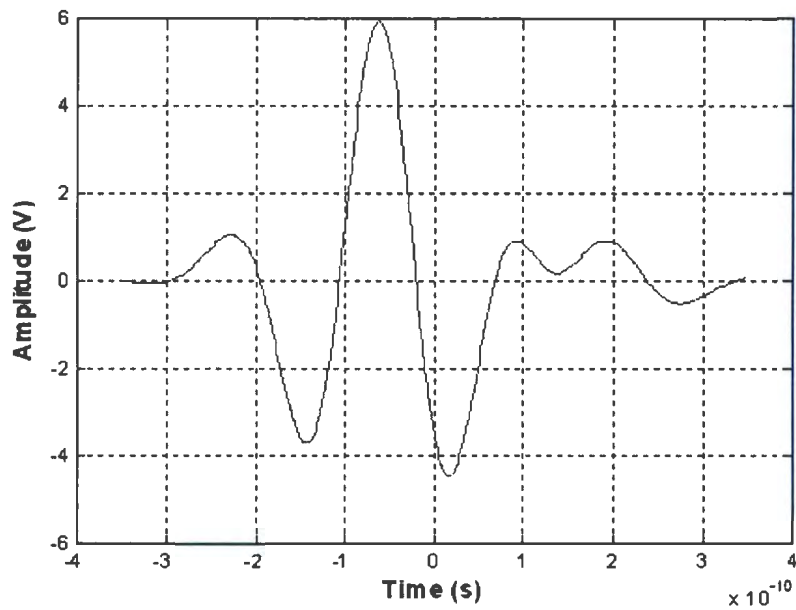


Figure 4.5: Pulse combined by 7<sup>th</sup> and 14<sup>th</sup> Gaussian derivatives

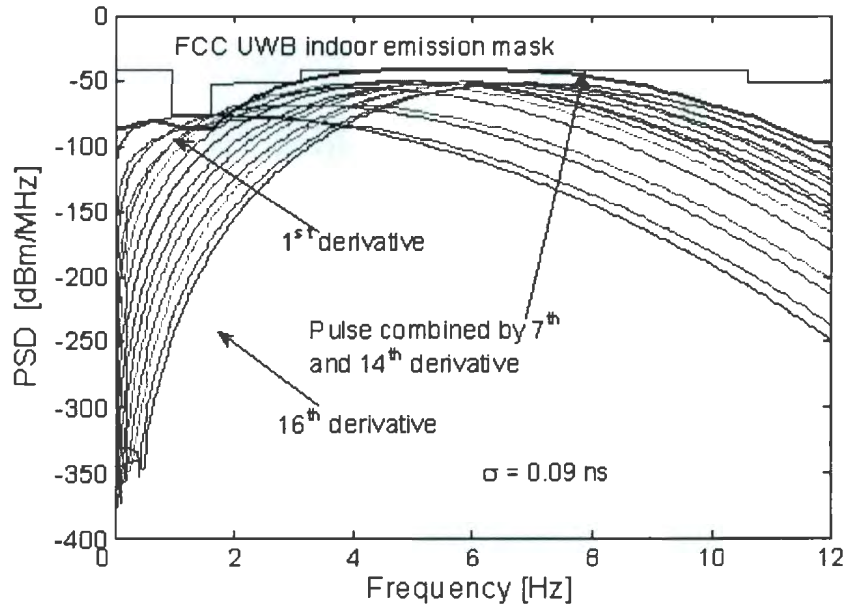


Figure 4.6: PSD of combination of 7<sup>th</sup> and 14<sup>th</sup> Gaussian derivatives

best pulse combined by 3 different derivatives and its PSD, as shown in Figure 4.7 and Figure 4.8, respectively. We can see that this pulse's PSD are even closer to the mask. Its energy is 0.30556 mW and a little bigger  $\eta$  value than the previous pulse.

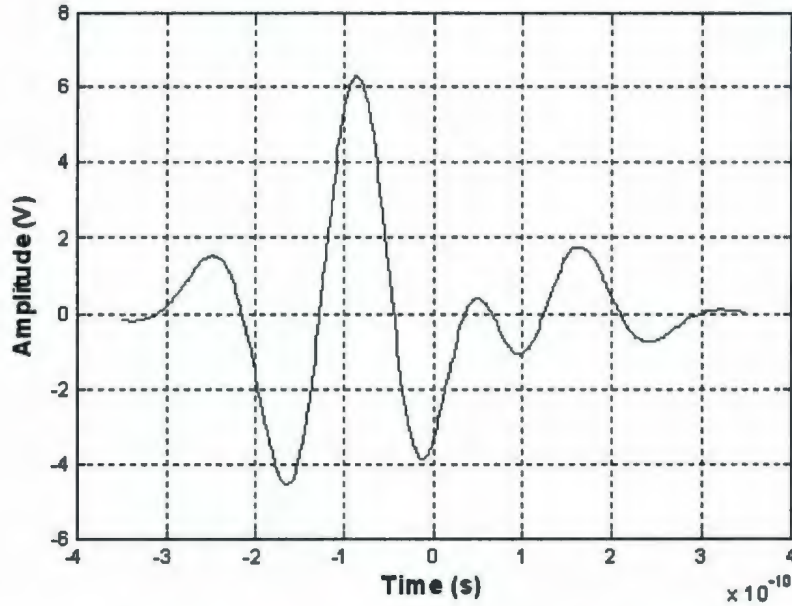


Figure 4.7: Pulse combined by 7<sup>th</sup>, 10<sup>th</sup> and 15<sup>th</sup> Gaussian derivatives

Table 4.5: Parameters of different pulses

Pulse	Pulse power (W)	$\eta$ value
Gaussian 2 <sup>nd</sup> derivative(small)	$1.358 \cdot 10^{-7}$	$1.618 \cdot 10^{-10}$
Gaussian 2 <sup>nd</sup> derivative(big)	$1.4898 \cdot 10^{-4}$	$1.6158 \cdot 10^{-10}$
Gaussian 5 <sup>th</sup> derivative	$1.3519 \cdot 10^{-4}$	$1.5878 \cdot 10^{-10}$
Pulse combined by 7 <sup>th</sup> and 14 <sup>th</sup> G.D.	$2.7564 \cdot 10^{-4}$	$1.0737 \cdot 10^{-10}$
Pulse combined by 7 <sup>th</sup> , 9 <sup>th</sup> and 15 <sup>th</sup> G.D.	$3.0556 \cdot 10^{-4}$	$1.0424 \cdot 10^{-10}$

Table 4.5 listed the power and  $\eta$  values of different pulses. We can find that our designed pulses not only have more energy than the other two, but also have smaller  $\eta$  values. One thing need to be mentioned here: in the table, there are two Gaussian

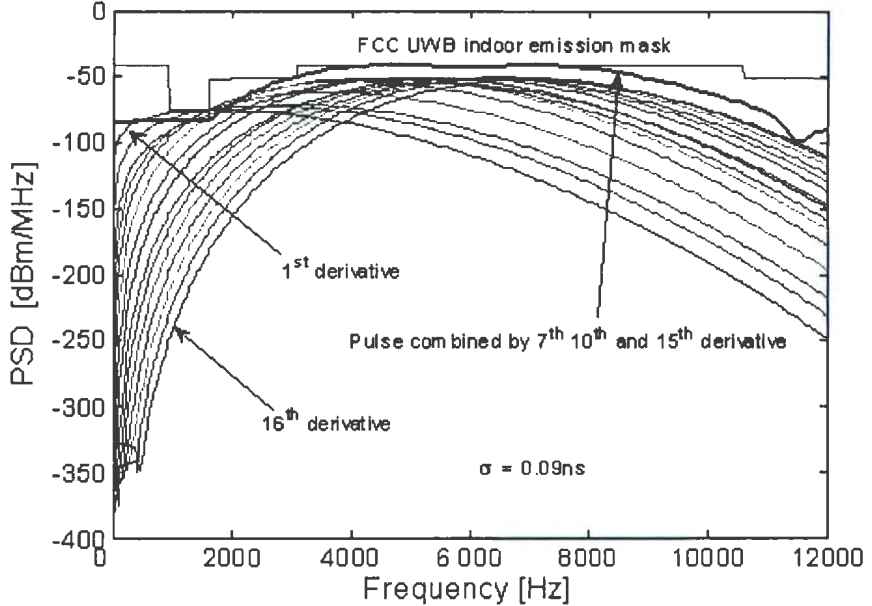


Figure 4.8: PSD of combination of  $7^{th}$ ,  $10^{th}$  and  $15^{th}$  Gaussian derivatives

$2^{nd}$  derivative pulses. The “small” one has a sufficient low power and its PSD fits in the FCC indoor mask, but it does not exploit the FCC mask in a power efficient manner; whereas the “big” one trying to maximize transmission power and its PSD violates the FCC mask in some bands. However, the latter pulse is actually most widely referenced in many papers [5][8][29][26][16]. Therefore, for the convenience of comparisons with other people’s work, in our following simulation, when we refer to the “Gaussian  $2^{nd}$  derivative pulse”, we mean the latter one, even though its PSD violates the mask. Figure 4.9 shows the PSD of these two Gaussian  $2^{nd}$  derivative pulses.

In order to show the importance of the  $\eta$  value in the BER calculations, we

compare two pulses combined by 3 different derivatives chosen from our candidate pool. These two pulses both combined by 7<sup>th</sup>, 10<sup>th</sup> and 15<sup>th</sup> Gaussian derivatives, their parameters are listed in Table 4.6. “Pulse A” in this table is actually the final choice of our method shown in Table 4.5. “Pulse B” has more power than “Pulse A” but also has a comparatively bigger  $\eta$  value. The calculation results are shown in Table 4.7. Other assumptions of this calculation is that there are 15 interferers in the system, all users work at the same data rate. Only one pulse is used to transmit one source data bit. The single link SNR is 5 dB and this system is an asynchronous system. The channel is an AWGN channel.

Table 4.6: Parameters of two pulses from candidate pool

Pulse	Pulse power (W)	$\eta$ value
Pulse A	$3.0556 \cdot 10^{-4}$	$1.0424 \cdot 10^{-10}$
Pulse B	$3.071 \cdot 10^{-4}$	$1.0468 \cdot 10^{-10}$

Table 4.7: Theoretical BER comparison of two pulses from candidate pool

Data Rate (Mb/s)	40	80	120	160
BER of pulse A	$2.4573 \cdot 10^{-2}$	$3.7799 \cdot 10^{-2}$	$5.1263 \cdot 10^{-2}$	$6.4404 \cdot 10^{-2}$
BER of pulse B	$2.4409 \cdot 10^{-2}$	$3.7683 \cdot 10^{-2}$	$5.1205 \cdot 10^{-2}$	$6.4402 \cdot 10^{-2}$
Data Rate(Mb/s)	200	240	280	320
BER of pulse A	$7.6956 \cdot 10^{-2}$	$8.8813 \cdot 10^{-2}$	$9.9953 \cdot 10^{-2}$	$1.1039 \cdot 10^{-1}$
BER of pulse B	$7.7005 \cdot 10^{-2}$	$8.8909 \cdot 10^{-2}$	$1.0009 \cdot 10^{-1}$	$1.1056 \cdot 10^{-1}$
Data Rate(Mb/s)	360	400	440	480
BER of pulse A	$1.2017 \cdot 10^{-1}$	$1.2293 \cdot 10^{-1}$	$1.3792 \cdot 10^{-1}$	$1.4599 \cdot 10^{-1}$
BER of pulse B	$1.2037 \cdot 10^{-1}$	$1.2955 \cdot 10^{-1}$	$1.3816 \cdot 10^{-1}$	$1.4625 \cdot 10^{-1}$

From Table 4.7, we observe that when all the users work at a lower data rate, “Pulse B” has a better performance. It is because when all users’ data rates are

low, the dominant noise is the thermal noise. “Pulse B” contains more power, which makes it have a better SNR at the receiver side. When all users’ data rates are high, the MUI becomes dominant in the noise and the pulse which causes less MUI will have a better BER. That is what happens to “Pulse A” at high data rate. Since in most cases, UWB communication systems’ target is to work at high speed in a short range environment where many other UWB systems also work, we choose the pulse that can cause less MUI, “Pulse A”, as our designed pulse shape.

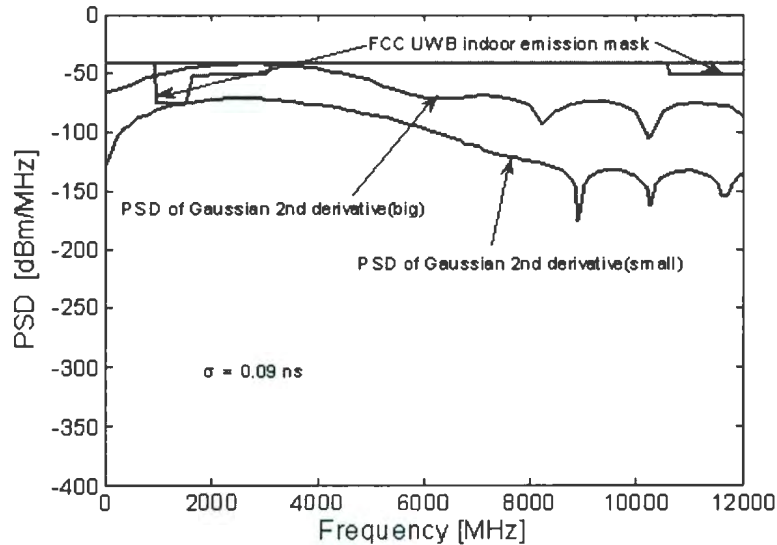


Figure 4.9: PSD of two  $2^{nd}$  Gaussian derivative pulses

### 4.3 Performance comparisons

From the literature review in Chapter 2, we find that not much work has been done in the pulse shape design research to demonstrate how the shape of the pulse affects

bit-error performance. Most researchers focused on how to make the PSD of the pulse approach the FCC mask as close as possible. Although this also indirectly affects the receiver SNR and the system BER, it is not explicitly studied. In our design, we not only pay attention to the optimal exploitation of the mask, but also the pulse effects on MUI, which explicitly relate the pulse shape to system bit-error performance. In this section, we show that our designed pulses have better performance than other frequently used UWB pulse shapes in some aspects. Among them, system BER is a fundamental factor to compare.

In order to conduct fair comparisons, we established a UWB end to end system model using MATLAB. On this simulation platform, we can use different pulse shapes to transmit information bits. The system is shown in Figure 4.10. In this system, by modifying the block “Pulse Shaper”, different pulse waveforms can be introduced into the system. Performance under other channel conditions, for example, the IEEE 802.15 standard channel, can be easily achieved by replacing the “AWGN channel” block with the desired channel block. The parameters of the UWB system model are listed in Table 4.8.

Table 4.8: Parameters of the simulation UWB systems

Parameter	Notation	Value
Pulse Width	$T_p$	0.7ns
Chip Width	$T_c$	0.9ns
Frame Width	$T_f$	28.8ns
Number of Chips per Frame	$N_c$	32
Repetition Code Length	$N_s$	2

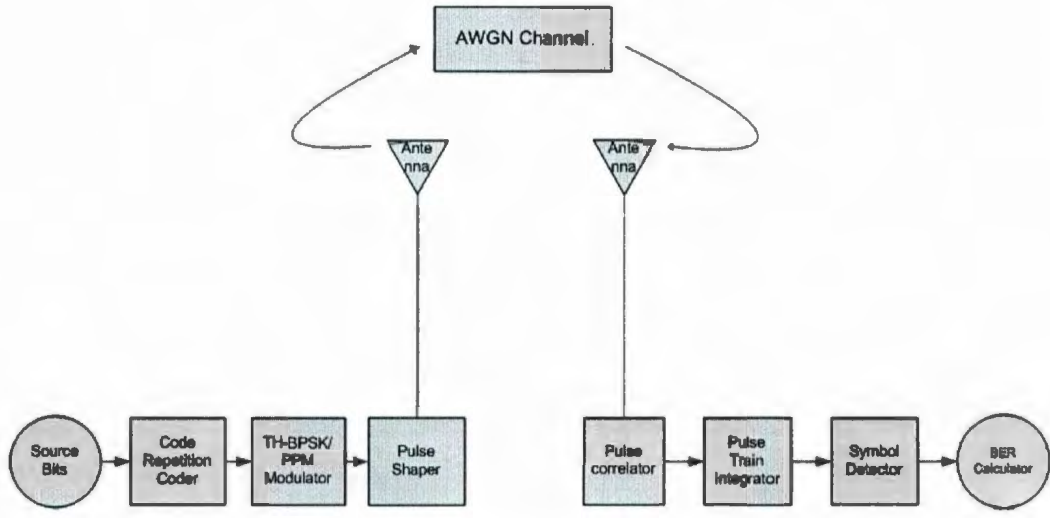


Figure 4.10: System model for the single link UWB transmission chain with AWGN channel

The pulses we choose to compare are the second order Gaussian derivative introduced in [16] and many other papers, the fifth order Gaussian derivative introduced in [26] with several different parameters, our designed pulse combined by 2 Gaussian derivative pulses and pulse combined by 3 Gaussian derivatives. The basic parameters for all the pulses are listed in Table 4.8. Except that the second order Gaussian derivative's PSD dose not conform to the FCC mask at 0-960 GHz, the PSD of other pulses all conform to the FCC indoor mask. We will explain why we choose these pulses in the next section.

#### 4.3.1 BER comparisons of different pulses

We first compare the BER performance of indoor TH-BPSK and TH-PPM UWB systems using different pulses. It should be noted that although the BER curves are

presented in the figures as a function of SNR, the SNR value is correct only for the Gaussian 2<sup>nd</sup> derivative pulse. That is, we use the signal power of the Gaussian 2<sup>nd</sup> derivative pulse as a reference signal to normalize the powers of all other waveforms. Therefore, we refer to this SNR as Normalized SNR in order to differentiate it from the real SNR.

In the following series of figures, we show the simulation results of the system BER of different pulses in several scenarios. The exact evaluation of the bit-error rate  $P_r$  is complex and requires the full characterization of the statistics of the multiple-access interference terms. In our case, for the purpose of comparing different pulse waveforms, it is sufficient to consider the average bit energy to noise plus interference density ratio, which, for simplicity, will be referred to as the SNR defined by the ratio of the squared expected value of the decision statistic to its variance. The bit-error probability is then approximated by  $P_r \approx Q[\sqrt{SNR}]$ , where  $Q$  denotes the error function  $Q(x) = (1/\sqrt{2\pi}) \int_x^\infty e^{-u^2/2} du$ . This estimation method is called Gaussian approximation (GA). Figure 4.11 shows the simulated BER of single link TH-PPM systems with different pulses. The symbol “G.D.” in the legend of the figure means Gaussian Derivative(s).

In Figure 4.12, the performance of indoor multi-user TH-PPM UWB systems with one target user and seven asynchronous interferers using different pulses are compared.

Figure 4.13 shows the performance of indoor multi-user TH-PPM systems with

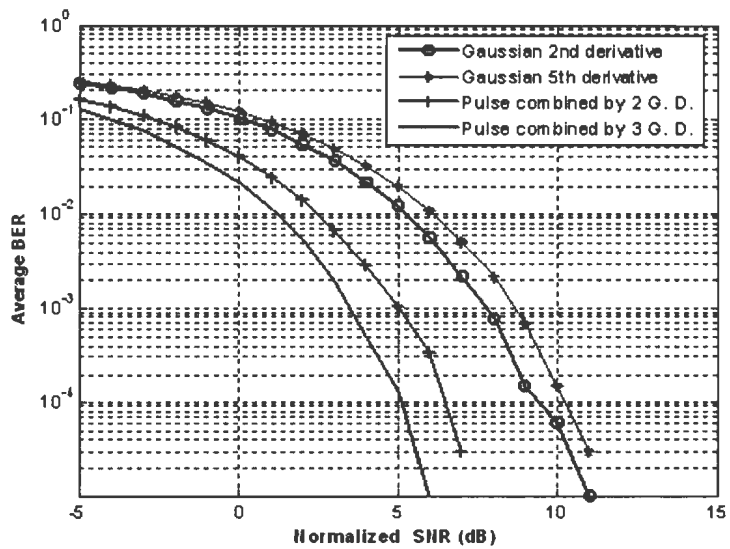


Figure 4.11: Comparison of indoor Single Link TH-PPM UWB systems using different pulses

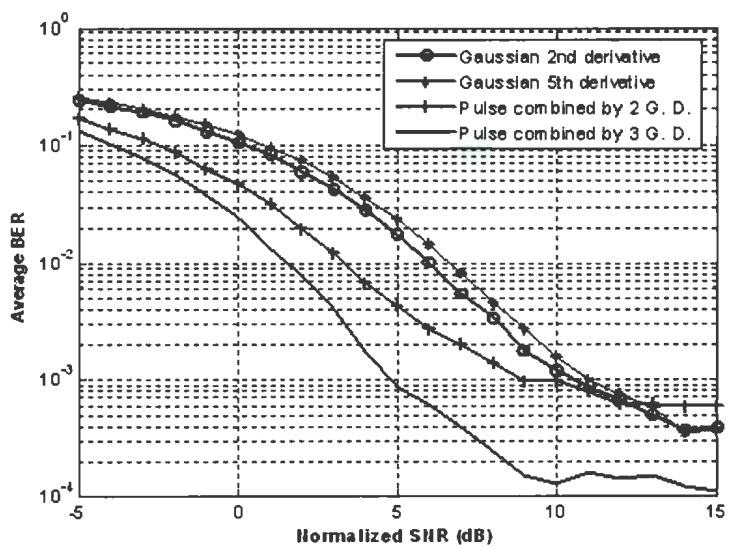


Figure 4.12: Comparison of indoor TH-PPM UWB systems using different pulses with 7 asynchronous interferers

one target user and fifteen asynchronous interferers.

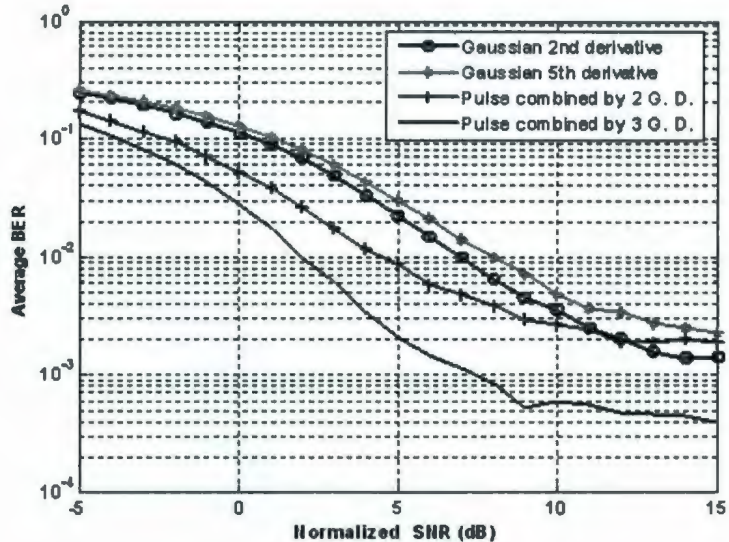


Figure 4.13: Comparison of indoor TH-PPM UWB systems using different pulses with 15 asynchronous interferers

The same series of comparisons for indoor TH-BPSK systems are shown from Figure 4.14 to Figure 4.16.

From those comparisons, we observe that in the single link scenario, for both TH-PPM and TH-BPSK systems, at the same noise level (the same “Normalized SNR” value), our designed pulses have lower BER than the 2<sup>nd</sup> and 5<sup>th</sup> Gaussian derivative pulses. The pulse combined by 3 different Gaussian derivatives has even lower BER than the pulse combined by 2 Gaussian derivatives. For TH-BPSK systems, the BER gap between our designed two pulses and the other two popular pulses are even more apparent.

Figure 4.12 and Figure 4.15 show the BER versus normalized SNR for TH-PPM

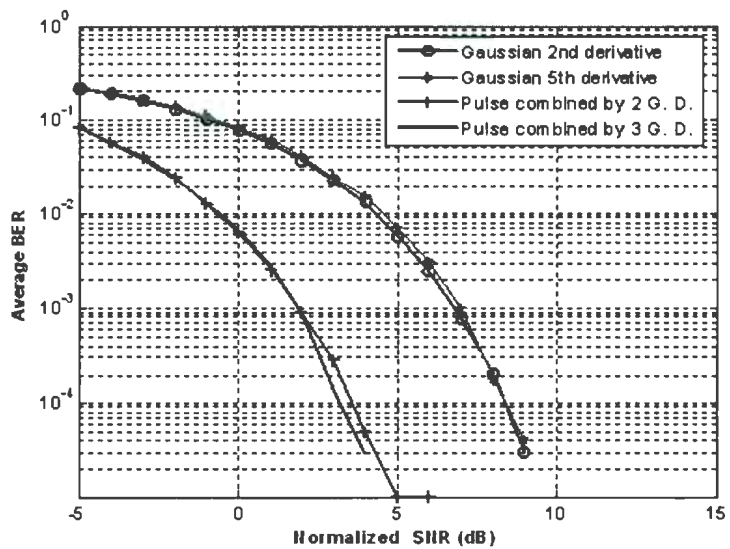


Figure 4.14: Comparison of indoor Single Link TH-BPSK UWB systems using different pulses

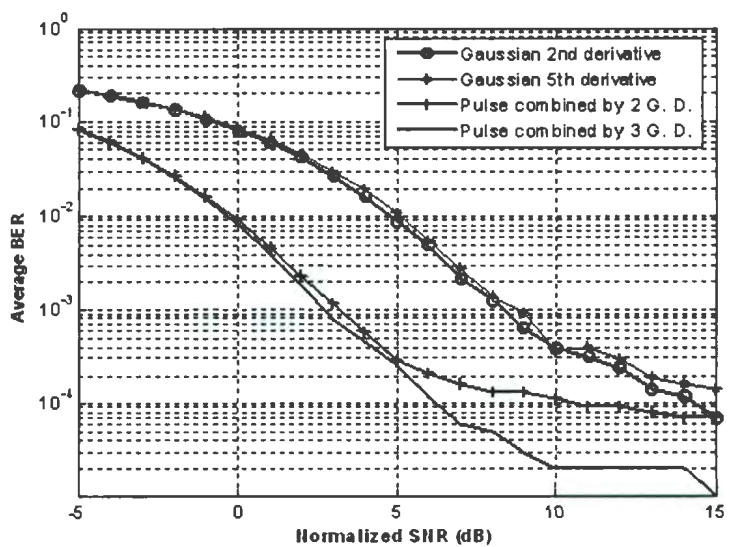


Figure 4.15: Comparison of indoor TH-BPSK UWB systems using different pulses with 7 asynchronous interferers

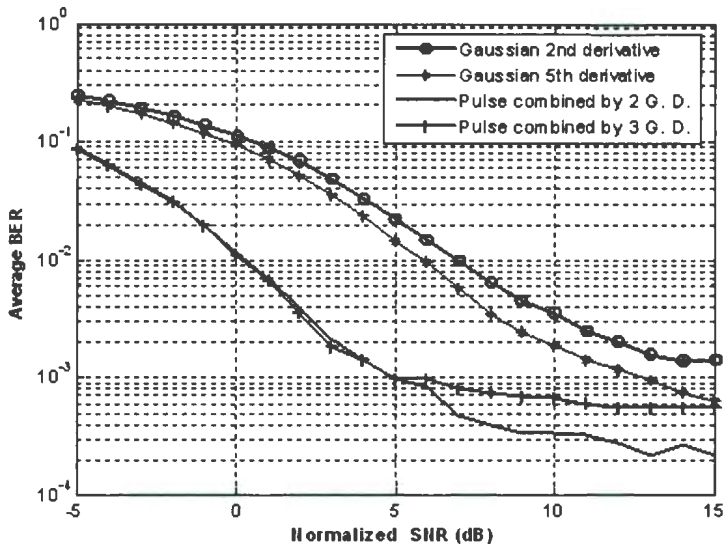


Figure 4.16: Comparison of indoor TH-BPSK UWB systems using different pulses with 15 asynchronous interferers

and TH-BPSK system using different pulses when 7 interfering users are present. In these cases, we notice that for the BER curves of all pulses tend asymptotically to a constant value, leading to the conclusion that system performance in the presence of high SNR values is dominated by MUI. That is to say, the system performance is dominated by MUI when the SNR is high, and the AWGN almost can be ignored. When the SNR is low, the decrease of probability of error and the growth of the transmitted power is linear. In this situation, when the transmitter power is low or when the user number is very small, the probability of error is mainly determined by thermal noise. In that case, by increasing the transmission power, we can get better system performance (low BER). In the other case, the probability of error reaches a value where however the transmission power is increased, it does not change

much. That means the MUI is dominating the noise part. In other words, the system performance is limited by the MUI. From the figures, we observe that pulse combined by 2 Gaussian derivatives has better performance than 2<sup>nd</sup> and 5<sup>th</sup> Gaussian derivative pulses when SNR value is small, but when SNR value is big, the system performance is greatly affected by MUI and the BER is not better than those single Gaussian derivatives. The pulse combined by 3 Gaussian derivatives, however, shows better performance to that of the other three pulses for all SNR values. Figure 4.13 and Figure 4.16 also show similar results. Since the interfering users are 15, the BER value will be higher than that with 7 interfering users.

In Section 4.2.2, we showed the importance of  $\eta$  value in the reduction of MUI in a multi-user system by calculation. Here, in this part, we will use this simulation platform to verify the conclusion draw by the calculations. We take two multi-user TH-BPSK UWB systems use “Pulse A” and “Pulse B” respectively to compare. The system has 15 interferers.

Figure 4.17 shows the average BER of two systems using “Pulse A” and “Pulse B” respectively. We can find that when “Normalized SNR” is small which means thermal noise is dominant in the noise, the system using “Pulse B” has a better SNR. When “Normalized SNR” become big, which means thermal noise is small and MUI is dominant, the system using “Pulse A” has a better BER. These observations are consistent with the conclusion we have drawn from the calculation in Section 4.2.2, which indicates that carefully choice of  $\eta$  value can reduce MUI and thus reduce

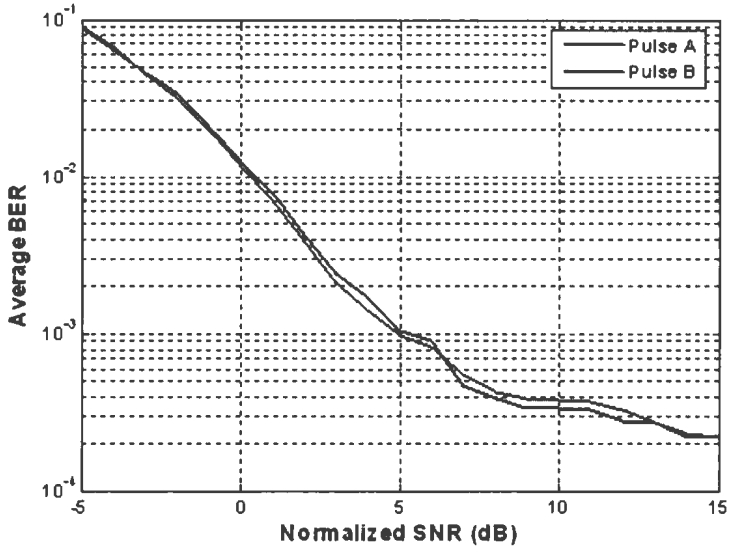


Figure 4.17: BER comparison of two pulses from candidate pool

system BER. Hence, we are more confident to choose “Pulse A” as our designed pulse shape.

In Figure 4.18, we compare the theoretical calculation results with the simulation results. The theoretical results (based on Gaussian approximation) is in good agreement with the simulation for small SNR values. However, it does not accurately predict the error rate floor of the system (caused by the interference) for large SNR values. This is consistent with the conclusion in [37] that GA is not a reliable approximation to calculate the bit error probability at big SNR scenarios. Since this is not the focus of our research, we will not investigate further on this.

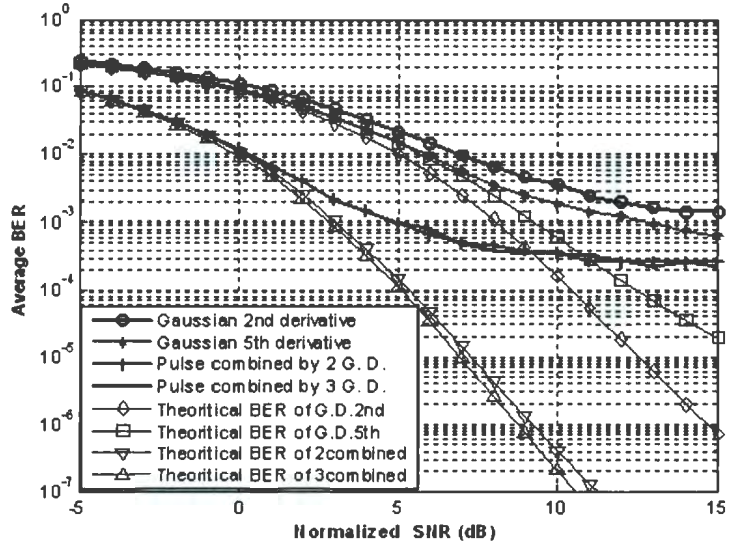


Figure 4.18: Comparison both theoretical and simulation results of indoor TH-BPSK UWB systems using different pulses with 7 asynchronous interferers

#### 4.3.2 Maximum user number comparisons for different pulses

In this section, we try to make the comparisons between different pulses for the maximum user number they can support in a TH-PPM UWB system operating at a certain data rate and a certain BER level.

The comparisons are based on the maximum user number expressions derived by Win and Scholtz in [16].

In our case, based on their maximum user number expression, SNR is fixed so as to ensure a probability of error of  $10^{-3}$ . The number of users  $N_u$  vs. the additional increase in power  $\Delta P$  needed to maintain the same SNR in multiple access condition

is given by [16]

$$N_u - 1 = \frac{1}{\eta R_d} \frac{1}{SNR} \left( 1 - \frac{1}{\Delta P} \right). \quad (4.1)$$

As  $\Delta P \gg 1$ , we get

$$N_{u,max} = \frac{1}{\eta R_d SNR} + 1. \quad (4.2)$$

From this equation we can see that the maximum user number has a direct relation with the parameter  $\eta$  we derived in the last chapter. System data rate  $R_d$  and SNR also directly relate to maximum user number. In Figure 4.19, the maximum user number of a system using different pulses is shown as a function of data rate while the system BER is maintained at  $10^{-3}$ . As shown, our designed pulses can support more users for all data rate values. In particular, at lower system data rate such as 10 Mb/s, the pulse combined by 3 Gaussian derivatives can support almost two times the users as Gaussian 5<sup>th</sup> derivative pulse can.

#### 4.3.3 Transmission distance comparisons of different pulses

The PSD limitation defined by emission masks determines the maximum allowable transmit power. In this subsection, under rather simplified hypotheses, we evaluate the maximum distance when a predetermined BER and a given data rate must be guaranteed at the receiver. In this study, a simple link budget analysis is considered.

For a narrowband signal, the received power at distance  $d$  is given by [38]

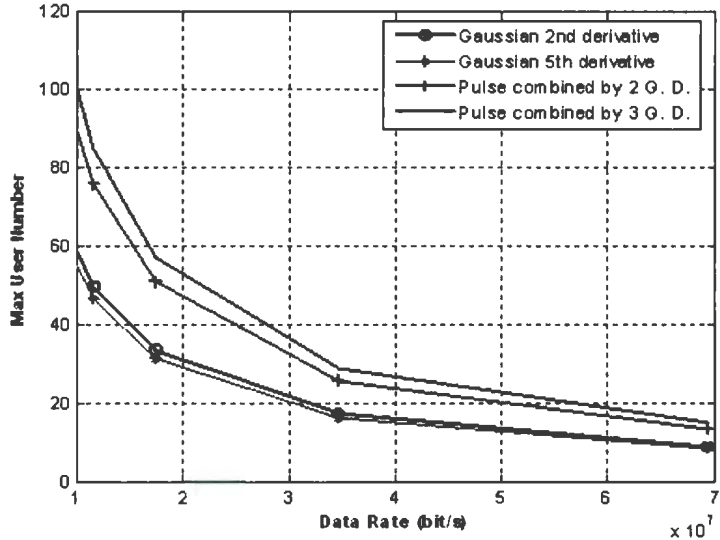


Figure 4.19: Maximum number of users vs. system data rate for system BER at  $10^{-3}$  using different pulses

$$P_r(d) = \frac{P_t}{PL(d)}, \quad (4.3)$$

and the free-space path loss dimension ratio,  $PL(d)$ , is given by

$$PL(d) = \frac{(4\pi)^2 d^2 f_c^2}{G_t G_r c^2}, \quad (4.4)$$

where  $P_t$  is the transmitted power,  $G_t$  and  $G_r$  are the transmitter and receiver antenna gains, respectively,  $f_c$  is the carrier frequency, and  $c$  is the speed of light.

For indoor UWB system using very short time duration pulses, the PSD is very wideband and, therefore, Equation 4.4 must be modified to account for variations across the bandwidth of the signal. In particular, the transmitted and received

powers should be calculated using the integral of the PSD within a frequency region. Therefore, the transmitted power is

$$P_t = \int_{f_L}^{f_H} A_{max} |P(f)| df, \quad (4.5)$$

where  $P(f)$  is normalized PSD and  $A_{max}$  can be changed according to the mask restraints.  $[f_L, f_H]$  is the band that the PSD mainly occupies or the band we are interested in. The received power at distance  $d$  is given by

$$P_r(d) = \int_{f_L}^{f_H} \frac{A_{max} |P(f)|}{PL(d, f)} df, \quad (4.6)$$

where  $PL(d, f)$  is the wideband path loss dimension ratio for the free-space propagation model, with the center frequency in Equation 4.4 replaced by the variable  $f$ . With this frequency-dependent path loss dimension ratio, the received power becomes [26]

$$P_r(d) = \frac{A_{max} G_t G_r c^2}{(4\pi)^2 d^2} \int_{f_L}^{f_H} \frac{|P(f)|}{f^2} df. \quad (4.7)$$

In the noise spectral density calculations that follows, we use the data from [26].  $N_0 = kT_0 F \cdot LM$ , where  $k$  is Boltzmann constant  $1.38 \times 10^{-23} \text{ Joules/K}$ ,  $T_0$  is room temperature (300 K),  $F$  is the noise figure in dB, and link margin,  $LM$ , is also in dB.

The received power  $P_r(d)$  necessary at distance  $d$  to achieve a given average SNR can be computed from the relation

$$P_r(d) = SNR + P_N + LM, \quad (4.8)$$

where  $P_N$  is the received noise power and is equal to  $N_0B$ , and  $B$  is the noise equivalent bandwidth of the receiver. The distance expression is derived as [26]

$$d = \frac{c}{4\pi} \sqrt{\frac{A_{maxG_tG_r}}{Eb/N_0 \cdot R_d \cdot kT_0F \cdot LM} \int_{f_L}^{f_H} \frac{|P(f)|}{f^2} df}. \quad (4.9)$$

In Equation 4.9,  $A_{max} \cdot |P(f)|$  can be seen as the maximum PSD of different pulses under the FCC mask, which is different from pulse to pulse. So the transmission distances of signal represented by different pulses will vary.

We calculate the transmission distance of signals represented by different pulses. The results are shown in Figure 4.20. In the figure, we consider an ideal pulse whose PSD exploits the 0-10.6 GHz FCC interval. This case is interesting because it provides the upper limit for the reachable distance on an UWB communication link. As seen from the figure, our two designed pulses are not the pulses that can transmit farthest. The reason is that these two pulse are combined by different Gaussian derivatives, and the higher order of the derivative, the more the high frequency components in the pulse's PSD. According to Equation 4.9, the more high frequency components in spectrum, the shorter distance the signal can transmit. However, we

can see our designed pulses can transmit farther than the Gaussian 5<sup>th</sup> derivative. The transmission distance of the pulse combined by 3 Gaussian derivatives has very small difference from the Gaussian 2<sup>nd</sup> derivative and the ideal pulse. For the pulse combined by 2 Gaussian derivatives, this difference is also very small when the system data rate is high, and we know that UWB indoor communication systems are designed to work at very high data rates.

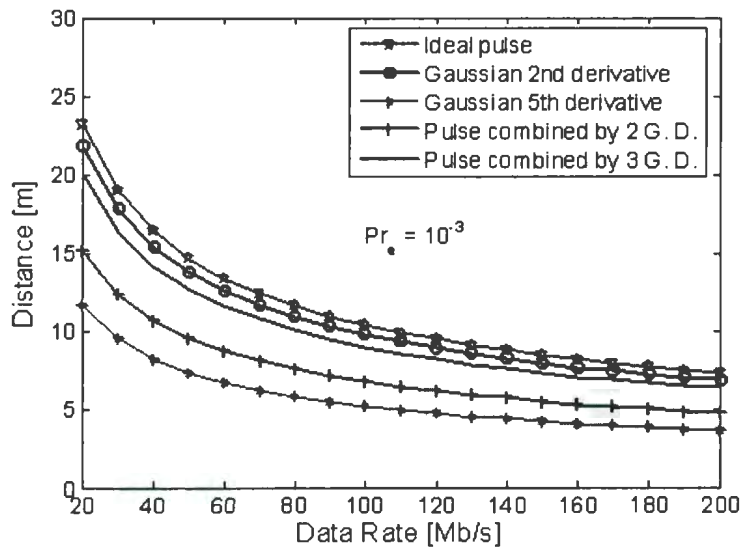


Figure 4.20: Maximum transmission distance vs. system data rate for signal representing by different pulses

## **4.4 Simulation comparisons of pulse performance in system model using UWB standard channel**

Propagation of signals represented by different pulses through AWGN channel is studied in previous sections. In this section, we present the UWB standard multiple path channel model, and compare the pulses' performance in system models that use this channel.

### **4.4.1 IEEE 802.15.3 UWB channel model**

The channel model is a result of the work carried out by the channel modeling sub-committee of the IEEE 802.15 Task Group 3a (TG3a) and is intended to assess the performance of physical (PHY) layer proposals submitted to the group [39]. The model came as a best fit of all channel model contributions which were accomplished based on numerous data collections. It was developed to best reflect the possible measurements of realistic channel environments, where IEEE 802.15.3a devices using the frequency spectrum allocated by the FCC (3.1-10.6 GHz) are going to operate. From these measurements, it is found that the clustering phenomenon exists. Cluster creation is caused by the building's superstructure like external and internal walls and doors, while rays within the cluster are caused by various reflections from objects in the vicinity of the transmitter and the receiver like furniture and people.

By far, the Saleh-Valenzuela channel model [40] seems to fit with the measurements. The model was adopted with some modifications which consists of using a lognormal distribution instead of Rayleigh distribution for the multipath amplitude attenuation since it has been shown through observations that the lognormal distribution is a better fit of the measurements taken. Independent fading is assumed for each cluster as well as each ray within the cluster. The multipath discrete time impulse response of the channel can be described as

$$h(t) = X \sum_{l=0}^L \sum_{k=0}^K \alpha_{k,l} \delta(t - T_l - \tau_{k,l}), \quad (4.10)$$

where  $X$  is the lognormal shadowing term such that  $20\log_{10}(X) \propto N(0, \sigma_x^2)$ .  $\alpha_{k,l}$  is the multipath gain coefficient for the  $l^{th}$  cluster and the  $k^{th}$  ray,  $T_l$  is the arrival time of the first path of the  $l^{th}$  cluster,  $\tau_{k,l}$  is the delay of the  $k^{th}$  ray within the  $l^{th}$  cluster relative to the first path arrival time  $T_l$ . By definition, for the first cluster  $T_0 = 0$ , and for the first ray within the  $l^{th}$  cluster  $\tau_{0,l} = 0$ .

The multipath gain coefficient, including the amplitude and the phase, is defined as

$$\alpha_{k,l} = p_{k,l} \xi_l \beta_{k,l}, \quad (4.11)$$

where  $p_{k,l}$  is chosen from  $\{\pm 1\}$  with equal probability to account for the signal inversion due to reflections,  $\xi_l$  is the fading associated with the  $l^{th}$  cluster, and  $\beta_{k,l}$  is the fading associated with the  $k^{th}$  ray of the  $l^{th}$  cluster. The amplitude  $|\alpha_{k,l}|$  has

a lognormal distribution and can be expressed as

$$|\alpha_{k,l}| = 10^{(\mu_{k,l} + n_1 + n_2)/20}, \quad (4.12)$$

where  $n_1 \propto N(0, \sigma_1^2)$  and  $n_2 \propto N(0, \sigma_2^2)$  are independent and correspond to the fading on each cluster and ray. Thus  $20\log_{10}(\xi_l \beta_{k,l}) \propto N(\mu_{k,l}, \sigma_1^2 + \sigma_2^2)$ ; i.e.,  $|\alpha_{k,l}|$  is lognormally distributed. The  $\mu_{k,l}$  is given by

$$\mu_{k,l} = \frac{10\ln(\Omega_0) - 10T_l/\Gamma - 10\tau_{k,l}/\gamma}{\ln(10)} - \frac{(\sigma_1^2 + \sigma_2^2)\ln(10)}{20}, \quad (4.13)$$

where  $\Omega_0$  is the mean energy of the first path of the first cluster,  $\Gamma$  and  $\gamma$  is a cluster-decay and a ray-decay factor. The averaged power delay profile is

$$E[|\alpha_{k,l}|^2] = \Omega_0 e^{-T_l/\Gamma} e^{-\tau_{k,l}/\gamma}, \quad (4.14)$$

which reflects the exponential decay of each cluster, as well as the decay of the total cluster power with delay. The cluster arrival time, i.e. the arrival time of the first ray of the cluster, are modeled as a Poisson process with some fixed rate  $\Lambda$ . In each cluster, rays also arrive according to a Poisson process with some fixed rate  $\lambda$ . The distribution of the cluster and the ray arrival time are independently and

exponentially distributed and can be expressed as

$$p(T_l|T_{l-1}) = \Lambda e^{[-\Lambda(T_l - T_{l-1})]}, l > 0 \quad (4.15)$$

$$p(\tau_{k,l}|\tau_{k-1,l}) = \lambda e^{[-\lambda(\tau_{k,l} - \tau_{k-1,l})]}, k > 0 \quad (4.16)$$

As a conclusion, the received rays' amplitude follows a lognormal distribution and their variances decay exponentially with cluster delay and with ray delay within the cluster. The corresponding phase angles take on values 0 and  $\pi$  to reflect the signal inversions due to reflections from the surrounding objects. The clusters and the rays that arrive within the cluster form Poisson arrival processes with rates  $\Lambda$  and  $\lambda$ , respectively. The interarrival time of rays and clusters are exponentially distributed.

#### 4.4.2 Channel model realizations

In [39], four different measurement environments are defined, namely CM1, CM2, CM3, and CM4. CM1 describes a LOS (line-of-sight) situation when the separation between transmitter and receiver is less than 4m. CM2 describes the same range, but for a non-LOS situation. CM3 describes a non-LOS situation for a distance of 4-10m between transmitter and receiver. Finally, CM4 describes an extreme non-LOS situation, which results in a delay spread of 25ns.

Because channel model is not the main focus of this thesis, we will not have more

details about the channel model here. The details can be found in [39].

In our simulations, we replaced the “AWGN” block in Figure 4.10 with this standard channel block, and did the system SNR comparisons for different pulses. The simulations are not only in a single link system, but also in a multi-user system that the number of interferers can be changed. We use parameters of CM1 in our channel model. Figure 4.21 and Figure 4.22 show the continuous time and discrete time channel impulse responses. Figure 4.21 shows that the transmission of a pulse generates multiple contributions at the receiver. The presence of different clusters is not evident. The same conclusion is suggested by the discrete time impulse response in Figure 4.22.

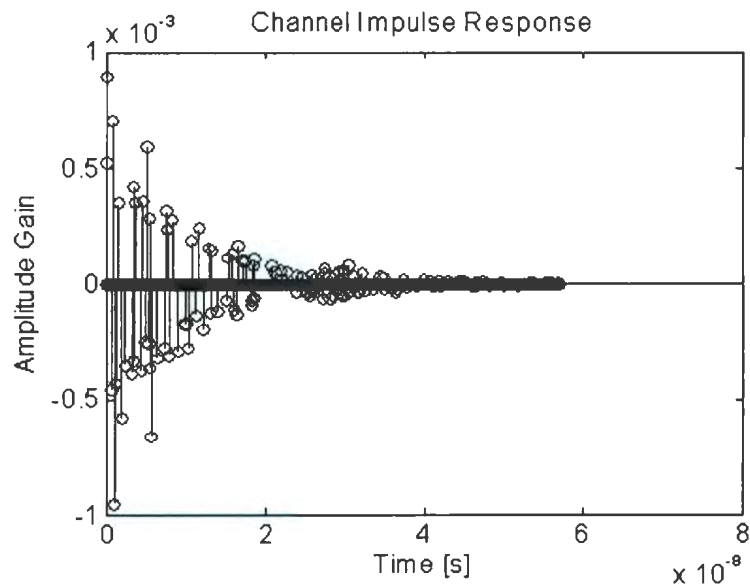


Figure 4.21: Channel impulse response for CM1

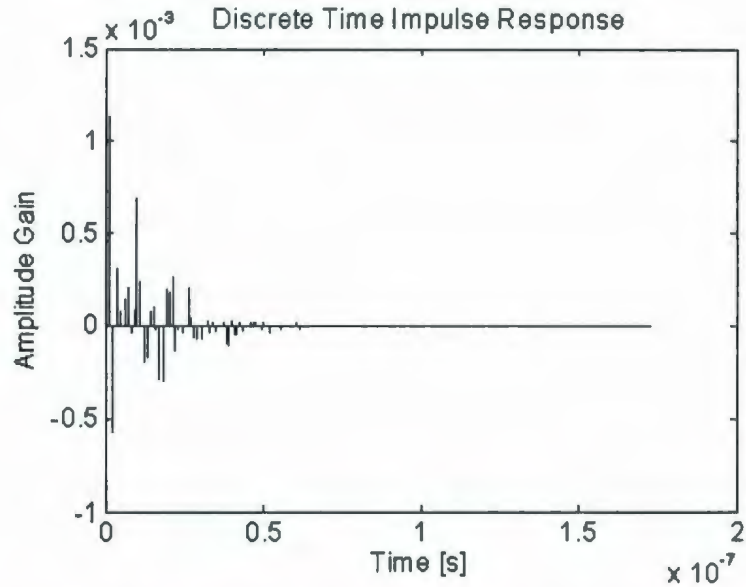


Figure 4.22: Discrete time channel impulse response for CM1

#### 4.4.3 Simulation comparisons of pulse performance

When the signals transmit through the multipath channel, the analytical expression of system BER will be very hard to obtain. As a matter of fact, so far there is not a widely accepted theoretical expression in the literature. We show the results from our simulations here. For the receiver part, we use an ideal RAKE, which processes all the multi-path contributions being resolved at the receiver. From the figures, we observe that the performances of our designed pulses are better comparing to the other two pulses. Our designed pulses perform much better in multi-path environments. Figure 4.23 to Figure 4.25 show the BER versus normalized SNR for TH-PPM and TH-BPSK system using different pulses when 1,8,16 users are present, respectively. From Figure 4.23, we can see that in a single link system, the BER

curves of pulses combined by 2 and 3 Gaussian derivatives always perform better than those from the curves of 2<sup>nd</sup> and 5<sup>th</sup> Gaussian derivative pulses. However, the gap between them are not obvious. From Figure 4.24 and Figure 4.25, we can see clearly that the BER of pulses combined by 2 and 3 Gaussian derivative pulses are much lower than that of 2<sup>nd</sup> and 5<sup>th</sup> Gaussian derivative pulses. In particular, the pulse combined by 3 different Gaussian derivatives outperforms all the other pulses for all “Normalized SNR” values in all three scenarios. These figures reveal that our designed pulses have much better performance in multi-user system with multipath channel than single 2<sup>nd</sup> and 5<sup>th</sup> Gaussian derivative pulses.

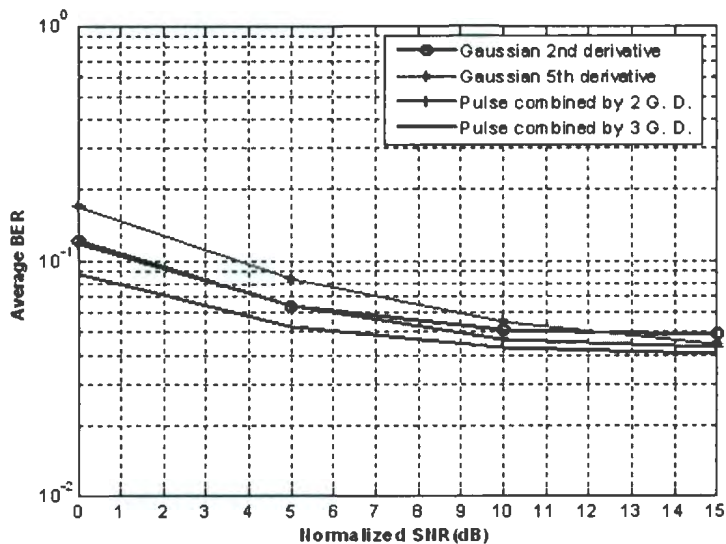


Figure 4.23: Comparison of indoor Single Link TH-BPSK UWB systems using different pulses through IEEE standard channel

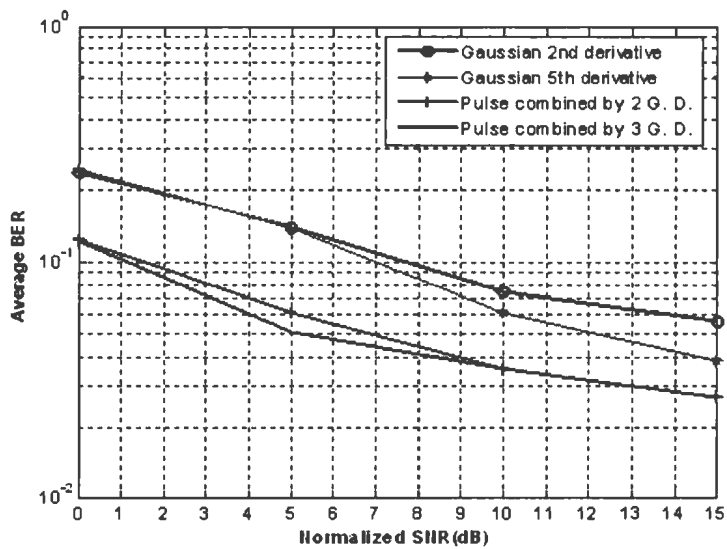


Figure 4.24: Comparison of indoor TH-BPSK UWB systems using different pulses with 7 asynchronous interferers through IEEE standard channel

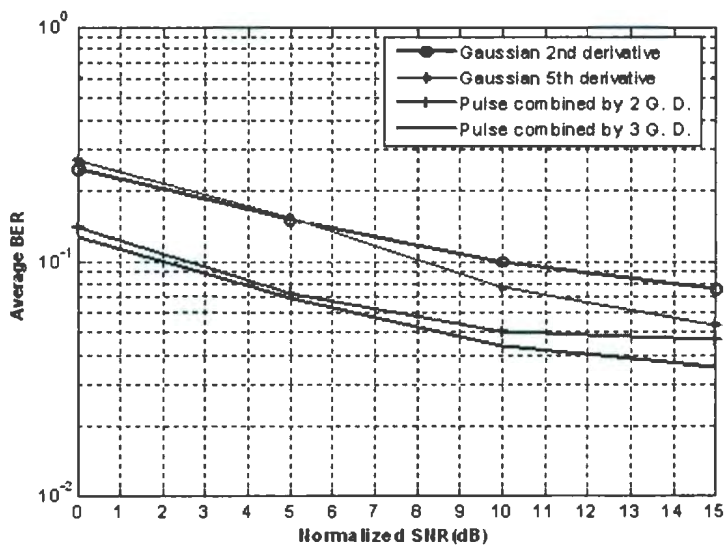


Figure 4.25: Comparison of indoor TH-BPSK UWB systems using different pulses with 15 asynchronous interferers through IEEE standard channel

## 4.5 Chapter summary

In this chapter, through various calculations and simulations, the performance of our designed pulses and that of the other two widely referenced UWB pulse shapes are compared in several different aspects. The results showed that our designed pulses not only meet the regulatory requirements, but also contain more power. The energy of the pulse combined by 3 Gaussian derivatives are twice as that of the  $2^{nd}$  or  $5^{th}$  Gaussian derivative pulses. Since our pulse can contain more energy under the FCC restraints, both in single link and multi-user environments, the systems using our designed pulses have a higher SNR at the receiver and hence lower BER, which has been verified by the calculations and simulations in different scenarios including the systems using TH-BPSK modulation and TH-PPM modulation through a non-fading AWGN channel, and the system using TH-PPM modulation through the IEEE standard channel. The systems that use our designed pulses also can support more users than the systems using other pulses. Although for transmission distance our designed pulses are not the farthest, their performance is better than the Gaussian  $5^{th}$  derivative pulse and very close to the Gaussian  $2^{nd}$  derivative pulse and the ideal pulse at the interested system data rate range.

# **Chapter 5**

## **Conclusion and future work**

### **5.1 Conclusions**

UWB technology is one of the hot topics today because of a tremendous promise it holds especially in the field of high data rate and short distance wireless communications. Once realized, UWB can hold its sway over a varied range of applications with small hardware complexity.

In this thesis, we have first given a review of previous literature of impulse UWB pulse shaping techniques including introduction of the widely used pulse generation techniques unique to UWB communication systems. We have presented a new UWB pulse shape design method. This method is based on the linear combination of a set of different Gaussian derivative pulses. By combining certain numbers (2 and 3 in this thesis) of different Gaussian derivative pulses, we can get a single pulse that not

only offers efficiency in meeting the FCC spectral mask, but also effectively exploits the allowable bandwidth and power. Since our design scheme also takes into account the pulse's effect on system BER with the presence of multi-user interference, our designed pulses have comparatively better performance in multi-user systems than single 2<sup>nd</sup> and 5<sup>th</sup> Gaussian derivative pulses which are the most frequently used UWB pulses in academia.

Another contribution of this thesis is the development of an end-to-end UWB signal transmission simulation models coded using MATLAB. Comparisons of the performance of different pulses on TH-PPM and TH-BPSK UWB system models using AWGN channel and IEEE 802.15.3a standard channel has been simulated on this platform. The results show that our design pulses have lower BER in single link systems as well as multi-user systems. Systems that use our designed pulse can support more users than the 2<sup>nd</sup> and 5<sup>th</sup> Gaussian derivative pulses when the data rate and system BER are fixed. Since our designed pulses have relatively more high frequency components, their transmission distance is not as far as the Gaussian 2<sup>nd</sup> derivative pulse, whose energy are concentrated in lower frequency band. However, since the pulses contain more energy, they still transmit further than the Gaussian 5<sup>th</sup> derivative pulse.

## 5.2 Recommendations for future work

This thesis work has opened numerous areas for future work which could be done to better understand the performance of the pulse shaping in UWB communication systems. Opportunities for further research exist and provide motivation for additional investigations across several areas such as:

- Better understanding of the effects of pulse shape on the system performance in a multi-user environment using multipath channel. We have learned that pulse shape can affect the performance of multi-user systems with simple AWGN channel. In a multipath channel, the received signal's multipath components will also affect the useful signal, which will also relate to the pulse shape. A better understanding of pulse shape's effects in such an environment can help us design a more useful pulse for real applications.
- A more precise theoretical approximation of the performance of a time-hopping binary pulse position modulation and BPSK ultra-wideband system with multiple user and multiple path interference. Gaussian approximation is known to be not sufficient to calculate the bit error rate under high SNR scenarios. Hence, a more precise closed form theoretical method is a preferred choice to provide system performance results on a theoretical basis.
- A more modularized practical UWB simulation platform. We have developed an end-to-end simulation platform in our project. We believe this platform can be

enhanced by considering more realistic situations.

- The design of a simple and power efficient all-digital CMOS pulse generator that can generate our designed pulses. We have introduced an all-digital low-power CMOS pulse generator for UWB systems which can generate Gaussian 5<sup>th</sup> derivative pulses. Further work can be extended to develop a similar pulse generator which can generate the pulses of arbitrary combination of different pulse waveforms. It also would be interesting to compare different pulse generation methods with the one that designed in this thesis based on the complexity criterion.

## References

- [1] S. Roy, J. R. Foerstern, V. Somayazulu, and D. G. Leeper, "Ultrawideband radio design: The promise of high-speed, short-range wireless connectivity," *Proceedings of IEEE*, vol. 92, pp. 295-311, February 2004.
- [2] FCC, "Revision of part 15 of the commission rules regarding ultra-wideband transmission systems," *First Report and Order, ET Docket 98-153*, February 2002.
- [3] B. Manny and E. Tsui, "Adaptive radio constructs," *Intel Developer Forum*, Intel Corporation, September 2003.
- [4] T. W. Barrett, "History of ultrawideband (uwb) radar and communications: Pioneers and innovators," *Proceedings of Progress In Electromagnetics Symposium 2000*, pp. 47-55, Cambridge July 2000.
- [5] G. Ross, "A time domain criterion for the design of wideband radiating elements," *IEEE Trans. on Antennas and Propagation*, vol. 16, pp. 335-344 1968.

- [6] G. Ross, "Transmission and reception system for generating and receiving base-band duration pulse signals without distortion for short base-band pulse communication systems." U. S. Patent 3,7828,632, April 17, 1973.
- [7] "A brief history of UWB communications." Website: <http://www.ferret.com.au/articles/04/0c01fc04.asp>.
- [8] R. A. Scholtz, "Multiple access with time hopping impulse modulation," *Proceedings of IEEE Conference on Military Communications*, MILCOM' 93, Bedford, MA, pp. 447-450, 1993.
- [9] J. H. Reed, *An Introductiong to Ultra Wideband Communication Systems*. New Jersey: Pentice Hall, March 1998.
- [10] M. Wellborn, "Xtreme spectrum cfp presentation," May 2003. Website: [http://grouper.ieee.org/groups/802/15/pub/2003/May03/03153r4P802-15\\_TG3a-Xtre meSpectrum-CFP-Presentation.pdf](http://grouper.ieee.org/groups/802/15/pub/2003/May03/03153r4P802-15_TG3a-Xtre meSpectrum-CFP-Presentation.pdf).
- [11] Batra, "Multiband OFDM physical layer proposal for IEEE 802.15 task. Group 3a," November 2003.
- [12] "Ultra wideband in the news." Website: <http://www.sss-mag.com/uwb.html>.
- [13] "Sg3a alternate PHY selection criteria." IEEE, IEEE P802.15-02/105r25, 2002.
- [14] J. G. Proakis, Digital Communications. New York: McGraw-Hill, Third edition, 1995.

- [15] J. D. Taylor, *Introduction to Ultra Wideband Radar Systems*. Boca Raton, FL: CRC, 1995.
- [16] M. Z. Win and R. A. Scholtz, "Ultra-wide bandwidth time-hopping spread-spectrum impulse radio for wireless multiple-access communications," *IEEE Transactions on Communications*, vol. 48, pp. 679-691. April 2000.
- [17] D. Benedetto and M. G. B. Vojcic, "Ultra wide band (UWB) wireless communications: Atutorial," *Journal of Communication and Networks, Special Issue on Ultra-Wideband Communications*, vol. 5, pp. 290-302, December 2003.
- [18] "Effective isotropical-radiate power." Website: <http://en.wikipedia.org/wiki/Eirp>.
- [19] X. Luo, L. Yang, and G. Giannakis, "Designing optimal pulse-shapers for ultra-wideband radios," *Proceedings of IEEE Conference on Ultra Wideband Systems and Technologies*, Reston, Virginia, pp. 349-353, November 2003.
- [20] T. W. Parks and J. H. McClellan, "Chebysherv approximation for non-recursive digital filters with linear phase," *IEEE Trans. on Circuit Theory*, pp. 189-194, 1972.
- [21] B. Parr, B. Cho, K. Wallace, and Z. Ding, "A novel Ultra wideband pulse design algorithm," *IEEE Comm. Letters*, pp. 219-221, 2003.
- [22] X. Wu, Z. Tian, T. Davidson, and G. Giannakis, "Optimal waveform design for uwb radios," *Proceedings of IEEE International Conference on Acoustics, Speech, and Signal Processing*, vol. 4, Montreal, Canada, pp.521-524, May 2004.

- [23]L. Vandenberghe and S. Boyd, "Semi-definite programming," *SLAM. Review*, vol. 31, pp.49-95, March 1996.
- [24]Y. Wu, A. Molisch, S. Y. Kung, and J. Zhang, "Impulse radio pulse shaping for Ultra Wideband (UWB) systems," *Proceedings of Personal, Indoor and Mobile Radio Communications*, vol. 1, Beijing, China, pp. 877-881, September 2003.
- [25]D. Zeng, J. Annamalai, and A. Zaghloul, "Pulse shaping filter design in uwb system," *Proceedings of IEEE International Conference on Ultra Wideband Systems and Technologies*, Reston, Virginia, pp. 66-70. November 2003.
- [26]H. Sheng, P. Orlik, A. M. Haimovich, L. j Cimini, and J. Zhang, "On the spectral and power requirements for ultra-wideband transmission," *Proceedings of IEEE International Conference on Communications*, vol. 1, Anchorage, Alaska, pp. 718-722, May 2003.
- [27]L. B. Michael, M. Ghavami, and R. Kohno, "Multiple pulse generator for ultra-wideband communication using Hermite polynomial based orthogonal pulses," *Proceedings of IEEE Conference on Ultra Wideband Systems and Technologies*, pp. 47-51, March 2002.
- [28]M. Matsuo, M. and Kamada and H. Habuchi, "Design of UWB pulses based on b-splines," *Proceedings of IEEE International Symposium on Circuits and Systems, 2005*, vol. 6, pp. 5425-5428, May 2005.

- [29]N. Beaulieu and B. Hu, "A novel pulse design algorithm for ultra-wideband communications," *Proceedings of IEEE Global Telecommunications Conference, 2004*. vol. 5, Dallas, TX. pp. 3220-3224, November 2004.
- [30]L. De Nardis, G.Giancola, and D. B. M. Gola, "Power limits fulfillment and MUI reduction based on pulse shaping in UWB networks," *Proc. of International Conference on Communications*, vol. 6, Paris, France, pp. 3576-3580, June, 2004.
- [31]Morgan. Morel, "Ultra-wideband impulse scattering measurements," *IEEE Trans. on Antennas and Propagation*, vol. 42, pp .840-846, April 1994.
- [32]N. C. Lee J. S. and S. T., "New uniplanar subnano-second monocycle pulse generator and transformer for time-domain microwave applications," *IEEE Transactions on Microwave Theory and Techniques*, vol. 6, pp. 1126-1129, April 2001.
- [33]D. Kim H., Park and Y. Joo, "Design of Scholtz monocycle pulse generator," *Proceedings of IEEE Conference on Ultra Wideband Systems and Technologies*, Reston, Virginia, pp. 77-80, November 2003.
- [34]H. Kim and Y. Joo, "Fifth-derivative Gaussian pulse generator for UWB system," *Proc of Radio Frequency Integrated Circuit Symposium*, pp. 671-674, June 2005.
- [35]R. J. Cramer, R. A. Scholtz, and M. Z. Win, "Evaluation of an ultra-wideband propagation channel," *IEEE Transactions on Antennas and Propagation*, vol. 50, pp. 561-570, May 2002.

- [36] O.U. and Y. Li, "On the optimum pulse-position modulation index for ultra-wide band communication," *Proceedings of IEEE Circuits and Systems Symposium*, vol. 1, Shanghai, China, pp. 77-80, 2004.
- [37] B. Hu and N. Beaulieu, "Exact bit error rate analysis of TH-UWB systems in the presence of multiple-access interference," *Communications Letters*, vol 7, pp . 572-574, December 2003.
- [38] T. S. Rappaport, *Wireless Communications Principles and Practice*. Upper Saddle River, NJ: Prentice-Hall, 1996.
- [39] J. Foerster, "Channel modeling sub -committee report final," *IEEE P802.15 Work Group for Wireless Personal Area Networks (WPANs)*, IEEE P802.15-02/490rl-Sg3a, February 2003.
- [40] A. M. Saleh and R. A. Valenzuela, "A statistical model for indoor multipath propagation," *IEEE Journal on Selected Areas in Communications*, pp. 128-137, February 1987.







